

Simplified Phosphorescent Organic Light-Emitting Devices: A Study of Efficiency and Stability

by

Yingjie Zhang

A thesis
presented to the University of Waterloo
in fulfillment of the
thesis requirement for the degree of
Doctor of Philosophy
in
Electrical and Computer Engineering

Waterloo, Ontario, Canada, 2016

©Yingjie Zhang 2016

AUTHOR'S DECLARATION

I hereby declare that I am the sole author of this thesis. This is a true copy of the thesis, including any required final revisions, as accepted by my examiners.

I understand that my thesis may be made electronically available to the public.

Abstract

Organic light-emitting devices (OLEDs), compared to their inorganic counterparts, have potentially lower fabrication costs, lighter weight and better mechanical flexibility. Since its invention almost three decades ago, OLED technology has attracted tremendous interest, and has now produced a multi-billion-dollar industry. Currently, the two major applications of OLEDs are display panels and solid state lighting. As OLED development has progressed, its efficiency and stability have improved dramatically. However, these improvements come with the cost of increasing complexity in device structure. Consequently, the initial promise that OLEDs can provide a significant advantage in fabrication cost has unfortunately diminished. Recently, a device utilizing a simplified phosphorescent OLED, or PHOLED, structure with only three organic layers sparked interest in the field. Despite its simpler structure, this simplified PHOLED exhibits high efficiency. The origin of this high efficiency is, however, unclear. Considering that the device does not utilize blocking layers, it is uncertain if device efficiency can be further optimized. Moreover, simplified PHOLEDs have much lower stability than that of the conventional devices.

This work aims to be the first scientific investigation directed towards simplified PHOLEDs, with the goal of understanding the underlying processes that govern efficiency and stability of these devices, and then to utilize this knowledge to try to further improve device performance.

Investigations of the efficiency behavior of these devices show that charge balance in simplified PHOLEDs is not optimal. Particularly, the devices are generally hole-rich, and that the leakage of electrons to the counter electrode also presents a major mechanism that results in efficiency loss. By using hole transport layers (HTLs) that can also block electrons, device efficiency is found to increase by 25%. Results also show that by using a rougher ITO, light trapped in the ITO/organic wave-guided mode can be efficiently extracted, and a light outcoupling enhancement as high as 40% is achieved. Furthermore, it is found that the ITO thickness can also influence light outcoupling by 40%. These results demonstrate the significant efficiency benefits of using ITO with optimal thicknesses and higher roughness in OLEDs.

Investigations of the factors governing device stability show that the exciton-induced degradation of the ITO/organic interface plays an important role in limiting the lifetime of simplified

PHOLEDs. It is found that the lack of electron blocking layers in these devices allows electrons to leak from the emission layers and recombine with holes to form excitons near the ITO/organic interface. Furthermore, it is shown that introducing an electron blocking HTL can increase device lifetime by one order of magnitude. These results also show that the interactions between excitons and positive polarons in the host lead to host aggregation followed by the formation of exciton quenchers within. It is found that the rate of host aggregation limits the lifetime of PHOLEDs, and is also influenced by the guest material and its concentration. The findings explain why PHOLEDs utilizing different guest materials but otherwise identical material systems can have significantly different lifetimes and provide an answer to a long-lasting question in the field. Finally, it is found that reducing the exciton and polaron densities within the emission layer can further improve the lifetime of simplified PHOLEDs by one order of magnitude.

Acknowledgements

I would like to express my deepest gratitude to my supervisor, Professor Hany Aziz, for his guidance and encouragement throughout my PhD years. His wisdom and character have changed me as a researcher and as a person. Without his support, this work would not have been possible.

I would also like to thank my advisory committee members, Professor Irene Goldthorpe, Professor Bo Cui, Professor Pavle Radovanovic, and Professor Zheng-Hong Lu for their valuable advice and input in this thesis work.

I would like to acknowledge Mr. Richard Barber, the manager of the G2N lab, for his technical support.

I am grateful for all the helpful discussions and moral support from my colleagues, especially Dr. Qi Wang, Dr. Hossein Siboni, Dr. Yoshitaka Kajiyama, Dr. Graeme Williams, Dr. Dong-Ying Zhou, Mr. Sibi Sutti, Mr. Mina Abdelmalek, Mr. Thomas Borel, and Mr. Tyler Davidson-Hall.

I want to thank my parents, Qiuju Ma and Wenqing Zhang, for their never-ending love. Last but not least, I would like to thank my dear wife, Dr. Guanru Feng, for her constant support, patience, kindness and love.

Table of Contents

AUTHOR'S DECLARATION.....	ii
Abstract.....	iii
Acknowledgements.....	v
Table of Contents.....	vi
List of Figures.....	viii
List of Tables.....	xiii
List of Abbreviations.....	xiv
Chapter 1 Introduction.....	1
1.1 Background & Literature Review.....	2
1.1.1 OLED Operation Mechanism.....	2
1.1.2 A Review of Common OLED Architectures.....	8
1.1.3 Introduction to Simplified PHOLED.....	10
1.2 Device Efficiency.....	11
1.2.1 Internal Quantum Efficiency.....	11
1.2.2 Light Outcoupling.....	12
1.3 Device Stability.....	16
1.3.1 Bulk Material Degradation Mechanisms.....	17
1.3.2 Interfacial Degradation Mechanisms.....	18
1.4 Outstanding Issues Related to the Efficiency and Stability of Simplified PHOLEDs.....	22
1.5 Research Objectives.....	23
Chapter 2 Methodology & Experimental Procedures.....	25
2.1 Methodology.....	25
2.2 Material selection.....	26
2.3 Device Layout and Fabrication.....	29
2.4 Device & Material Characterization.....	30
2.4.1 IVL Characteristics.....	30
2.4.2 EL Spectroscopy.....	31
2.4.3 Delayed EL Measurements.....	31
2.4.4 EL Stability Measurements.....	31
2.4.5 Photo-stability Measurements.....	31
2.4.6 PL Spectroscopy.....	31

2.4.7 Exciton Lifetime Measurements.....	31
Chapter 3 Charge Balance in Simplified PHOLEDs.....	32
3.1 Limitations on Charge Balance	32
3.2 Approaches for Improving Charge Balance	42
3.3 Conclusions	44
Chapter 4 Light Outcoupling in Simplified PHOLEDs.....	45
4.1 Approaches for Improving Light Outcoupling	45
4.2 Conclusions	56
Chapter 5 Exciton-induced Degradation at the ITO/Organic interface	57
5.1 Degradation Mechanism.....	57
5.2 Approaches to Suppress Degradation.....	64
5.3 Conclusions	67
Chapter 6 Exciton-polaron Induced Degradation at the Organic/Organic Interface	68
6.1 Degradation Mechanism.....	69
6.2 Approaches for Suppressing Degradation	88
6.2.1 Reducing Exciton Concentration at the Organic/Organic Interface	88
6.2.2 Reducing Polaron Concentration at the Organic/Organic Interface	97
6.3 Conclusions	107
Chapter 7 Conclusions & Future Work.....	109
7.1 Conclusions	109
7.2 Future work	113
7.2.1 Using Pre-Aggregated Neat Emitting Layer to Suppress Exciton-Polaron Induced Aggregation.....	113
Appendix A List of Publications Derived from this Work.....	114
Bibliography.....	115

List of Figures

Figure 1.1 Device structure used in Tang and VanSlyke [2].	2
Figure 1.2 Operation mechanism of a generic bi-layer OLED: ① charge carrier injection; ② charge carrier transport; ③ exciton formation; and ④ radiative decay of exciton (or photon emission).	3
Figure 1.3 Tunneling and thermionic emission models for charge carrier injection from a metal contact to an organic semiconductor.	4
Figure 1.4 Electronic structure presented with potential wells for (a) molecules, (b) inorganic crystalline semiconductors and (c) organic semiconductors.	5
Figure 1.5 Hopping transport in organic semiconductor (a) without and (b) with the assistance of an external electric field.	6
Figure 1.6 Jablonski diagram showing some common electronic transitions that occurs in OLEDs.	8
Figure 1.7 Energy level diagram of an example device with multiple organic layers for optimizing charge balance.	9
Figure 1.8 Device structure of a simplified PHOLED.	11
Figure 1.9 Light outcoupling scheme	15
Figure 1.10 Light extraction working principle for shaped substrates.	15
Figure 1.11 Device structures of an OLED and a hole-only device	20
Figure 1.12 Scheme showing hole accumulation and their interactions with excitons near the CBP/TPBi interface in simplified PHOLEDs	21
Figure 2.1 Device layout on the pre-patterned ITO substrate	30
Figure 3.1 (a) Current density-voltage characteristics of devices with various CBP thickness. (b) Current efficiency vs. CBP thickness of these devices 100 cd/m^2 .	34
Figure 3.2 Delayed EL signals of devices with (a) 30 nm, (b) 90 nm, (c) 150 nm and (d) 210 nm CBP HTL under 0 and 0.74 MV/cm reverse electric field.	36
Figure 3.3 (a) Current density-voltage characteristics of devices with various TPBi thickness. (b) Current efficiency vs. TPBi thickness of these devices at 100 cd/m^2 .	38
Figure 3.4 Delayed EL signals of devices with (a) 45 nm, (b) 95 nm, (c) 145 nm and (d) 195 nm TPBi ETL under 0 and 0.83 MV/cm reverse electric field.	39
Figure 3.5 (a) Current density vs. voltage and (b) current efficiency vs. current density characteristics of devices with various NPB doping concentrations in the hole trapping layer. (a) Inset: energy level diagram for NPB and CPB.	41

Figure 3.6 (a) Current density vs. voltage and (b) current efficiency vs. current density characteristics of devices with various Bphen doping concentrations in the electron trapping layer. (a) Inset: energy level diagram for TPBi and Bphen.	42
Figure 3.7 Current efficiency vs. luminance characteristics of devices with 45 nm BmPyPhB ETL and various HTL/EML structures: Device A – CBP (30 nm)/CBP:Ir(ppy) ₃ (5%) (15 nm); Device B - TCTA (30 nm)/TCTA:Ir(ppy) ₃ (5%) (15 nm); Device C - TCTA (30 nm)/CBP:Ir(ppy) ₃ (5%) (15 nm); and Device D - TCTA (30 nm)/CBP:Ir(ppy) ₃ (acac) (5%) (15 nm).	43
Figure 3.8 Delayed EL signals of device D under 0 and 0.74 MV/cm reverse electric field.	44
Figure 4.1 (a) Simplified PHOLED structure. (b) Current density vs. voltage characteristics of devices fabricated on ITO _{130/3.3} and ITO _{130/8.5}	47
Figure 4.2 Current efficiency (solid symbols) and power efficiency (open symbols) vs. luminance of devices fabricated on ITO _{130/3.3} and ITO _{130/8.5}	47
Figure 4.3 AFM images of (a) ITO _{130/3.3} and (b) ITO _{130/8.5}	48
Figure 4.4 Measured brightness due to light scattered off the neighboring ITOs on ITO _{130/3.3} and ITO _{130/8.5}	48
Figure 4.5 Changes in EL and driving voltage with time under 20 mA/cm ² current density for devices fabricated on ITO _{130/3.3} and ITO _{130/8.5}	50
Figure 4.6 AFM images of (a) ITO _{130/3.3} , (b) MoO ₃ on ITO _{130/3.3} , (c) CBP on MoO ₃ and ITO _{130/3.3} , (d) entire organic stack on ITO _{130/3.3} , (e) ITO _{130/8.5} , (f) MoO ₃ on ITO _{130/8.5} , (g) CBP on MoO ₃ and ITO _{130/8.5} and (h) entire organic stack on ITO _{130/8.5} . Notice the difference in color scale.	50
Figure 4.7 Current efficiency (solid symbols) and power efficiency (open symbols) vs. luminance characteristics of devices fabricated on ITO _{100/3.3} and ITO _{100/9.9}	51
Figure 4.8 Transmittance of ITO _{100/3.3} , ITO _{100/9.9} , ITO _{130/3.3} and ITO _{130/8.5} substrates.	52
Figure 4.9 Current efficiency vs. luminance characteristics of the device with structure (inset) fabricated on ITO _{130/8.5} and ITO _{130/3.3}	53
Figure 4.10 Measured transmittance of ITO _{100/3.3} and ITO _{130/8.5} . (b) Current efficiency vs. luminance of devices fabricated on ITO _{100/3.3} and ITO _{130/8.5}	54
Figure 4.11 (a) Measured transmittance of ITO _{100/3.3} and ITO _{130/8.5} . (b) Current efficiency vs. luminance of devices fabricated on ITO _{100/3.3} and ITO _{130/8.5}	55
Figure 4.12 Current density vs. voltage characteristics of devices fabricated on ITO _{100/3.3} and ITO _{130/8.5}	56

Figure 5.1 Changes in (a) EL and (b) driving voltage with time under 20 mA/cm ² current density for pristine and illuminated devices without MoO ₃ . (c) Changes in EL with time for pristine and illuminated devices with MoO ₃	60
Figure 5.2 (a) JV characteristics of devices with x% FIrpic doping concentrations. x = 0, 5, 10, 15, 20. (b) Current efficiency vs. current density characteristics. (c) Changes in EL with time under 20 mA/cm ² current density.	62
Figure 5.3 Changes in EL with time under 20 mA/cm ² current density for devices with x nm thick CBP HTL, where x = 20, 40, 60, 80, 100.	64
Figure 5.4 (a) JV and (b) current efficiency vs. current density characteristics of devices with ITO/CBP and ITO/26DCzPPy/CBP interfaces. (c) Changes in EL with time of devices with ITO/CBP and ITO/26DCzPPy/CBP interfaces under 20 mA/cm ² current density.	66
Figure 5.5 Changes in EL with time of pristine and illuminated devices under 20 mA/cm ² current density.	67
Figure 6.1 EL spectra (normalized to the guest emission peak intensity) of devices with (a) 0.25% Ir(ppy) ₃ , (d) 0.25% Ir(ppy) ₂ (acac) and (g) 0.25% Ir(piq) ₃ as dopant, collected before and after electrical driving at 20mA/cm ² for certain periods of time. (b), (e) and (h) The enlarged views of (a), (d) and (g) centered around the host emission peaks, respectively. The arrows highlight the direction of changes in the CBP monomer and aggregate peaks relative to the guest emission peaks. (e), (f) and (i) Normalized EL spectra from (a), (d) and (g), respectively, after removing the guest emission peaks.	70
Figure 6.2 Changes in device EL and CBP monomer emission over time of devices using (a) 1.5% Ir(ppy) ₃ , (c) 1.5% Ir(ppy) ₂ (acac) and (e) 1.5% Ir(piq) ₃ as dopant, under electrical driving at 20 mA/cm ² . EL spectra (normalized to the guest emission peak intensity) of devices with (b) 1.5% Ir(ppy) ₃ , (d) 1.5% Ir(ppy) ₂ (acac) and (f) 1.5% Ir(piq) ₃ as dopant, collected before and after electrical driving at 20mA/cm ² for certain periods of time.	72
Figure 6.3 Changes in CBP-to-dopant EL peak ratio over time for devices using (a) Ir(ppy) ₃ , (b) Ir(ppy) ₂ (acac) and (c) Ir(piq) ₃ as dopant with various doping concentrations, under constant electrical driving at 20 mA/cm ²	74
Figure 6.4 Image of films (top) before and (bottom) after heating at 120°C for 6 minutes, taken under UV irradiation. The film compositions from left to right are: CBP (30 nm), CBP:Ir(piq) ₃ (5%) (30 nm), CBP:Ir(piq) ₃ (0.25%) (30 nm), CBP:Ir(ppy) ₂ (acac) (5%) (30 nm), CBP:Ir(ppy) ₂ (acac) (0.25%) (30 nm), CBP:Ir(ppy) ₃ (5%) (30 nm) and CBP:Ir(ppy) ₃ (0.25%) (30 nm).	76

Figure 6.5 Image of films after heating at 120°C for 30 minutes, under UV irradiation. The film compositions from left to right are: CBP (30 nm), CBP:Ir(piq) ₃ (5%) (30 nm), CBP:Ir(piq) ₃ (0.25%) (30 nm), CBP:Ir(ppy) ₂ (acac) (5%) (30 nm), CBP:Ir(ppy) ₂ (acac) (0.25%) (30 nm), CBP:Ir(ppy) ₃ (5%) (30 nm) and CBP:Ir(ppy) ₃ (0.25%) (30 nm).....	76
Figure 6.6 PL spectra of (a) CBP (30 nm), (b) CBP:Ir(ppy) ₃ (0.25%) (30 nm) and (c) CBP:Ir(ppy) ₂ (acac) (0.25%) (30 nm) films before and after heating at 120°C for 30 minutes, respectively.....	78
Figure 6.7 Exciton lifetime in neat CBP films measured at various detection wavelength (a) before and (b) after heating at 120°C for 6 minutes.....	81
Figure 6.8 Exciton lifetime of CBP films with various doping conditions measured at 389nm detection wavelength (a) before and (b) after heating at 120°C for 6 minutes.....	82
Figure 6.9 Image of films (top) before and (bottom) after heating at 160°C for 1 minute, taken under UV irradiation. The film compositions from left to right are: 26DCzPPy:Ir(ppy) ₃ (0.25%) (30 nm), 26DCzPPy:Ir(ppy) ₃ (5%) (30 nm), 26DCzPPy:Ir(ppy) ₂ (acac) (0.25%) (30 nm), 26DCzPPy:Ir(ppy) ₂ (acac) (5%) (30 nm), 26DCzPPy:FIrpic (0.25%) (30 nm), 26DCzPPy:FIrpic (5%) (30 nm) and 26DCzPPy (30 nm).	84
Figure 6.10 Microscope images of (a) 26DCzPPy:Ir(ppy) ₂ (acac) (0.25%) (30 nm), (b) 26DCzPPy:Ir(ppy) ₂ (acac) (5%) (30 nm), (c) 26DCzPPy:Ir(ppy) ₃ (5%) (30 nm) and (d) 26DCzPPy:FIrpic (5%) (30 nm) films after heating at 160°C for 1 minute.	85
Figure 6.11 Changes in device EL over time of devices with various dopant materials and concentrations under electrical driving at 20 mA/cm ²	86
Figure 6.12 Image of films (top) before and (bottom) after heating at 140°C for 2 minutes, taken under UV irradiation. The film compositions from left to right are: TAPC:Ir(ppy) ₃ (0.25%) (30 nm), TAPC:Ir(ppy) ₃ (5%) (30 nm), TAPC:Ir(ppy) ₂ (acac) (0.25%) (30 nm), TAPC:Ir(ppy) ₂ (acac) (5%) (30 nm).	86
Figure 6.13 Microscope images of (a) TAPC:Ir(ppy) ₂ (acac) (0.25%) (30 nm), (b) TAPC:Ir(ppy) ₂ (acac) (5%) (30 nm), (c) TAPC:Ir(ppy) ₃ (0.25%) (30 nm) and (d) TAPC:Ir(ppy) ₃ (5%) (30 nm) films after heating at 140°C for 2 minutes. Red circles indicate the average sizes of the crystallites.....	87
Figure 6.14 Changes in EL with time under 20 mA/cm ² current density for devices with 10, 20 and 30 nm EML all utilizing 30 nm CBP HTL and 40 nm TPBi ETL. (Inset) The structures of these devices.	89

Figure 6.15 Inset (a) EL spectra for devices with and without the 10 nm neat CBP layer. EL spectra for devices with 10, 15, 20, 25 and 30 nm EML and with 10 nm neat CBP marking layer, normalized to Ir(ppy) ₃ emission. Inset (b) EL spectra of these devices without normalization.	90
Figure 6.16 Current efficiency vs. current density characteristics of selected devices. (Inset) Current density vs. voltage characteristics of these devices.	91
Figure 6.17 Changes in EL with time of devices A, B and C. (Inset) The structures of these devices.	92
Figure 6.18 Current efficiency vs. current density characteristics of selected devices with different ETL/EIL configurations.	93
Figure 6.19 Current density vs. voltage characteristics of devices with various (a) BCP and (b) TPBi ETL thicknesses.	94
Figure 6.20 Current efficiency vs. current density characteristics of devices with various (a) BA1q, (b) BmPyPhB and (c) Alq ₃ ETL thicknesses.	96
Figure 6.21 Device structures of simplified PHOLEDs in (a) standard and (b) inverted architectures.	99
Figure 6.22 (a) JV characteristics, (b) current efficiency and (c) lifetime comparison of standard and inverted simplified PHOLEDs.	100
Figure 6.23 Device structures of (a) device C in the standard architecture and (b) device D in the inverted architecture with marking layers in TPBi, (c) device E in the standard architecture and (d) device F in the inverted architecture with marking layers in CBP.	102
Figure 6.24 EL spectra of devices A, B, C, D, E and F.	103
Figure 6.25 Delayed EL measurements of devices with (a) standard and (b) inverted structures with no reverse biases and with 10 V reverse biases.	105
Figure 6.26 Proposed device operating mechanisms in (a) standard and (b) inverted simplified PHOLEDs. Blue and red arrows indicate the movement of electrons and holes in the devices under operation, respectively.	106
Figure 6.27 Lifetime of simplified PHOLEDs using Ir(ppy) ₂ (acac) emitters with standard and inverted structures.	107

List of Tables

Table 2.1 List of materials used in this thesis.....	26
Table 5.1 Driving voltages and luminance at 20mA/cm ² for devices without and with MoO ₃ before and after external illumination.....	59

List of Abbreviations

AFM:	Atomic Force Microscopy
e-h:	electron-hole
EBL:	Electron Blocking Layer
EL:	Electroluminescence
EML:	Emission Layer
EIL:	Electron Injection Layer
EQE:	External Quantum Efficiency
ETL:	Electron Transport Layer
ETM:	Electron Transport Material
HTL:	Hole Transport Layer
HTM:	Hole Transport Material
HOMO:	Highest Occupied Molecular Orbital
ITO:	Indium Tin Oxide
IQE:	Internal Quantum Efficiency
IVL:	Current density vs. Voltage vs. Luminance (characteristics)
J-V:	Current density vs. Voltage (characteristics)
LUMO:	Lowest Unoccupied Molecular Orbital
MAM:	Molybdenum Oxide-Silver- Molybdenum Oxide (stack)
OLED:	Organic Light-Emitting Device
PHOLED:	Phosphorescent Organic Light-Emitting Device
PVD:	Physical Vapor Deposition
TIR:	Total Internal Reflection

Chapter 1

Introduction

Organic light-emitting devices (OLEDs) are electroluminescent thin-film devices that utilize organic semiconductor materials. In the most basic structure, an OLED consists of one layer of an electroluminescent material sandwiched between two electrodes. When an electrical bias is applied between the electrodes, electrons and holes are injected into the organic layer, where they recombine and produce photons. Compared to their inorganic counterparts, OLEDs have several advantages. They have potentially lower fabrication costs, lighter weight and better mechanical flexibility, because they can be fabricated via solution processing techniques, and the devices in general are only a few hundred nanometers thick. Since its invention almost three decades ago, OLED technology has attracted tremendous interest, and has now produced a multi-billion-dollar industry. The two major applications of OLEDs today are display panels and solid state lighting.

The two major performance parameters of OLEDs are efficiency and stability (commonly specifically referred to the stability of electroluminescence under device operation). As OLED development has progressed, both efficiency and stability have improved dramatically. The advancement comes from the emergence of better-performing organic semiconducting materials (e.g. phosphorescent emitters) as well as improved and more sophisticated device structures that often consist of five or more organic layers. As this process has evolved, however, the initial promise that OLEDs can produce significant fabrication cost advantages has unfortunately diminished, because of the growing complexity in device structure. As a result, commercial OLED products have high price tags, and have yet to be competitive in the consumer electronics market. Meanwhile, as the OLED technology is being developed, a device utilizing a simplified phosphorescent OLED, or PHOLED, structure with only three organic layers recently sparked interest in the field. Not only does this device have the advantage of much simpler fabrication due to the reduced number of organic layers that require material deposition, but the device also showed record-high efficiency. Due to these advantages, simplified PHOLEDs are the focus of this thesis. In particular, studies of approaches to further improve device efficiency as well as investigations of the stability issues associated with simplified PHOLEDs will be presented.

In this chapter, Section 1.1 gives a brief background on OLED operation mechanism and simplified PHOLED. Sections 1.2 and 1.3 discuss the issues with device efficiency and lifetime in general. Section 1.4 lists some issues related to simplified PHOLEDs. Finally, Section 1.5 presents the motivations behind this work and its objectives.

1.1 Background & Literature Review

Electroluminescence (EL) for organic materials was first observed by Pope et al. in anthracene single crystals in 1963 [1]. This device utilized a single layer of an organic material sandwiched between two electrodes. Producing EL, however, required very high driving voltage (> 400 V) and the brightness was very low. A breakthrough came in 1987, when Tang and VanSlyke invented the first bi-layer OLED which consisted of one hole transport material (HTM) — Tetraphenyldiamine (TPD), and one electron transport material (ETM) — Tris(8-hydroxyquinolino)aluminum (Alq_3) [2]. This device was able to exhibit a brightness measuring higher than 1000 cd/m^2 with a driving voltage below 10 V. The structure of the device is illustrated in Figure 1.1. In order to understand why this device was able to perform better and signal the birth of OLED technology as we know it today, it is important to first understand the operation mechanism of OLEDs.

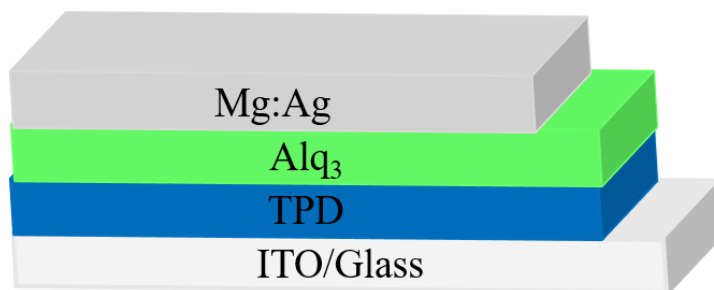


Figure 1.1 Device structure used in Tang and VanSlyke [2].

1.1.1 OLED Operation Mechanism

The operation of OLED is a process of converting electrical energy into electromagnetic radiation, or more specifically, converting electrons into photons. This process is done in four steps: (1) charge carrier injection from the electrodes into the organic layers; (2) charge carrier transport in the organic layers; (3) exciton formation and (4) radiative decay of exciton (or photon emission). Figure 1.2 presents the energy level diagram of a generic bi-layer OLED under an electrical bias and illustrates the four steps of the operation mechanism in these devices.

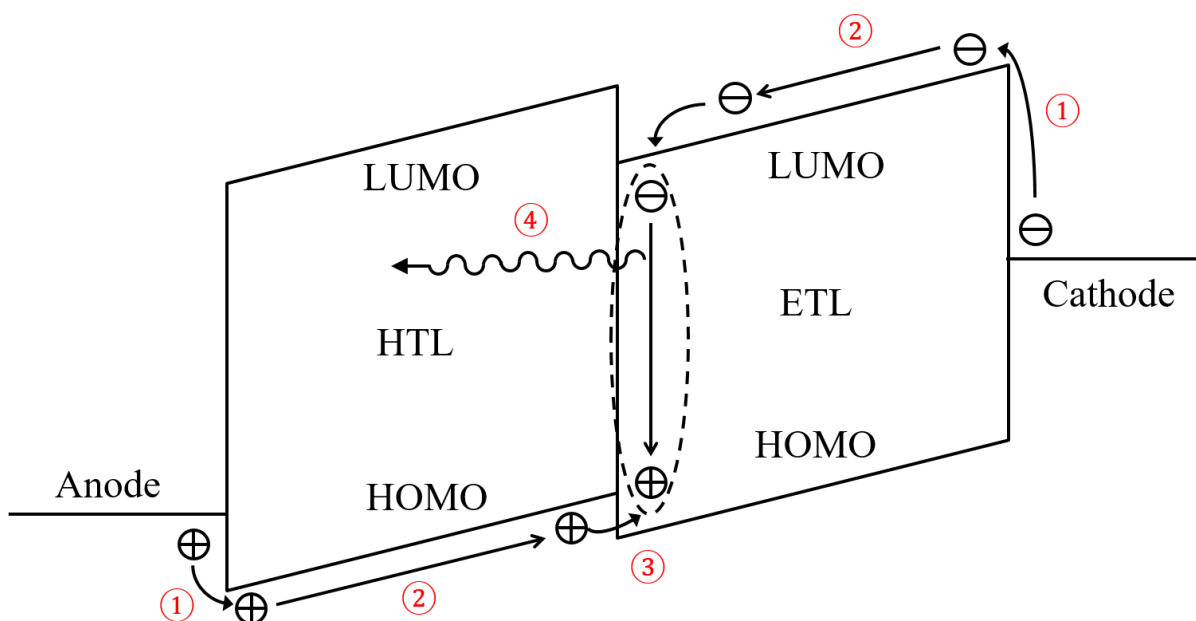


Figure 1.2 Operation mechanism of a generic bi-layer OLED: ① charge carrier injection; ② charge carrier transport; ③ exciton formation; and ④ radiative decay of exciton (or photon emission).

Charge carrier injection is the first step in OLED operation. In Figure 1.2, this step is denoted by ①. In this step, electrons are injected from the cathode into the lowest unoccupied molecular orbitals (LUMO) levels of the electron transport layer (ETL) and holes are injected from the anode into the highest occupied molecular orbitals (HOMO) levels of the hole transport layer (HTL). In both cases, an injection barrier is present due to the Schottky contact formed at the metal/semiconductor interface. Charge injection through this barrier can be described using two models: tunneling or thermionic emission [3], [4]. Figure 1.3 illustrates the working principles for electron injection using these two models. In the tunneling model, Φ_B represents the injection barrier between the work function of the metal and the LUMO level of the organic layer¹. When an electric field is applied across the organic layer, its energy levels are tilted. The charge injection efficiency is related to the

¹ To be more accurate, the height of the injection barrier is not actually the difference between the work function of the metal and the LUMO level of the organic layer. When an organic semiconductor is placed next to a metal, there is usually a layer of dipoles formed at the interface, causing the vacuum level of the organic material to shift [116]. In general, the dipole layer reduces the injection barrier. Moreover, the band bending effect, similar to what is seen in inorganic semiconductors, is also present in the organic layer, but only occurs over a short distance from the interface. Although both the band bending and the dipole layer can affect the injection barrier, the simplified scenario shown in Figure 1.3 can be used sufficiently for the understanding of the electron injection process in OLEDs.

barrier thickness x . Obviously, reducing Φ_B and increasing the applied electric field decrease x , and thus lead to more efficient injection. On the other hand, in the thermionic emission model, electrons require sufficient thermal energy to surpass the energy barrier Φ_B for the charge injection to occur. It is important to note that the energy barrier Φ_B is lowered in this model due to the effect of the image force potential. Image force describes a phenomenon whereby when an electron is placed a distance of y from the surface of a metal, it experiences a force that is the same as having a positive charge $2y$ away. As a result, when an electron is close to a metal surface, there is a force that tries to prevent the electron from escaping the metal. The potential that arises from the image force would then influence the applied electric field, resulting in a combined potential that allows the injection of electrons with lower thermal energy into the organic material. Similar to the tunneling model, the injection efficiency is related to the barrier height Φ_B . By increasing the applied electric field, the injection barrier can be lowered.

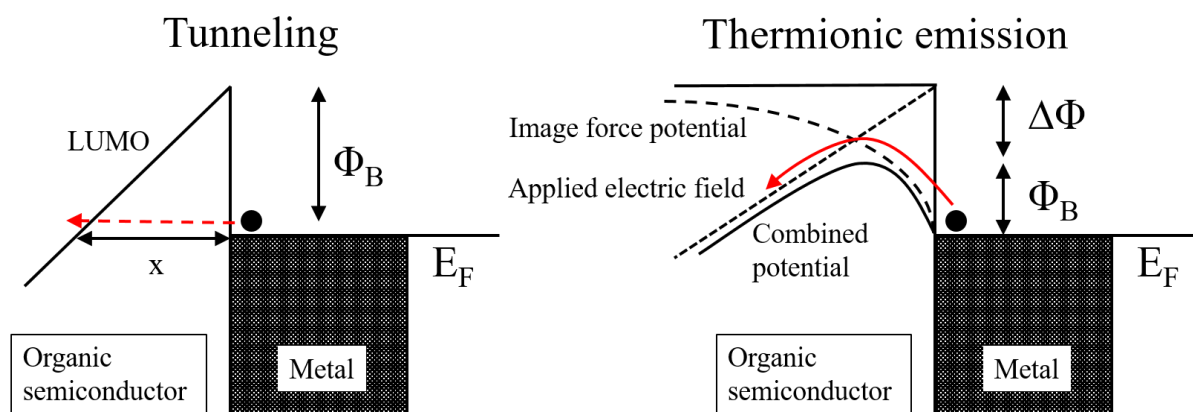


Figure 1.3 Tunneling and thermionic emission models for charge carrier injection from a metal contact to an organic semiconductor

Charge carrier transport is the second step in OLED operation. In Figure 1.2, this step is denoted by ②. After holes and electrons are injected into the HTL and ETL, respectively, the carriers are then transported across the two layers towards the HTL/ETL interface. One major difference between OLEDs and inorganic LEDs (or to a broader extent, organic semiconductors and inorganic semiconductors in general) is that organic material is generally amorphous instead of crystalline. Figure 1.4 (a) presents the electronic structures with potential wells for molecules in general. In inorganic crystalline semiconductors, where molecules are arranged in a highly ordered structure, conduction and valence bands are formed, as shown in Figure 1.4 (b). On the other hand,

because organic semiconductors are amorphous molecular solids, i.e. they lack long-range order and have only weak intermolecular interactions, conduction and valence bands are not formed, and the energy diagram is different from that of conventional semiconductors, as illustrated in Figure 1.4 (c) [5]. In contrast to inorganic crystalline solids, where charge transport is generally modelled by band transport, charge transport in organic amorphous materials occurs by hopping. More specifically, holes transport along the organic semiconductors by hopping from the HOMO levels of one molecule to another while electrons hop on the LUMO levels. In addition, it should be noted that in order for the hopping to occur, the charge carriers need to have sufficient thermal energy to surpass the potential barrier between molecules. As a result, mobility in organic materials increases at higher temperatures [6]. Furthermore, carrier mobility depends on the external electric field applied across organic semiconductors. Figure 1.5 illustrates the charge transport process with and without an external electric field. As can be seen clearly, when an external field is present, the potential barrier ΔE between neighboring molecules is lowered, resulting in easier hopping, and thus faster charge transport.

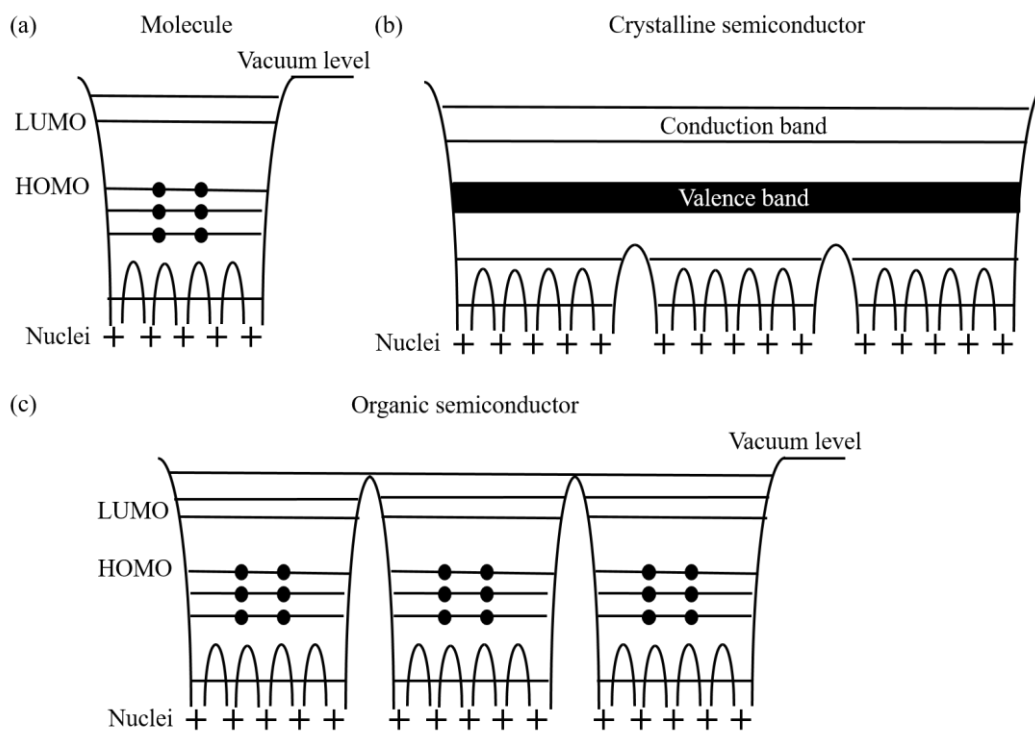


Figure 1.4 Electronic structure presented with potential wells for (a) molecules, (b) inorganic crystalline semiconductors and (c) organic semiconductors.

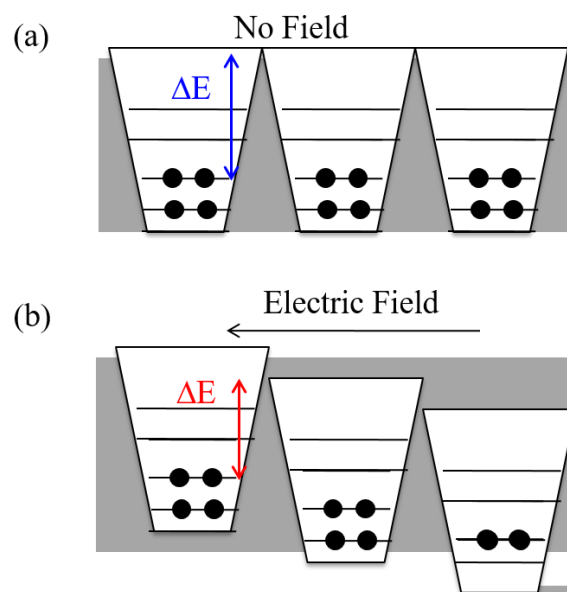


Figure 1.5 Hopping transport in organic semiconductor (a) without and (b) with the assistance of an external electric field.

Exciton formation is the third step in OLED operation. In Figure 1.2, this step is denoted by ③. After holes and electrons are transported across the HTL and ETL, they recombine to form excitons, i.e. electron-hole (e-h) pairs bond together by electrostatic interactions. In the case of organic semiconductors, the bond holes and electrons reside on the same molecules and thus form Frenkel (localized) excitons. Obviously, the efficiency of the exciton formation process is related to the probability of holes recombining with electrons, and thus the hole and electron densities. In fact, the high efficiency of the first bi-layer OLED by Tang and Van Slyke [7] is due to the high carrier density near the HTL/ETL interface, hence more efficient exciton formation. The high charge density in bi-layer OLED is generally due to the mismatch in HOMO or LUMO levels and/or the difference in carrier mobility in the two transport materials. For example, in the device shown in Figure 1.2, because the LUMO level of the HTL is much shallower than that of the ETL, the electron injection from the ETL to the HTL is difficult, resulting in electron accumulation at the interface. Furthermore, despite the easier injection of holes from the HTL to the ETL due to a small HOMO level difference, if the hole mobility in the ETL is low, a high density of holes in the ETL near the interface is also formed. Because of the high density of holes and electrons in the ETL near the interface, excitons are created efficiently nearby. It is also important to note that when an exciton is formed, both the electron and the hole have an equal probability of being in a spin $|\uparrow\rangle$ or $|\downarrow\rangle$ state. Consequently,

the formed exciton has a 25% chance of being in a singlet state, i.e. the exciton has a total spin number of 0 with the state $\frac{1}{\sqrt{2}}(|\uparrow\downarrow\rangle - |\downarrow\uparrow\rangle)$, and a 75% chance of being in a triplet state, i.e. the exciton has a total spin number of 1 with possible states $|\uparrow\uparrow\rangle$, $|\downarrow\downarrow\rangle$ and $\frac{1}{\sqrt{2}}(|\uparrow\downarrow\rangle + |\downarrow\uparrow\rangle)$.

Radiative decay of exciton (or photon emission) is the last step in OLED operation. In Figure 1.2, this step is denoted by ④. As an exciton is a pair consisting of an electron in a higher energy level and a hole in a lower energy level, it is in a metastable state, and so the electron eventually loses its energy and fills the hole. There are several pathways for the excitons to lose their energy and relax to the ground state. The Jablonski diagram, as shown in Figure 1.6, presents some common electronics transitions that the excitons can experience which occur in OLEDs. As can be seen in the figure, the created excitons can undergo non-radiative (denoted by squiggly lines) and radiative relaxations (denoted by solid lines). If the excitons undergo non-radiative decay, such as internal conversion and then vibrational relaxation, the exciton energy is then dissipated via phonons. On the other hand, if the excitons undergo radiative decay, such as fluorescence (resulted from the decay of singlet excitons) or phosphorescence (resulted from the decay of triplet excitons), photons are then produced. This photon emission step, which directly influences the efficiency of OLEDs, depends on two main factors. The first one is whether the emission is fluorescent or phosphorescent. As stated above, when an OLED is under operation, according to spin statistics, 25% of the excitons formed in step ③ are singlets (occupying the S1 state) and 75% of the excitons are triplets (occupying the T1 state). If fluorescent emitters are used in OLEDs, only the 25% singlets are able to relax to emit photons, due to the Pauli Exclusion Principle. As a result, the maximum quantum efficiency of such devices is 25%. However, if a phosphorescent emitter is used in an OLED, the 75% triplets can emit photons via phosphorescence, due to the strong spin-orbit coupling resulted from the heavy metal atom incorporated in the molecule (e.g. iridium in tris(2-phenylpyridine)iridium(III) (Ir(ppy)_3)). Moreover, the remaining 25% of excitons which are singlets can also be converted to photons by first relaxing to the T1 state through intersystem crossing and vibrational relaxation. Therefore, the theoretical maximum quantum efficiency is 100% for phosphorescent emitters. The second important factor that affects the efficiency of OLEDs is the quantum yield of the emitting material. The quantum yield describes how likely an exciton goes through radiative decay to emit photons, and is related to the rates of the radiative transitions relative to the other non-radiative transitions, such as intersystem crossing and internal conversion. For some of the benchmark emitters, such as

$\text{Ir}(\text{ppy})_3$, the quantum yield can be greater than 90% [8]. It is also important to note that in order for the emitted photons to be observed outside of the devices, most OLEDs consist of one transparent and one reflective electrode (so that light emits in a single direction). Due to its high optical transmittance ($> 90\%$ in visible range at 150 nm film thickness), high electrical conductivity (with $< 20 \Omega/\square$ sheet resistance at 150 nm film thickness) and deep work function ($\sim 4.7 \text{ eV}$), tin-doped indium oxide (ITO) has been the most widely used transparent anode in OLED community. On the other hand, both silver and aluminum are generally used as the reflective cathode.

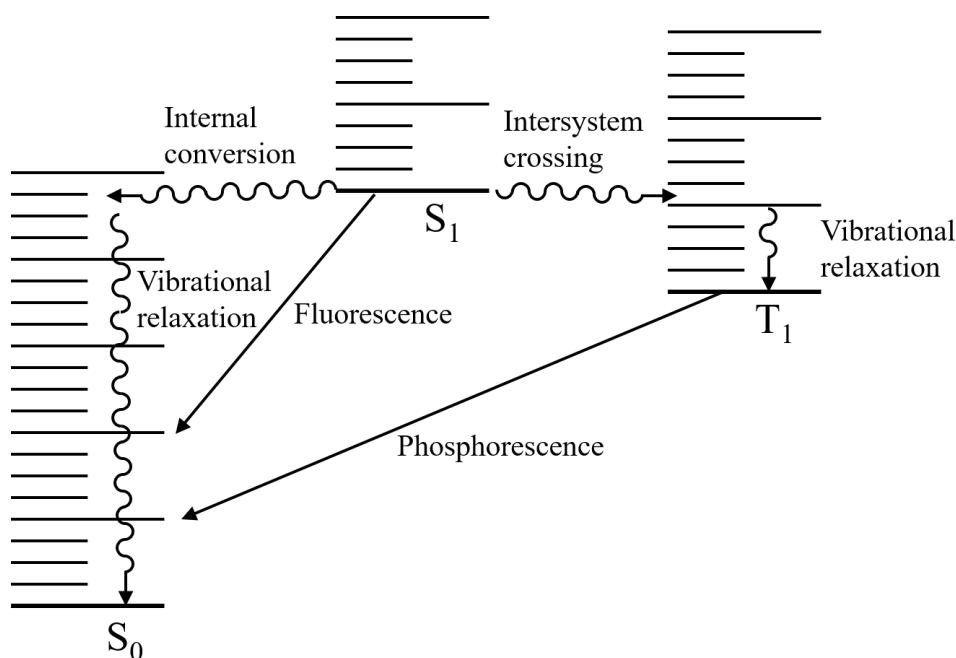


Figure 1.6 Jablonski diagram showing some common electronic transitions that occurs in OLEDs.

1.1.2 A Review of Common OLED Architectures

Ever since the first bi-layer device made by Tang and VanSlyke, the structure of OLEDs has been growing in complexity in order to improve device performance [9]–[14]. For instance, Figure 1.7 presents the structure of an example device with seven organic layers. In order to enhance carrier injection efficiency, thus lowering the voltage needed to drive a device at a constant current, hole injection layers (HILs) and electron injection layers (EILs) are often used between the electrodes and the corresponding transport layers (e.g. HIL is inserted between the anode and the HTL) in state-of-the-art OLEDs. The purpose of the injection layers is to facilitate charge injection by reducing the

corresponding injection barriers. Some commonly used materials include MoO_3 as the HIL and LiF as the EIL. In addition to these barrier-lowering injection layers, HTLs doped with strong acceptor and ETLs doped with metal have been used as the injection layers and eliminations of injection barriers have been demonstrated [9].

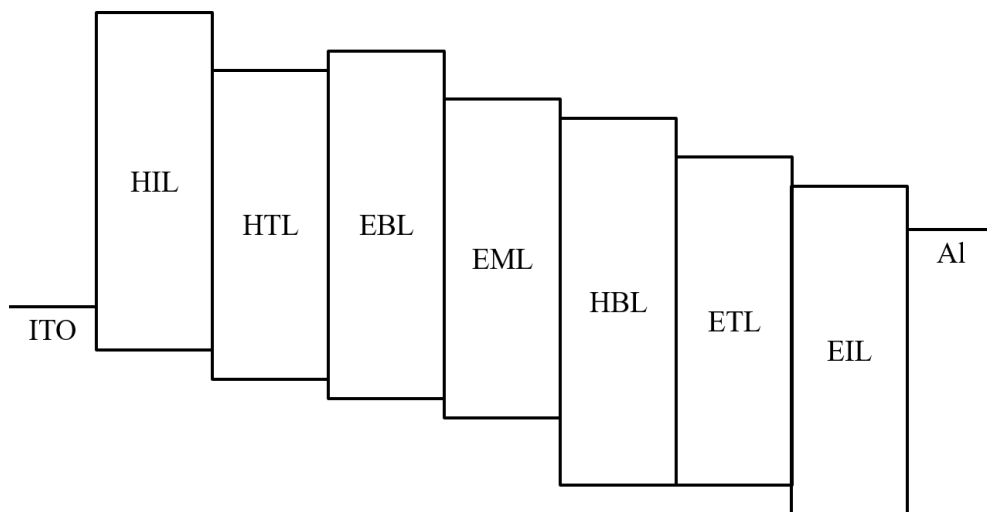


Figure 1.7 Energy level diagram of an example device with multiple organic layers for optimizing charge balance.

In addition to HILs and EILs, dedicated emission layers (EMLs) are often used in OLEDs. In a generic bi-layer OLED, such as the device shown in Figure 1.2, excitons are created and undergo radiative decay on the ETL. In this case, the ETL also acts as the EML. On the other hand, when a dedicated EML is inserted between the HTL and ETL, excitons are formed on the EML by having the holes and electrons accumulating at either the HTL/EML or EML/ETL interface. The benefit of this structure is to have better confinement of excitons within the EML by having the energy levels of excited states (S_1 and/or T_1) on the EML be lower than those on the HTL and ETL. Another common practice in OLEDs is that the EML generally consists of a host material and a guest emitter. The excitons are usually created on the host and then transferred to the guest molecules via Förster and Dexter energy transfer processes. By diluting the emitter in the host, concentration quenching, a process that lowers fluorescent and phosphorescent decay rates via non-radiative energy transfer between identical molecules or through aggregates, can be avoided [15]. A three-fold efficiency enhancement has been observed when such a host:guest system is used [16].

Lastly, charge blocking layers such as EBL and HBL can also be introduced to confine charges within the EML. The benefits of using these charge blocking layers are: (1) both hole and electron density within the EML can be maximized so that the exciton formation process is efficient; and (2) leakage current, which corresponds to the electrical energy that cannot be converted into photons, can be limited.

1.1.3 Introduction to Simplified PHOLED

Clearly, one disadvantage of having OLEDs with such complex structures is the increased cost of device fabrication. Opposite to the general approach, in 2011, Helander et al. demonstrated a simplified PHOLED that consists of only three organic layers (compared to the traditional devices that consists of 7 organic layers), yet showing record-high efficiency at the time [17]. As a result, this simplified PHOLED structure soon attracted a great deal of interest in the community.

Figure 1.8 presents the structure of the simplified PHOLED in Helander et al. [17]. Same as in most OLEDs, ITO is the transparent anode. To facilitate hole injection, chlorine plasma is used to treat the ITO surface to increase its work function to ~ 6 eV. CBP (chemical abbreviation for 4,4'-bis(carbazol-9-yl)biphenyl), a bipolar (i.e. the material has high hole and electron mobility) organic semiconducting material, is employed as both the HTM and the host. Bis(2-phenylpyridine)(acetylacetonate)iridium(III) ($\text{Ir}(\text{ppy})_2(\text{acac})$), a phosphorescent green emitter that has 94% quantum yield [18], is doped into the CBP at 8% concentration to form the EML. A wide bandgap ETM, 2,2',2''-(1,3,5-benzinetriyl)-tris(1-phenyl-1-H-benzimidazole) (TPBi), is used so that excitons can be confined on the EML. Lastly, a thin layer of LiF is inserted between the ETL and the Al cathode to help electron injection. To understand how the simplified PHOLED can exhibit very high efficiency, it is important to first look at factors that influence OLED efficiency in general. A background on this topic can be found in Section 1.2.

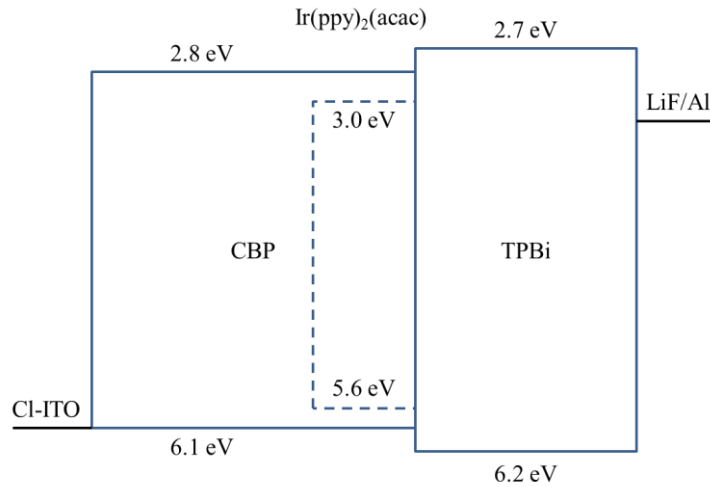


Figure 1.8 Device structure of a simplified PHOLED

Although the simplified PHOLED by Helander et al. exhibited the highest efficiency at the time, it suffered one major drawback: its lifetime is shorter than that of traditional PHOLEDs [19], [20]. Therefore, understanding the mechanism behind the limited lifetime becomes a priority before this structure can be used in industry. A background on some of the degradation mechanisms that limit the lifetime of OLEDs in general are discussed in Section 1.3. Some possible mechanisms that could be causing the limited lifetime of simplified PHOLEDs are also presented.

1.2 Device Efficiency

1.2.1 Internal Quantum Efficiency

One important efficiency parameter in any electroluminescent device is its internal quantum efficiency (IQE). It is defined as the efficiency of a device in converting electrical current into photons, and is given by:

$$IQE = \frac{n_{photon\ output}}{n_{electron\ input}} \quad \text{Equation 1.1}$$

where $n_{photon\ output}$ is the number of photons produced by the device, and $n_{electron\ input}$ is the number of electrons injected into the device. In case of OLEDs, the IQE is affected by three factors: the fraction of excitons that can decay radiatively — η_{ER} , the quantum yield of the light emitting material — η_{QY} , and the charge balance factor — η_{CB} . The IQE can thus be represented as the product of these terms

$$IQE = \eta_{ER} \cdot \eta_{QY} \cdot \eta_{CB} \quad \text{Equation 1.2}$$

The η_{ER} term depends solely on the emitter type. For fluorescent emitters, since only singlets can decay radiatively, η_{ER} is 0.25. For phosphorescent emitters, such as the ones used in simplified PHOLEDs, both singlets and triplets can undergo radiative relaxation, hence η_{ER} is 1. The η_{QY} term describes the percentage of singlet excitons that decays radiatively as opposed to through non-radiative mechanisms such as internal conversion. For state-of-the-art phosphorescent emitters, the quantum yield is usually close to unity [8]. Therefore, for simplified PHOLEDs, the only factor that requires optimization in order to maximize IQE is charge balance. The charge balance factor describes how efficiently the current is converted into excitons on the emitter and is determined by three factors: (a) the electron-to-hole (e/h) ratio; (b) how well charges are confined on the emitter; and (c) how well excitons are confined on the emitter. If the ratio between electrons and holes is not unity, leakage current of the carrier with larger numbers would occur. Similarly, leakage current can also arise if the charges are not confined on the emitter. Finally, if the excitons are not confined on the emitter, they may transfer into other materials and will not contribute to light emission from the emitter.

In general, the charge balance term can be optimized by changing the thickness of the hole and electron transport layers [21] and using p-doped and n-doped transport layers to balance the e/h ratio or, more commonly, by introducing charge and exciton blocking layers to confine both charges and excitons [10]. For example, Figure 1.7 presents an example device illustrating how all the factors can be optimized. Firstly, the HIL and EIL are introduced to facilitate hole and electron injection into the device. Secondly, the HTL and ETL with similar mobility for their respective carrier are chosen so that the e/h ratio can be kept close to unity. Thirdly, the EBL and HBL layers are used next to the EML to avoid electron and hole leakage. Finally, the EBL and HBL also have large bandgaps and high triplet energies so that the excitons are also confined on the EML to avoid exciton losses to adjacent layers.

1.2.2 Light Outcoupling

While IQE describes how efficient an OLED is at converting electrical current into photons, the more practical and arguably more important parameter that defines the efficacy of an OLED is its external quantum efficiency (EQE). The EQE is a parameter that characterizes the proficiency of an OLED at converting electrical current into photons that can be observed outside of the device. In

OLED, the photons are generated in the EML. Due to total internal reflection (TIR), some of the photons get trapped inside the device and cannot be extracted. The light outcoupling efficiency — $\eta_{light\ outcoupling}$, which specifies the ratio of photons that can be extracted versus all generated photons, relates to the EQE and IQE as follows:

$$EQE = IQE \times \eta_{light\ outcoupling} \quad \text{Equation 1.3}$$

Obviously, in order to maximize the EQE of an OLED, both the IQE and the light outcoupling efficiency need to be optimized. Unfortunately, the light outcoupling efficiency of OLEDs, which are point source emitters on flat substrates, is not inherently high. Figure 1.9 presents a common light outcoupling scheme. According to ray optics, usually 30% of produced light is trapped in the glass wave-guided mode, and 50% is trapped in the ITO/organic wave-guided mode via TIR. When light travels from medium A to medium B, if the refractive index of medium B is smaller than that of medium A, i.e. $n_B < n_A$, TIR would occur. In this case, only rays inside a cone defined by the critical angle can be transmitted. It is important to note that even if there are additional media between A and B, as long as none of them has a refractive index lower than n_B , the size of the cone remains the same [22]. The equation for calculating the critical angle is:

$$\theta_c = \sin^{-1} \frac{n_B}{n_A} \quad \text{Equation 1.4}$$

Assuming light emission is isotropic, the percentage of light within a cone can be presented as the ratio of the solid angle of the cone and that of a hemisphere (not a full sphere due to total reflections at the metal cathode), described as

$$1 - \cos \theta_c \quad \text{Equation 1.5}$$

Substituting Equation 1.4 into Equation 1.5 yields

$$1 - \sqrt{1 - \left(\frac{n_B}{n_A}\right)^2} \quad \text{Equation 1.6}$$

Generally, in OLEDs, the refractive index of the light emitting organic material is ~ 1.7 . Therefore, the total amount of light that can theoretically escape is

$$1 - \sqrt{1 - \left(\frac{1}{1.7}\right)^2} = \sim 20\%$$

There is one important assumption for the above analysis to be valid: the thickness of the EML needs to be sufficient for ray optics (i.e. the thickness of the EML needs to be much greater than the emission wavelength). However, in state-of-the-art PHOLEDs (including simplified PHOLEDs), the total thickness of the organic stack is around 100 nm, which is smaller than the wavelength of the light within the organic stack (i.e. ~ 310 nm for green emission in the organic stack with a refractive index of ~ 1.7). As a result, the wave-guided mode within the organic layers is suppressed [23]. Therefore, the predicted EQE using ray optics is an underestimate. The actual EQE limit when taking interference into consideration is around 30% [24]. Although this limit obtained by ray optics is not precise, the majority of light loss is still due to light trapped in the organic/ITO wave-guided mode and the glass wave-guided mode. Clearly, in order to increase the EQE of simplified PHOLEDs, the most effective way is to improve light extraction of these two wave-guided modes. The light trapped in the glass wave-guide mode can usually be partially extracted using roughened substrates [25], shaped substrates [22], [26]–[28] and micro-lenses [29]–[35]. The underlying mechanisms for these techniques are very similar. Figure 1.10 presents the working principle on how light extraction is achieved using a spherically shaped substrate. When the glass substrate is initially flat, light with an incident angle greater than the critical angle θ_c would experience TIR, and therefore be trapped within the glass substrate. However, when the spherical glass is attached to the flat substrate, light emitted from the emitter has a smaller incident angle when it arrives at the glass/air interface. The total amount of light that would be subjected to TIR is significantly reduced. As a result, more light is able to be extracted from the glass wave-guided mode. In general, techniques for extracting light at the glass/air interface are well developed and cost-effective.

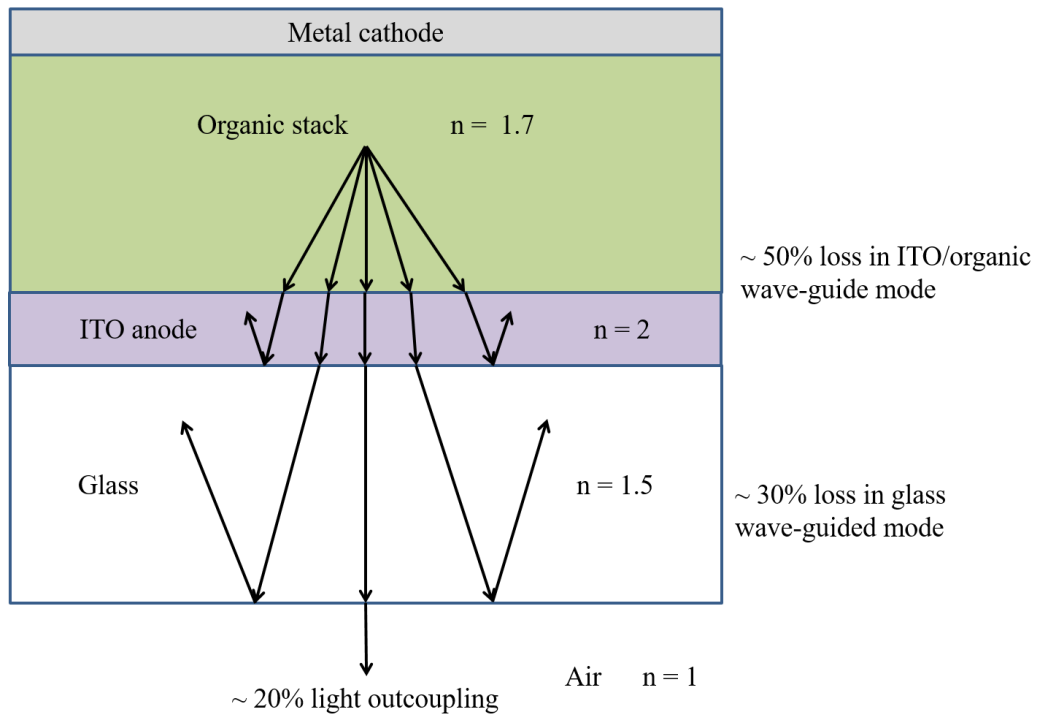


Figure 1.9 Light outcoupling scheme

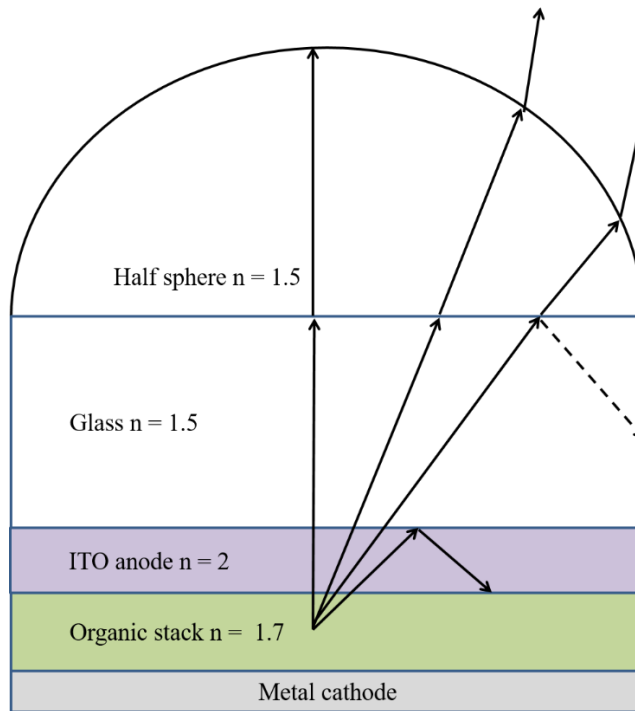


Figure 1.10 Light extraction working principle for shaped substrates

In contrast, the extraction of light trapped in the ITO/organic wave-guided mode (trapped due to the refractive index mismatch between ITO, i.e. ~ 2 and glass, i.e. 1.5) is more challenging. Numerous techniques have been developed to improve the light extraction so far. For example, a layer of low-refractive index silica aerogel with a refractive index of 1.03 can be placed between the ITO anode and the glass substrate to effectively double the light outcoupling efficiency [23]. Moreover, photonic crystal structures produced by nanoimprint lithography can be used to diffract light in the glass wave-guided mode to a direction that light can escape, thereby improving light outcoupling by a factor of 1.5 to 2 [36], [37]. Furthermore, a low-refractive index grid can also be inserted between the ITO anode and glass substrate to collimate light within the organic/ITO layers, thereby increasing the EQE by a factor of 2 [38]. Unfortunately, these techniques introduce additional complicated processing steps into OLED fabrication, and are therefore cost-extensive. More drastic solutions such as replacing the ITO anode with PEDOT:PSS [39] or using top-emitting device structure [40], [41] have shown devices with record-high efficiencies. However, these two approaches have their own limitations. Due to the acidic nature of PEDOT:PSS, OLEDs made on top generally have low stability [42]. On the other hand, encapsulating the top-emitting devices (to control ambient degradation) would re-introduce glass wave-guided mode within the encapsulation structure, thereby significantly reducing the light outcoupling of the top-emitting devices.

1.3 Device Stability

The relatively shorter lifetime of OLEDs (with lifetime usually defined as the amount of time it takes for the luminance of an OLED operating at a constant current to drop to 50% of its initial value) compared to other light-emitting technologies such as LCD and LED has been a major factor that has limited their competitiveness in consumer electronics since their invention. In general, the degradation mechanisms in OLEDs are usually categorized into ambient-induced and intrinsic. Ambient-induced degradation, characterized by the growth of non-emissive areas on the devices, is caused by cathode oxidation and delamination due to the presence of oxygen and moisture [43]–[45]. This process can be suppressed using encapsulation techniques [46], or by using materials that are less susceptible to ambient attack [47]. Currently, ambient-induced degradation of OLEDs fabricated on rigid substrates can be well controlled. However, devices made on flexible substrates are still prone to ambient-induced degradation due to insufficient encapsulation of the devices. Intrinsic degradation, on the other hand, is associated with a gradual decrease in device EL intensity over time. This decrease in device EL originates from phenomena that occur in the active organic materials, and

can happen through either physical or chemical means. Unlike ambient-induced degradation, suppressing intrinsic degradation still remains challenging, and therefore, continues to be an active research field in the OLED community. In general, the intrinsic degradation mechanisms can be classified into bulk material or interfacial depending on where they primarily occur.

1.3.1 Bulk Material Degradation Mechanisms

Up until recently, the intrinsic degradation of OLEDs has been mostly attributed to the degradation of the bulk materials. Several models of the mechanisms have been proposed. The most significant ones include: (1) the unstable cationic Alq₃ model [48], [49]; (2) exciton-induced chemical degradation model [50]–[54]; and (3) exciton polaron annihilation model [55], [56].

The ground-breaking work on uncovering intrinsic degradation in OLEDs was done on the most widely used fluorescent emitter – Alq₃. The operation mechanism in a generic NPB/Alq₃ (NPB is the HTL and Alq₃ is the ETL) device is similar to the one shown in Figure 1.2, where excitons are formed on Alq₃ due to a high density of holes and electrons in the ETL. By using photoluminescence (PL) spectroscopy, Aziz et al. discovered that the cationic Alq₃ species (i.e. positively charged Alq₃ molecules) form over time due to holes being injected into the ETL and can act as fluorescent quenchers [48]. As a result, the fluorescent decay rate for Alq₃ emitters, and hence their quantum yield decreases over time, leading to a gradual loss in device EL.

The exciton-induced chemical degradation model attributes the device EL degradation to chemical decomposition arising from materials being in the excited states (i.e. excitons). High-performance liquid chromatography [50] and laser desorption/ ionization time-of-flight mass spectrometry [52] techniques are used to detect the chemical changes in OLEDs before and after the devices have been subjected to extensive electrical driving. (Usually the device luminance is ~ 5% of the initial value after electrical driving.) In both techniques, the presence of new chemical compositions that are capable of quenching excitons has been detected in the degraded devices, suggesting that bond cleavage of organic materials occurs during OLED operation. It is also believed that the energy required for bond dissociation comes from the organic molecules being in the excited states.

Unlike the previous two models where either single charge carriers or excitons alone can produce exciton quenchers, the exciton polaron annihilation model suggests that the interaction between the host negative polaron (i.e. electrons on host molecules) and the guest triplet excitons results in faster device degradation, particularly in PHOLEDs only [56]. It is shown that when the host negative polaron and the guest triplet excitons are in close proximity to each other, the energy of the guest excitons can be transferred to the host molecules to form host excited polarons. The subsequent dissociation of the host molecules produces products that act as deep charge traps, and can therefore quench triplet excitons nearby.

1.3.2 Interfacial Degradation Mechanisms

Unlike the degradation of the bulk materials, degradation of the interfaces in OLEDs has not received much attention until recently. So far, it has been demonstrated that all three interfaces in OLEDs, namely, the ITO/organic [57], metal/organic [58]–[60] and organic/organic [61], [62] interfaces are all susceptible to degradation when excitons are present nearby.

1.3.2.1 Degradation at the ITO/organic Interface

Wang et al. show that the existence of excitons at the ITO/organic interface can result in a gradual loss in charge injection in fluorescent OLEDs [57]. The device structure in their studies is ITO/NPB (70 nm)/ Alq₃ (70 nm)/Mg:Ag (100 nm). The excitons at the ITO/organic interface are created by exposing OLEDs to external illumination that NPB absorbs. Untreated ITO, CF₄-plasma treated ITO, and ITO with 5 nm MoO₃ deposited on top are compared in their experiments. The changes in driving voltage over the illumination time of those devices are recorded. It is shown that the driving voltage of the untreated ITO increases most dramatically, indicating fast formation of a charge injection or transport barrier. On the other hand, when either CF₄-plasma treatment or MoO₃ is used at the ITO/organic interface, the change in driving voltage is significantly suppressed. Since the only difference among the three devices is the interface between ITO and NPB, the degradation is therefore concluded to be at this interface, and is related to hole injection. The authors suggest that the deterioration in hole injection is a result of loss of bonds between ITO and NPB, which is supported by the XPS data. When NPB is deposited on ITO, a new O-NPB bond is created, indicating bond formation between the oxygen in ITO and NPB. However, when the ITO/NPB interface is exposed to external illumination, this O-NPB bond intensity decreases, which is likely the reason for more difficult hole injection from the ITO into NPB. Finally, the authors show that similar degradation

trends in device driving voltage can also be observed in device EL stability. Considering that changes in hole injection would significantly alter charge balance, this correlation is not surprising.

The lifetime dependence on the ITO treatment is not specific to fluorescent OLED only. Gao et al. show that in a simplified PHOLED, when three different ITO treatments are used, namely, UV-ozone, UV-ozone + 1 nm InCl_3 and 1 nm CF_x , the devices exhibit very different lifetimes. Specifically, it is shown that coating the ITO anode with 1 nm InCl_3 or 1 nm CF_x can extend the lifetime of the simplified PHOLED by a factor of four [19].

1.3.2.2 Degradation at the Metal/organic Interface

Metal/organic interface in OLEDs has also been found to be susceptible to exciton induced degradation [58]–[60]. When excitons are present near the metal/organic interface, the adhesion between metal and the underneath organic layer is found to reduce over time. Similar to degradation at the ITO/organic interface, interfacial layers play an important role in affecting the lifetime of the device. According to Wang et al., LiF used in conjunction with aluminum cathode can effectively suppress this degradation [60].

1.3.2.3 Degradation at the Organic/organic Interface

Degradation at the organic/organic interface was first observed in fluorescent OLEDs [63], [64]. During device operation, defects that are capable of trapping holes are generated near the HTL/EML interface. It is known that these trapped charges can act as exciton quenchers, hence reduce the device EL. It is also possible that the trapped charges drive a chemical degradation process which results in byproducts that can quench excitons (similar to the aforementioned unstable cationic model). In either scenario, the root cause of the organic/organic interfacial degradation is attributed to the accumulation of positive charges or polarons.

In addition to polarons, there is usually a high concentration of excitons near the HTL/EML or EML/ETL (organic/organic in short) interface. Similar to the exciton polaron annihilation model, the interaction between host singlet excitons and host positive polarons can also lead to gradual loss in device EL over time reported by Wang et al. [61], [62]. In order to differentiate the influence of polarons only, excitons only and the interaction between the two on OLED stability, the authors compare the effects of exposing devices to each species and observe the change of driving voltage

over time. To allow only hole current inside a device, i.e. a hole-only device, the EIL in an OLED is replaced by a HIL that blocks electron injection from the cathode. Figure 1.11 presents the structures of an OLED and a hole-only device. Clearly, it can be seen that the only difference between an OLED and a hole-only device is the interfacial layer used at the metal/organic interface. The organic/organic interfaces remain the same in both devices. The benefit of using the hole-only device structure is that the effects of polarons only can be studied by simply running an electrical current through the device. Moreover, the effects of excitons alone can be tested by exposing the same hole-only device to external UV irradiation (at 365 nm where CBP absorbs). Finally, when the device is subjected to both constant current and UV irradiation, the effects of both polarons and excitons on the driving voltage can be observed. The results from Wang et al. clearly show that having polarons and excitons together near the organic/organic interface results in much faster voltage rise than the mathematical sum of polarons and excitons alone.

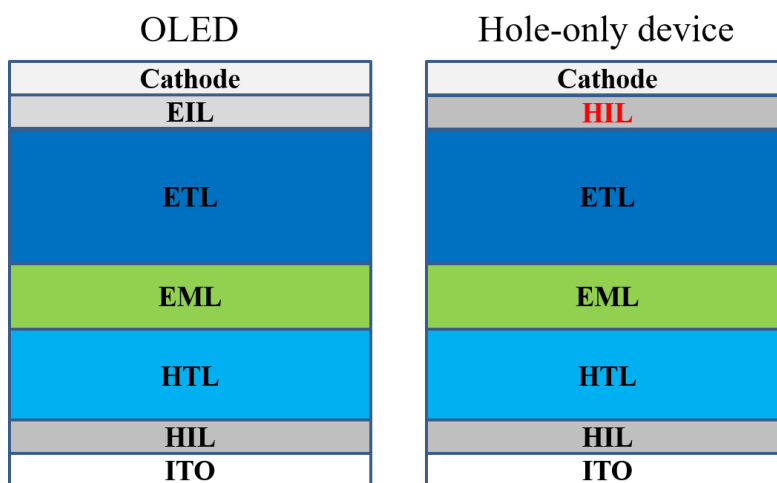


Figure 1.11 Device structures of an OLED and a hole-only device

In the case of simplified PHOLEDs, the mechanism for how the interaction between excitons and positive polarons occur is presented in Figure 1.12. When a simplified PHOLED is under operation, holes are injected from the ITO into CBP. Due to the HOMO level difference between CBP and TPBi, holes are accumulated at the CBP/TPBi (EML/ETL) interface. Similarly, electrons are injected from the Al cathode into TPBi, then into CBP. However, due to CBP being able to transport both holes and electrons efficiently, no electrons are accumulated at the CBP/TPBi interface. As a result, a net hole accumulation is formed nearby. In addition to having an

accumulation of holes, excitons are also formed near the CBP/TPBi interface. Therefore, the interaction between the holes and the excitons can occur and thus leads to the degradation of the interface. To understand how this exciton-polaron interaction degrades the interface (by either a physical or chemical process), a device with the CBP:Ir(ppy)₃ EML removed is studied. The structure for the device is ITO/MoO₃ (5 nm)/CBP (30 nm)/TPBi (30 nm)/LiF (0.5 nm)/Al (100 nm). It is important to point out that without the CBP:Ir(ppy)₃ layer, the excitons are then formed at the CBP/TPBi interface with hole accumulation nearby as well. Over the operation of this device, the authors are able to observe a drastic decrease in the intensity of the EL peak corresponding to the CBP emission, while also noticing a new peak emerging at 500 nm [62]. The change of EL spectrum is the signature of material aggregation, with the new peak at 500 nm being the aggregate band of CBP. Consequently, when CBP is used as the host material for the emitter in a simplified PHOLED, e.g. the device shown in Figure 1.12, the aggregation of the host material would then lead to the degradation of the device EL. Furthermore, the authors demonstrate a correlation between device EL lifetime and the rate by which this aggregation behavior occurs in a given host material [62]. Quite interestingly, the investigations also reveal a clear correlation between the rate of aggregation and the width of the energy band-gap of the material where materials with wider energy band-gap tend to aggregate faster. These new findings help explain, for the very first time, the generally lower stability of blue and other wide band-gap based OLEDs (i.e. PHOLEDs).

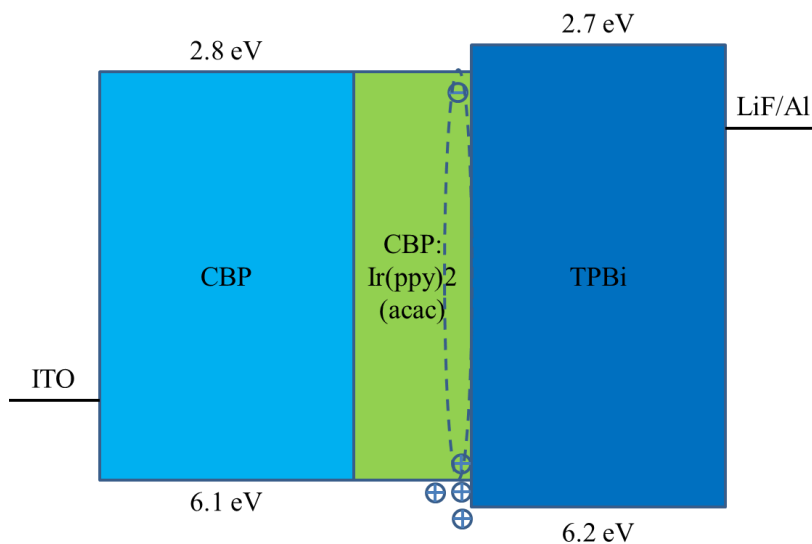


Figure 1.12 Scheme showing hole accumulation and their interactions with excitons near the CBP/TPBi interface in simplified PHOLEDs

1.4 Outstanding Issues Related to the Efficiency and Stability of Simplified PHOLEDs

Although simplified PHOLEDs with their simpler structure have the potential to achieve much lower fabrication cost while maintaining high efficiency, there are still a number of issues that need to be addressed in order to bring them towards utilization in commercial products.

In terms of efficiency, it has already been shown that in order to achieve high charge balance, and thus efficiency in PHOLEDs, multiple organic layers that can help confine charges and excitons to the EML are needed. As a result, most state-of-the-art devices comprise five or more organic layers. However, in a simplified PHOLED, where only three organic layers are employed, it is quite surprising that these devices showed record-high efficiency, especially without any electron blocking layer to confine electrons in the EML. It is therefore important to examine the extent of charge balance in simplified PHOLEDs.

In addition, since the extraction of light trapped in glass wave-guided mode can be easily achieved by using commercially available micro lens arrays, it is generally more demanding to find low-cost techniques that can extract light from ITO/organic wave-guided mode. One common technique that is used to improve light extraction from the ITO/organic wave-guided mode is to enhance light scattering at the ITO surface. Although several techniques have successfully shown improvement in light scattering, they are generally cost-extensive and require additional complicated fabrication steps. One possible economical way to increase light scattering at the ITO surface is to simply increase the ITO roughness. How effective this method can be therefore becomes an important question to investigate.

In terms of device stability, knowing that the lifetime of simplified PHOLEDs strongly depends on the interfacial layer between the ITO and CBP [19], and that excitons at the ITO/organic interface can lead to the degradation of hole injection, one question that immediately arises is whether the shorter lifetime in simplified PHOLED is related to the exciton-induced degradation at the ITO/organic interface. Furthermore, it is also important to understand how excitons are created nearby. By answering these two questions, the means of suppressing this degradation mode may be devised.

Finally, the lower stability of PHOLEDs that use wide bandgap emitters, especially blue, still remains a long standing problem that applies to all PHOLEDs, including the simplified one. It has been shown that the material aggregation phenomenon driven by the interaction of excitons and positive polarons is strongly correlated to the degradation of device EL, and that devices utilizing wide bandgap hosts are more prone to this degradation. However, one phenomenon that this theory still does not explain is why devices utilizing the same host material but different guest materials can sometimes have very different lifetimes [65]. In view of this phenomenon, a better understanding of the main factors governing device stability requires answering the following two questions (1) Is it the host or the guest that plays a more dominant role in governing device stability? (2) If the host plays a more dominant role, then how does the guest affect the stability of the host? Furthermore, knowing that the aggregation of the host material is a result of interactions of both excitons and polarons, it becomes important to find out the effects of reducing the exciton or polaron density near the organic/organic interface on device lifetime.

1.5 Research Objectives

This work aims to be the first scientific investigation directed towards simplified PHOLEDs, with the goal of unravelling the outstanding issues mentioned above. This work focuses on two aspects: device efficiency and stability. More specifically, the motivations of this work are to gain a better understanding of the underlying processes that govern the efficiency and stability of simplified PHOLEDs, and then to utilize this knowledge to try to improve the existing efficiency and lifetime. Towards this end, the following research objectives will be addressed:

- 1)** To investigate the factors governing the efficiency of simplified PHOLEDs and explore approaches to further increase it
 - a)** In consideration of the IQE
 - i)** Study the extent of charge balance in simplified PHOLEDs
 - ii)** If the charge balance is not optimal, explore approaches to further improve it
 - b)** In consideration of light outcoupling
 - i)** Examine the effects of increasing ITO roughness on light outcoupling efficiency
- 2)** To investigate the factors governing the stability of simplified PHOLEDs and explore approaches to further increase it
 - a)** In consideration of degradation at the ITO/organic interface

- i)** Study whether excitons near the ITO/organic interface are responsible for the shorter lifetime in simplified PHOLEDs
 - ii)** If the exciton-induced degradation at the ITO/organic interface is responsible, investigate the root cause for the existence of excitons nearby
 - iii)** Devise means to suppress this degradation mechanism
- b)** In consideration of degradation at the organic/organic interface
 - i)** Study whether the host or the guest plays a more dominant role in governing device stability
 - ii)** If it is the guest, investigate how the guest can affect the stability of the host
 - iii)** Examine whether reducing exciton or polaron density near the organic/organic interface can improve the lifetime of simplified PHOLEDs

Chapter 2

Methodology & Experimental Procedures

2.1 Methodology

In this work, investigations of the efficiency and stability of simplified PHOLEDs are performed purely through experiments. Although some theoretical models exist for describing each step of the operation of OLEDs (i.e. charge injection, charge transport, exciton formation and photon emission), the computation becomes increasingly complex when incorporating all four. Therefore, it is generally more straightforward and more accurate to study the underlying physics by comparing the performance of different devices.

In many of the experiments performed in this work, an archetypical simplified PHOLED with the structure ITO/MoO₃/CBP/CBP:Ir(ppy)₃/TPBi/LiF/Al is used. Compared with the common CF₄ treatment on ITO for improving hole injection, devices utilizing MoO₃ as the HIL generally have longer lifetime, and are therefore better suited for stability studies. CBP and TPBi are currently among some of the most widely used transport materials and are therefore chosen as the HTL and ETL, respectively. For the phosphorescent emitter, Ir(ppy)₃ and Ir(ppy)₂(acac) are the two most employed green dopants in the PHOLED community. Despite the fact that a device containing Ir(ppy)₂(acac) is slightly more efficient, a device that utilizes Ir(ppy)₃ has much longer lifetime, and is therefore more suitable for this work. Finally, due to being more resistant to exciton induced degradation at the metal/organic interface, LiF/Al cathodes are used.

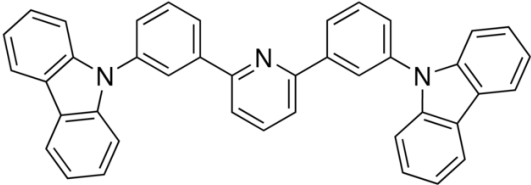
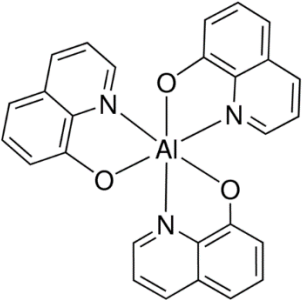
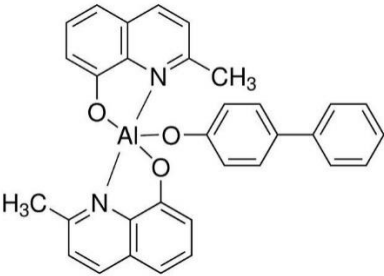
The performance of the devices in this work are evaluated in terms of efficiency and stability. To study device efficiency, current-voltage-luminance (IVL) measurements are used to characterize the optoelectrical properties of the devices by sweeping the applied voltage across them. The current response gives information about charge injection and transport, while the luminance response provides data for efficiency. In addition, the delayed EL technique is used to give insights into charge balance in simplified PHOLEDs. To study device stability, tests on device EL over time under both electrical driving (EL stability measurement) and external illumination (photo-stability measurement)

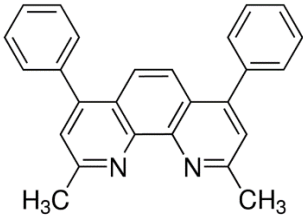
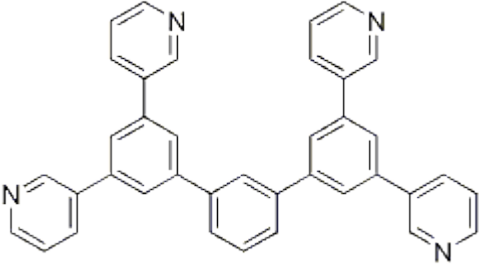
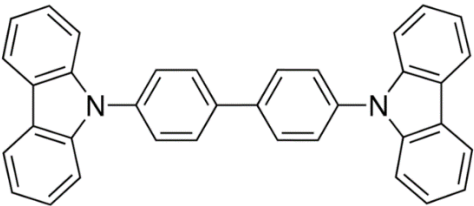
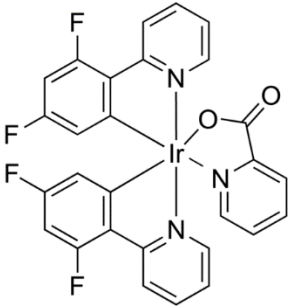
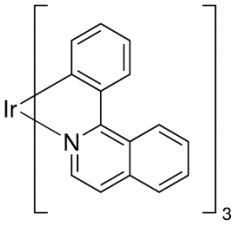
conditions are performed. Finally, in the cases where material comparisons are made, PL and exciton lifetime measurements on organic films are utilized.

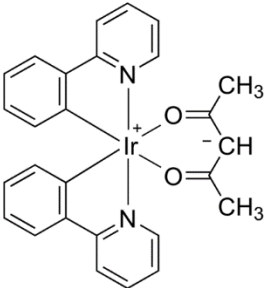
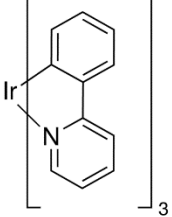
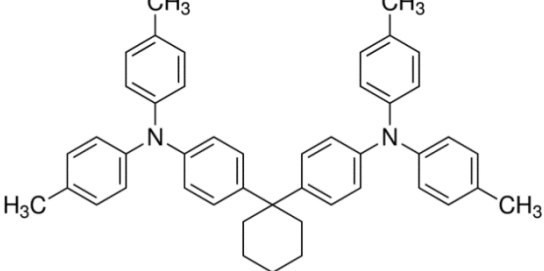
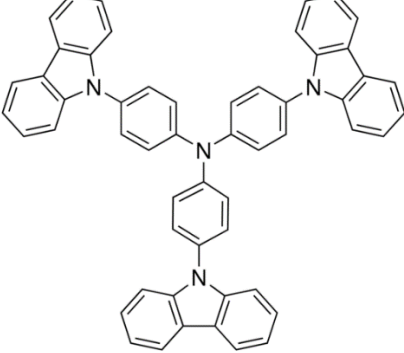
2.2 Material selection

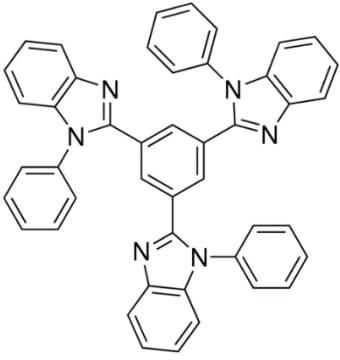
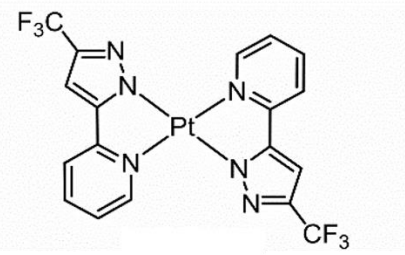
In addition to the typical CBP, TPBi and Ir(ppy)₃, many other organic materials are examined in order to study the device physics. These materials are listed in the table below along with their acronyms, structures and functionalities. All organic materials are obtained from either Luminescence Technology Corp. or HanFeng Chemicals and are used as received without any further sublimation.

Table 2.1 List of materials used in this thesis

Chemical names and acronyms	Chemical structures	Functions in OLEDs
2,6- bis[3-(carbazol-9-yl)phenyl] pyridine (26DCzPPy)		HTL and Host
Tris(8-hydroxy-quinolinato)aluminum (Alq3)		ETL
Bis(2-methyl-8-quinolinolate)-4-(phenylphenolato)aluminum (BALq)		ETL

2,9-dimethyl-4,7-diphenyl-1,10-phenanthroline (BCP)		ETL
1,3-Bis[3,5-di(pyridin-3-yl)phenyl]benzene (BmPyPhB)		ETL
4,4'-bis(carbazol-9-yl)biphenyl (CBP)		HTL and Host
Bis[2-(4,6-difluorophenyl)pyridinato-C ² ,N](picolinato)iridium (FIrpic)		Blue emitter
Tris(1-phenylisoquinoline)iridium (Ir(piq) ₃)		Red emitter

<p>Bis(2-phenylpyridine)(acetylacetonate) iridium(III) ($\text{Ir}(\text{ppy})_2(\text{acac})$)</p>		<p>Green emitter</p>
<p>Tris(2-phenylpyridine)iridium(III) ($\text{Ir}(\text{ppy})_3$)</p>		<p>Green emitter</p>
<p>Di-[4-(N,N -di-p -tolyl-amino)-phenyl]cyclohexane (TAPC)</p>		<p>HTL</p>
<p>4,4',4''-Tris(carbazol-9-yl)triphenylamine (TCTA)</p>		<p>HTL and Host</p>

<p>2,2',2''-(1,3,5-benzinetriyl)-tris(1-phenyl-1-H-benzimidazole) (TPBi)</p>		<p>ETL</p>
<p>Pt(II) bis(3-(trifluoromethyl)-5-(2-pyridyl)pyrazolate) (Pt(fppz)₂)</p>		<p>Red emitter</p>

2.3 Device Layout and Fabrication

All devices used in this thesis are fabricated on pre-patterned ITO-coated glass substrates. The ITO is 130 nm thick, and has a sheet resistance of $15\Omega/\square$, unless otherwise stated. The device layout is illustrated in Figure 2.1. There are usually 14 OLEDs on each substrate. The active area of each individual OLED is $2 \times 2 \text{ mm}^2$.

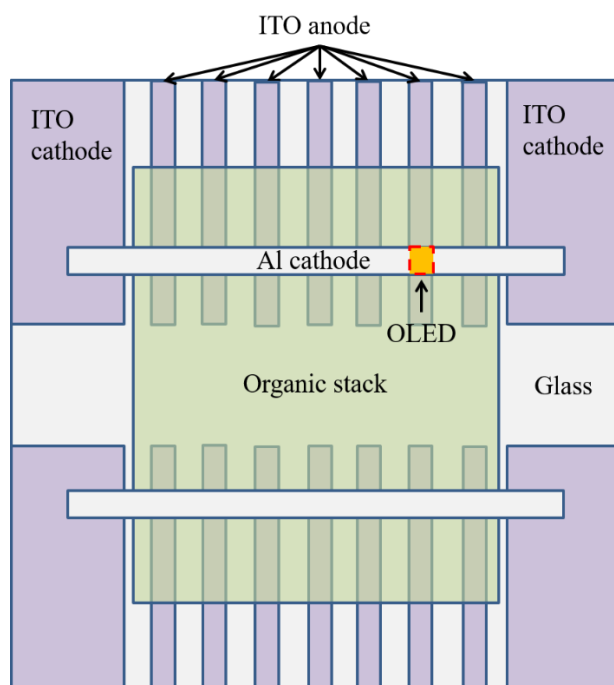


Figure 2.1 Device layout on the pre-patterned ITO substrate

Prior to device fabrication, the ITO substrates were sonicated in acetone and isopropanol for 5 minutes each in respective order. The substrates are then loaded into the vacuum chamber of the EvoVac system from Angstrom Engineering, where all materials are thermally evaporated at a rate of 0.1-2 Å/s at a base pressure of 5×10^{-6} torr. The rates of the evaporation are monitored using quartz crystals, and the thickness of the films are calibrated via a Dektak profilometer.

2.4 Device & Material Characterization

The characterization methods used in this work are described below. The devices are always kept in a N_2 environment during these measurements.

2.4.1 IVL Characteristics

The IVL characteristics of an OLED are measured using an Agilent 4155C semiconductor parameter analyzer with a 16442A test fixture. The driving voltage of the OLED is usually swept from 0 to 15 V while the current density through the device is recorded. Meanwhile, the luminance of the device is also recorded using a silicon diode. The luminance value is calibrated through a Minolta chroma meter cs-100.

2.4.2 EL Spectroscopy

The EL spectra of the OLEDs are acquired via an OceanOptics QE65000 spectrometer when the devices are electrically driven at 20 mA/cm².

2.4.3 Delayed EL Measurements

Delayed EL characteristics of the devices are measured using a home-built system from Xerox Research Center of Canada. The devices are driven using a square pulse driving scheme with a pulse width of 0.5 ms (the pulse is sufficiently long enough for prompt EL to reach its steady-state intensity). An optical shutter opens to collect delayed EL 0.3 ms after the end of the forward bias pulse, which is significantly longer than the lifetime of the triplet state of an Ir-based emitter (<1 μs) to ensure the absence of any contributions from prompt EL in the collected signal.

2.4.4 EL Stability Measurements

The EL stability of an OLED is measured using either a home-built system from Xerox Research Center of Canada or a commercial OLT lifetime test system from Botest. The device is electrically driven at either 40 mA/cm² alternating current with a duty cycle of 50% at a frequency of 100 Hz, or its equivalent of 20 mA/cm² DC. The change in EL and the driving voltage of the OLED are monitored by the testing system and plotted out as a function of time.

2.4.5 Photo-stability Measurements

The relationship between EL stability and exciton-induced degradation at the ITO/organic interface is studied using the photo-stability test. Excitons in the OLEDs are created by exposing the devices to light with a certain wavelength that can be absorbed by the organic material. A 200 W Hg lamp with an Oriel-77200 monochromator is used to create this light.

2.4.6 PL Spectroscopy

The PL spectra of organic films are obtained using an OceanOptics QE65000 spectrometer. A 200 W Hg lamp with an Oriel-77200 monochromator is utilized to excite the organic molecules to their S1 states.

2.4.7 Exciton Lifetime Measurements

The lifetime of excitons in organic films are measured using a FLSP920 spectrometer from Edinburgh Instruments.

Chapter 3

Charge Balance in Simplified PHOLEDs

The material presented in this chapter was published in Org. Electron., vol. 30, pp. 76–82, 2016. It is reproduced here with the permission from the publisher.

Simplified PHOLED, at the time of its introduction, exhibited record-high efficiency yet only employing three organic layers [17]. Without the additional charge carrier blocking layers, it is quite surprising for these simplified devices to have this high efficiency. Therefore, it is important to investigate the extent of charge balance and the factors that influence it in these devices.

Towards that end, this chapter addresses the charge balance question in simplified PHOLEDs. More particularly, the effects of altering charge balance in these devices are studied. This is done by means of changing the thickness of the charge transport layers or introducing charge traps in the transport layers. The results show that when using high carrier mobility charge transport materials, changing layer thickness does not impact charge balance appreciably. Therefore, unlike in conventional devices, this approach cannot be used for optimizing charge balance. Introducing charge traps in a thin layer within the HTL or ETL can, in comparison, influence charge balance more significantly, and proves to be a more effective approach for studying the factors limiting charge balance in these devices. The results reveal that simplified PHOLEDs are generally hole-rich, and that the leakage of electrons to the counter electrode is also a major mechanism behind the poor charge balance and efficiency loss in these devices. Finally, it is shown that by simply using an electron blocking HTL, the efficiency of the device can be enhanced by as much as 25%.

3.1 Limitations on Charge Balance

In order to test the extent of charge balance in simplified PHOLED and its dependence on the charge transport layer thickness, the effects of increasing the thickness of the HTL (CBP) in simplified PHOLED on device efficiency are first studied. The device structure used in this study is MoO_3 (5 nm)/CBP (x nm)/CBP:Ir(ppy)₃ (5%) (15 nm)/TPBi (45 nm)/LiF (1 nm)/Al (80 nm), where $x = 30, 60, 90, 120, 150, 180$ or 210. Figure 3.1 (a) shows the current density vs. voltage (J-V) characteristics of these devices. As expected, increasing the CBP thickness results in a shift in the characteristics to higher voltages. Despite the shift, the turn-on voltage is essentially the same for all

devices, indicating charge injection has not been altered. Figure 3.1 (b) shows the current efficiency of the devices at 100 cd/m^2 versus the CBP thickness. As can be seen, the efficiency trend exhibits an oscillating pattern. This curve is not different from the commonly observed microcavity effect trend that occurs when the ETL thickness is varied [66], [67], although with a much smaller oscillation amplitude (note the x axis does not cross y axis at 0 cd/A). This “weaker” microcavity can be attributed to the fact that light reflection at the ITO/organic interface is less than that at the organic/metal interface. This trend is however different from what is commonly observed in conventional fluorescent OLEDs (for example, one utilizing NPB and Alq₃ as HTL and ETL, respectively). In those devices increasing the HTL thickness generally leads to a monotonic (rather than an oscillating) change in efficiency as a result of the decrease in hole transport and the consequent increase in the electron-hole (e-h) ratio [21]. In contrast, in this experiment, despite the fact that driving voltage increases with the HTL thickness, indicating the charge balance also changes, such monotonic shift in current efficiency is not seen, and the trend is dominated by microcavity effects. For example, when the devices with 40 nm and 180 nm CBP are compared, with both representing nearly maximum constructive interference conditions, the current efficiency is almost the same. It is therefore reasonable to assume that charge balance does not change significantly even when the HTL thickness is increased by more than four times. Although the stark difference between the trend observed here versus that observed in conventional OLEDs [21] can at first glance appear surprising, when one considers that the hole mobility in CBP ($2 \times 10^{-3} \text{ cm}^2\text{V}^{-1}\text{s}^{-1}$ at the applied field of 0.5 MV/cm), is one order of magnitude higher than that in NPB ($1 \times 10^{-4} \text{ cm}^2\text{V}^{-1}\text{s}^{-1}$ at the applied field of 0.5 MV/cm) [68], [69], the much weaker effect of CBP thickness on charge balance becomes understandable.

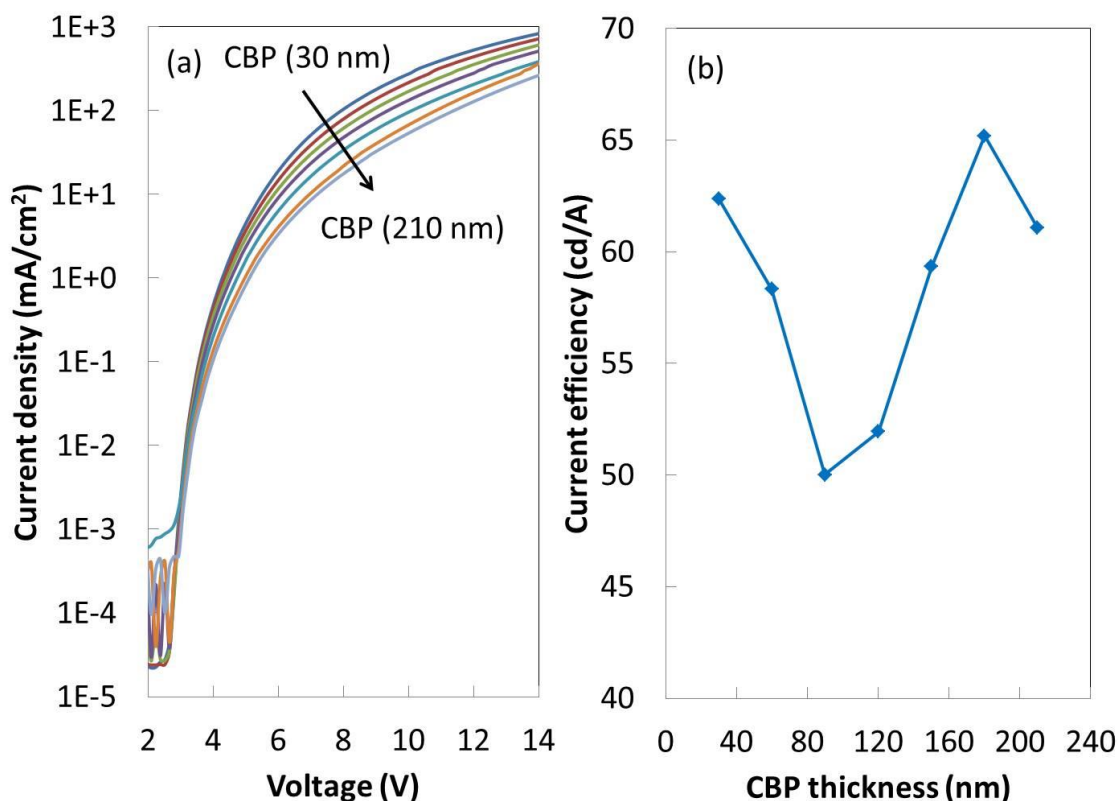


Figure 3.1 (a) Current density-voltage characteristics of devices with various CBP thickness. (b) Current efficiency vs. CBP thickness of these devices 100 cd/m².

Given the strong dependence of device current efficiency on microcavity effects, the traditional method of probing charge balance via monitoring device efficiency while varying layer thickness is clearly ineffective in devices utilizing high carrier-mobility materials. Therefore, for examining the factors influencing charge balance, a different technique is used: measuring device delayed EL. Delayed EL is the persistent EL that is emitted from a device after the end of the forward bias. In this technique, a device is driven using a square pulse with a pulse width of 0.5 ms (the pulse is sufficiently long enough for prompt EL to reach its steady-state intensity). An optical shutter opens to collect delayed EL 0.3 ms after the end of the forward bias pulse, which is significantly longer than the lifetime of Ir(ppy)₃ triplet state lifetime (<1 μs) and thus ensures the absence of any contributions from prompt EL in the collected signal. As such, any collected signal will arise from the radiative decay of excitons that are formed after the end of the forward bias pulse. A detailed description of the delayed EL measurement setup and signal detection protocol is reported elsewhere [70]. One common source of delayed EL is the recombination of charges that were initially trapped but get

released after the end of the forward bias pulse. In order to identify contributions by this mechanism to the observed delayed EL, a 0.5 ms reverse bias pulse (which produces a field of 0.74 MV/cm) is applied on the device during the delayed EL signal collection, and subsequent changes in delayed EL characteristics are monitored. Therefore, by comparing the delayed EL signal with and without the reverse bias for a given HTL thickness, the residual charge concentration, and thus the relative magnitude of charge balance, can be probed. Figure 3.2 shows the delayed EL signals from devices with 30 nm, 90 nm, 150 nm and 210 nm CBP under 0 and 0.74 MV/cm reverse electric field. It can be seen that in the absence of reverse bias, all devices show similar delayed EL. However, when the reverse electric field is applied, an initial spike as well as an unrecoverable loss in the delayed EL signal can be observed at the beginning and the end of the reverse bias pulse, respectively. Knowing that electron leakage from the EML to the HTL is significant in simplified PHOLED [71], the spike may be attributed to a fraction of the leaked electrons getting pulled back to the EML by the reverse field, that then recombines with residual holes in the EML and produce the delayed EL spike. In this case, the spike height would reflect the relative magnitude of the electron leakage current. From the figure, it can be seen that the spike height increases slightly from the device with 30 nm CBP to 150 nm CBP, which indicates a slight increase in electron leakage current when the HTL thickness is increased. Given that increasing the HTL thickness would necessarily hinder hole transport, and thus increases electron leakage current and, as a result, leads to a shift in the recombination zone away from the EML/ETL interface in the direction of the HTL/EML interface, it is not surprising to see the spike height increases with the CBP thickness. It is important to point out that a similar shift in recombination zone due to changing layer thickness was also observed by other groups [72]. Similarly, the un-recoverable loss in delayed EL can be attributed to holes and electrons that were originally trapped within the EML becoming swept away by the application of the reverse bias, resulting in a permanent loss in delayed EL. Knowing that the recombination zone shifts toward the HTL/EML interface when the HTL thickness is increased, it becomes apparent that the extraction of holes from the EML under a reverse bias also becomes easier in the devices with thicker HTL. Therefore, the un-recoverable loss in delayed EL increases with the CBP thickness monotonically, as can be seen from Figure 3.2. It is also important to point out that the initial spike height, which mirrors the magnitude of residual charges within the EML, is also affected by the un-recoverable loss. In the device with the thickest CBP (and thus the recombination zone is closest to the HTL/EML interface), the reverse bias is most effective in sweeping out the holes from the EML, resulting in the largest un-recoverable loss in delayed EL, as well as a loss in the initial spike. It is important to

emphasize that the changes in charge balance observed using delayed EL method are insignificant, evident from the negligible changes in device efficiency. Moreover, it is apparent that delayed EL is a sensitive technique for detecting small changes in charge balance without any influence from microcavity effects.

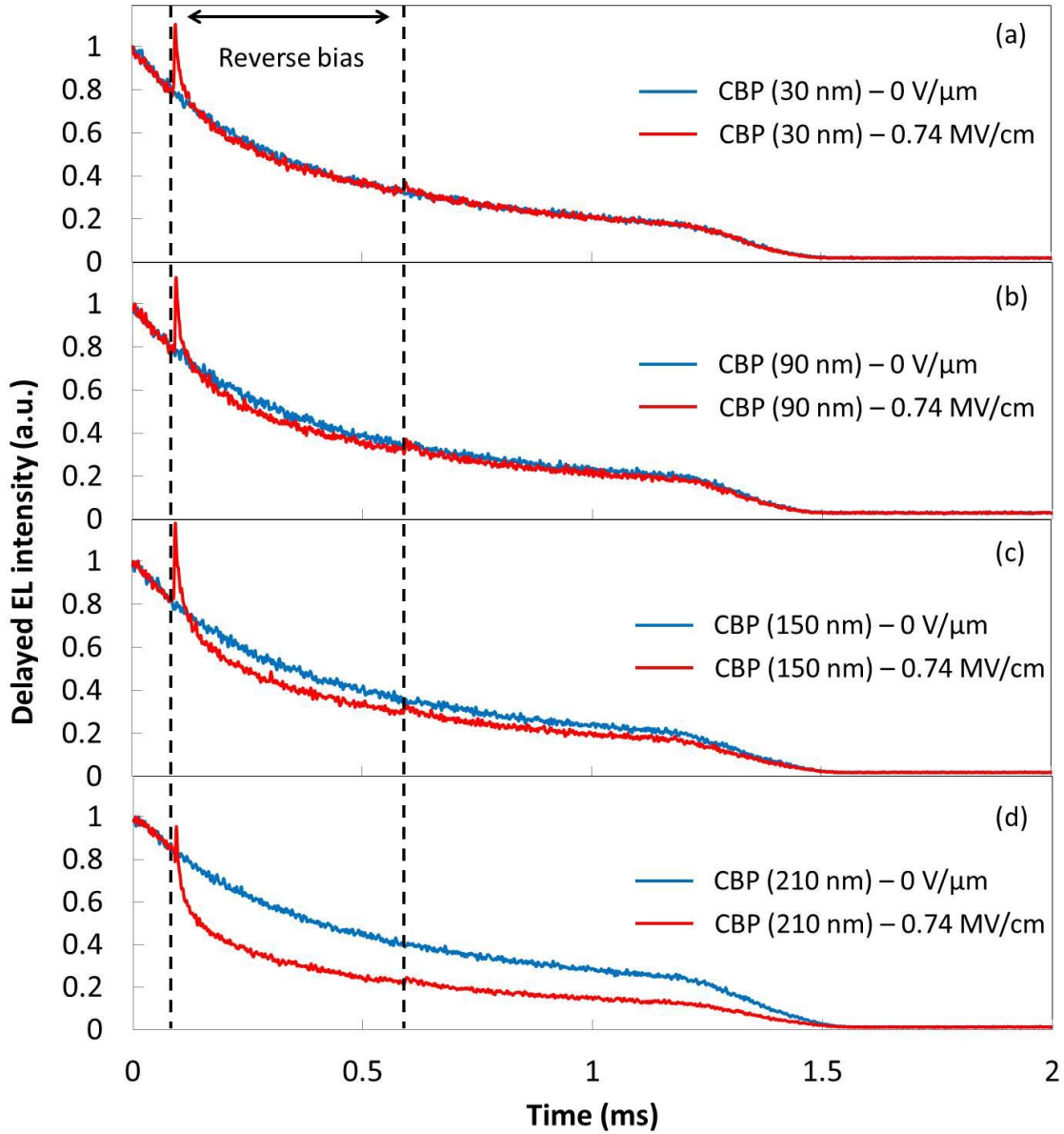


Figure 3.2 Delayed EL signals of devices with (a) 30 nm, (b) 90 nm, (c) 150 nm and (d) 210 nm CBP HTL under 0 and 0.74 MV/cm reverse electric field.

Similarly, the effects of changing the ETL (TPBi) thickness on charge balance are investigated. The device structure used is MoO₃ (5 nm)/CBP (30 nm)/ CBP:Ir(ppy)₃ (5%) (15 nm)/TPBi (x nm)/LiF (1 nm)/Al (80 nm), where x = 45, 70, 95, 120, 145, 170 and 195. Figure 3.3 (a) shows the J-V characteristics of these devices. It can be seen that increasing TPBi thickness results in a rise in driving voltage under the same current density, yet again leaving the turn-on voltage unaffected. Figure 3.3 (b) shows the current efficiency of these devices at 100 cd/m² versus TPBi thickness. Since TPBi is the layer that separates the EML from the reflective cathode, stronger microcavity effects in comparison to the previous case can be seen. Once again, due to the microcavity effects, the effect of the altered charge balance (due to the increase in TPBi thickness) on current efficiency cannot be observed. However, it is likely that the effect is once again not significant as evident from the similar efficiencies observed in devices with 45 nm TPBi and 170 nm TPBi. It is important to point out that the device with 195 nm TPBi is more efficient than that of the more commonly used 45 nm TPBi. This is because the EML is now sitting at the second antinode, which results in better light outcoupling [24]. Similar to the case when CBP layer thickness is increased, increasing TPBi layer thickness also does not seem to have a big impact on charge balance. This is again different from the case when the ETL in a traditional fluorescent OLED utilizing NPB and Alq₃ is altered, significant change in charge balance can be observed [21]. The reason is again related to the high electron mobility in TPBi ($4 \times 10^{-5} \text{ cm}^2\text{V}^{-1}\text{s}^{-1}$ at the applied field of 0.5 MV/cm), which is one order of magnitude higher than that in Alq₃ ($3 \times 10^{-6} \text{ cm}^2\text{V}^{-1}\text{s}^{-1}$ at the applied field of 0.5 MV/cm) [73], [74]. Therefore, the effects of changing TPBi thickness are not as dominant as the effects of changing Alq₃ thickness on charge balance.

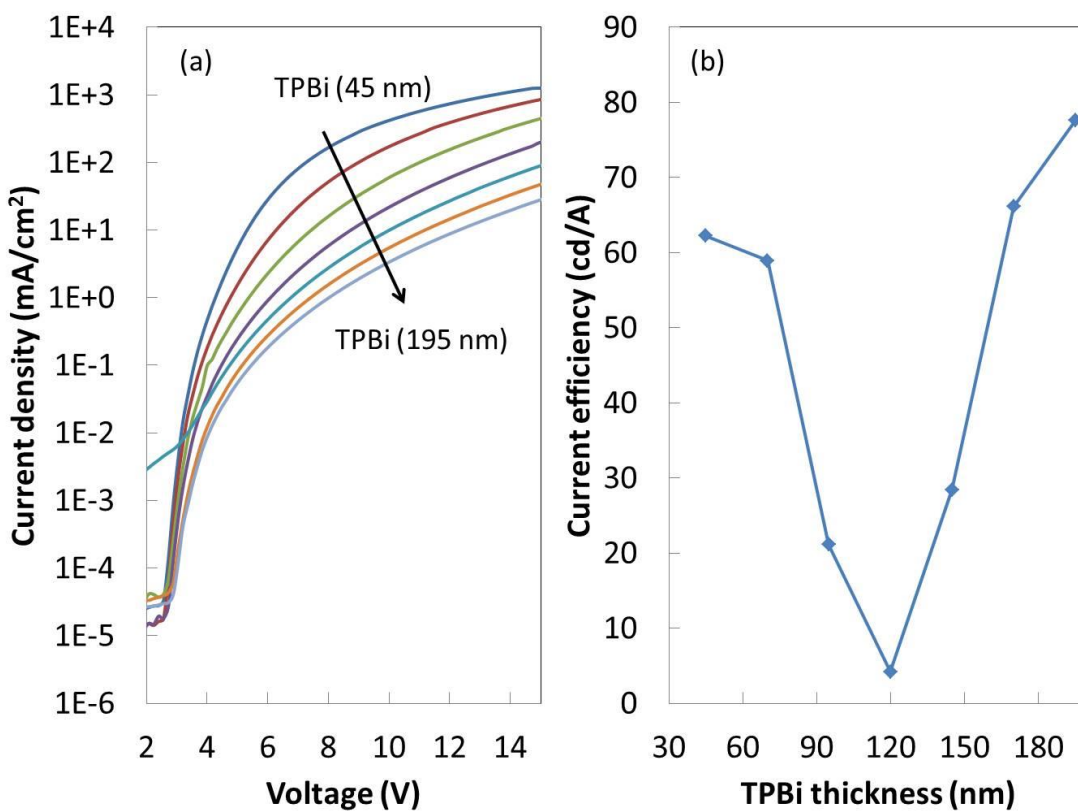


Figure 3.3 (a) Current density-voltage characteristics of devices with various TPBi thickness. (b) Current efficiency vs. TPBi thickness of these devices at 100 cd/m².

To examine how charge balance is changed by increasing TPBi thickness without being overshadowed by microcavity effects, delayed EL measurements are again used. Figure 3.4 shows the delayed EL signals of devices with various TPBi thickness (45, 95, 145 and 195 nm) under 0 and 0.83 MV/cm reverse electric field. It can be seen that the initial spike when the reverse bias is applied decreases slightly with increasing TPBi thickness, indicating a decrease in electron leakage current. Given that increasing the TPBi thickness would necessarily hinder electron transport (due to the longer electron travel path), the conclusion is not surprising. Furthermore, it can be seen that the devices with thick TPBi show a recoverable loss in delayed EL, rather than an un-recoverable loss, when a reverse bias is applied. The absence of the un-recoverable loss confirms that the recombination zone does not move when ETL thickness is increased. Since hole injection into TPBi is very difficult [75], the recombination zone does not shift with increasing TPBi thickness and thus remains at the EML/ETL interface. It can also be seen that as the TPBi gets thicker, the recoverable

loss in delayed EL increases, indicating an rise in triplet-triplet annihilation (TTA) [76]. This observation agrees with previous reports that increasing cavity thickness induces more TTA [67], [77].

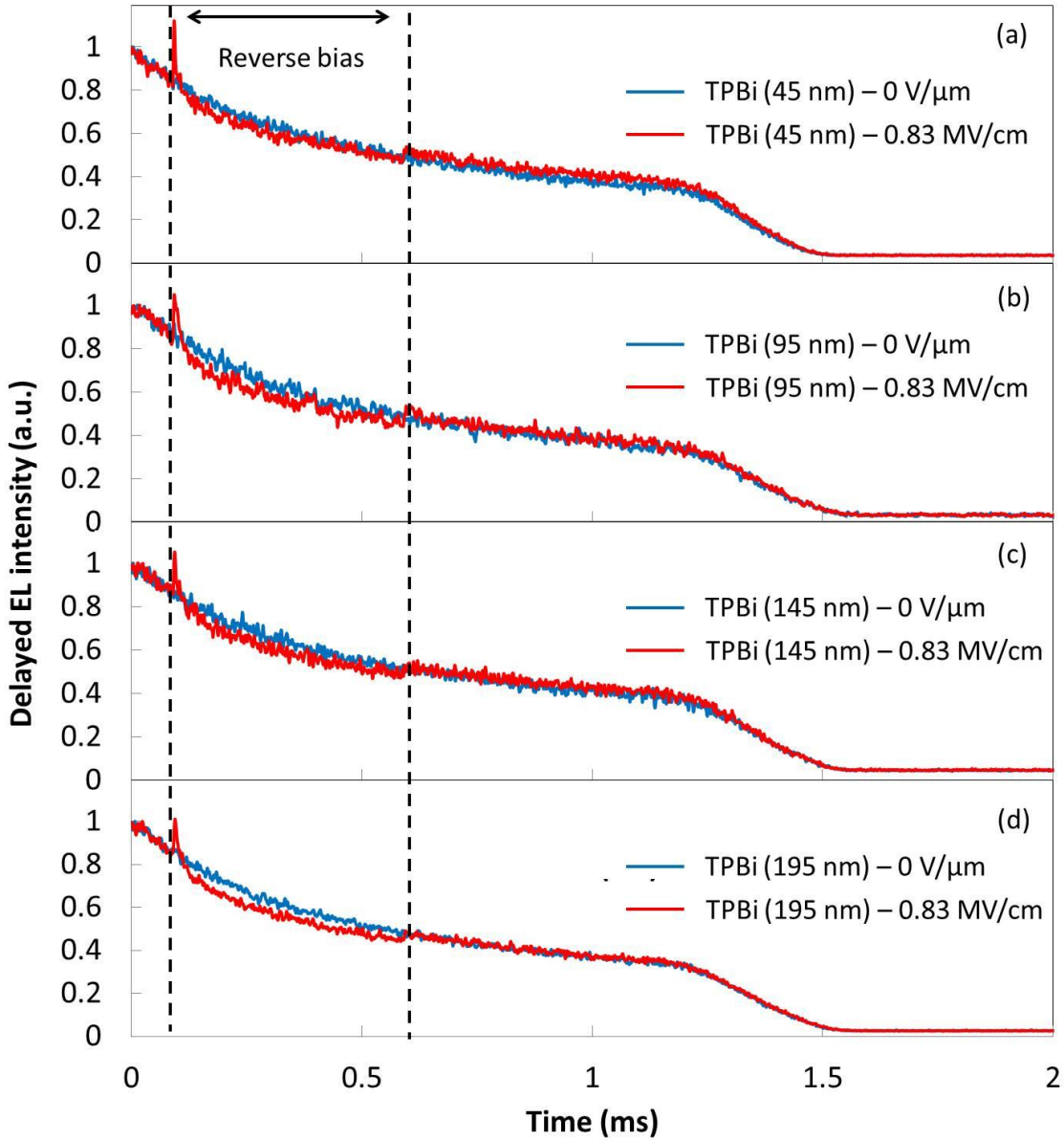


Figure 3.4 Delayed EL signals of devices with (a) 45 nm, (b) 95 nm, (c) 145 nm and (d) 195 nm TPBi ETL under 0 and 0.83 MV/cm reverse electric field.

Despite the fact that delayed EL is capable of probing how electron leakage current changes with the thickness of the hole and electron transport layers, the e-h ratio within the EML, which is the

quantity that most directly influences the charge balance factor, cannot be deduced using this technique. Therefore, in order to understand the effects of changing charge carrier transport on device current efficiency, an alternative approach that keeps microcavity effects unchanged must be used. One such approach is to introduce charge carrier traps within the transport layers without altering the layer thickness. First, the effects of introducing hole traps in the HTL are studied. Due to its shallower HOMO level than that of CBP, NPB can act as a hole trap when doped into CBP and therefore can be used for this purpose. The device structure used in this experiment is MoO₃ (5 nm)/CBP (10 nm)/CBP:NPB (x%) (5 nm)/CBP (165 nm)/CBP:Ir(ppy)₃ (5%) (15 nm)/TPBi (45 nm)/LiF (1 nm)/Al (80 nm), where x = 0, 0.08, 0.16, 0.32, 0.64 and 1. The CBP layer that separates the NPB doped layer and the EML is made sufficiently thicker than 16.8 nm, which is the exciton diffusion length in CBP [78], so that losses of excitons created in the EML to the NPB hole traps can be avoided. Moreover, it has recently been found that the presence of dopants near the EML/ETL interface can help electron injection [79]. By separating the NPB doped layer and the EML, such effect can be avoided. It is important to note that this device structure is significantly different from devices utilizing p-doped HTLs [10]. The thin layer of NPB doped CBP within the HTL serves to hinder hole transport, whereas in device with p-doped HTLs, the dopant is introduced to increase carrier concentration. Figure 3.5 (a) shows the J-V characteristics of the devices with various NPB concentrations. As expected, introducing the NPB results in a significant shift in the characteristics to lower currents, especially in the 5-15V range, consistent with trap-limited transport (e.g. the device with 1% NPB requires more than 5 V higher driving voltage than the device with 0% NPB at 100 mA/cm² current density). The subsequent fast rise in the characteristics in the 15-20V range can be attributed to the onset of trap-filling regime being approached. Clearly, as the NPB concentration increases, both the decrease in current and the subsequent rise become more pronounced, verifying the efficiency of NPB in trapping holes in CBP. Figure 3.5 (b) shows the current efficiency vs. current density characteristics of these devices. It can be seen that within the trap-limited regime (roughly from 0.1 to 10 mA/cm² current density), the device with more hole traps shows higher efficiency (i.e. more than 10% improvement with 1% NPB doping). This agrees with previous observations that the simplified PHOLED is hole-rich [80]. Thus, by impeding hole transport, charge balance, hence also efficiency, are improved. It is also important to note that in the trap-free regime, NPB containing devices show lower efficiency. This can be attributed to hole accumulation at the NPB trap sites which hinders hole transport significantly. As a result, the optimal charge balance is quickly lost at high currents, causing the efficiency to drop below that of the reference device. This suggests that the approach of

introducing traps for improving charge balance, and thus efficiency, may have limited benefits for practical applications. Nevertheless, the approach is clearly more useful relative to the more conventional approach of changing charge transport layer thicknesses for studying charge balance effects in these devices.

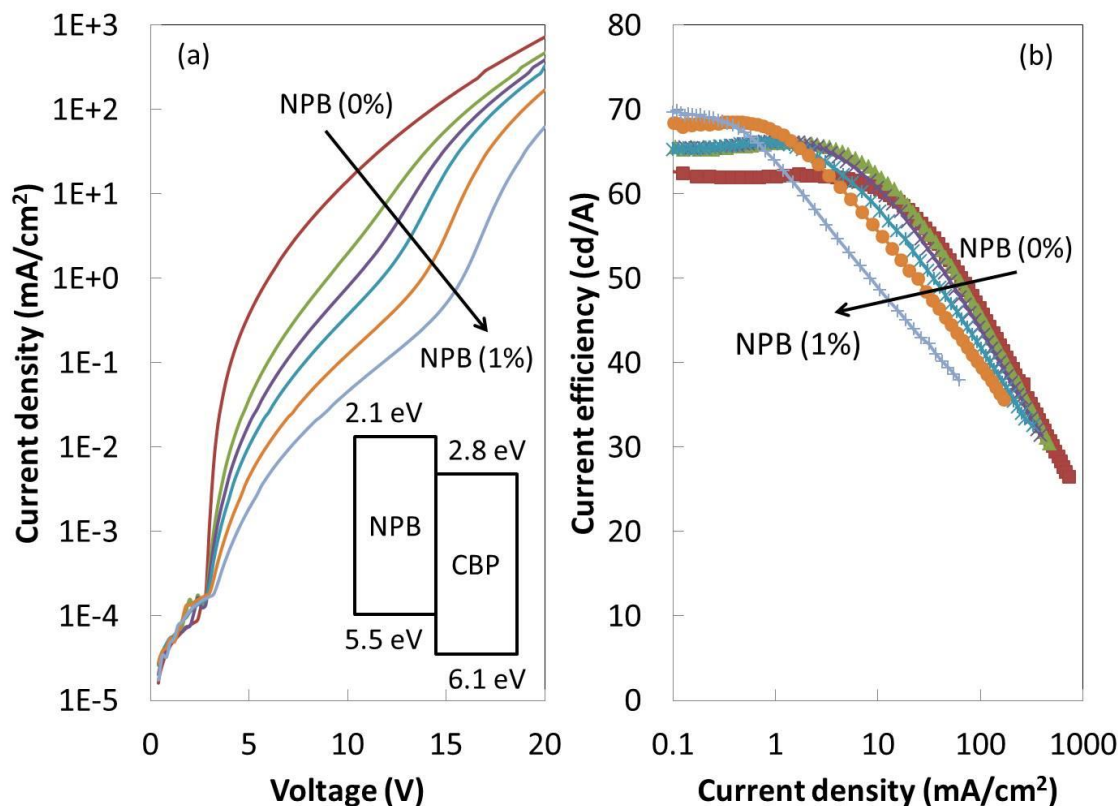


Figure 3.5 (a) Current density vs. voltage and (b) current efficiency vs. current density characteristics of devices with various NPB doping concentrations in the hole trapping layer. (a) Inset: energy level diagram for NPB and CPB.

Similarly, the effects of introducing electron traps in the ETL on device current efficiency are tested. Bphen is used as the trap due to its deeper LUMO level than that of TPBi. The device structure in this case is MoO₃ (5 nm)/CBP (30 nm)/CBP:Ir(ppy)₃ (5%) (15 nm)/TPBi (20 nm)/TPBi:Bphen (x%) (5 nm)/TPBi (20 nm)/LiF (1 nm)/Al (80 nm), where x = 0, 1, 2, 5, 10, 20 and 40. Figure 3.6 (a) presents the J-V characteristics of devices with various Bphen doping concentrations. Figure 3.6 (b) shows the current efficiency vs. current density of these devices. As expected, because the simplified

PHOLED is hole-rich, introducing electron traps in the ETL makes charge balance worse. Therefore, the device efficiency decreases as Bphen concentration increases. (Note: the change in J-V characteristics is not as significant as when NPB is introduced in CBP, perhaps due to a wider LUMO level distribution in Bphen that results in weaker electron trapping effect).

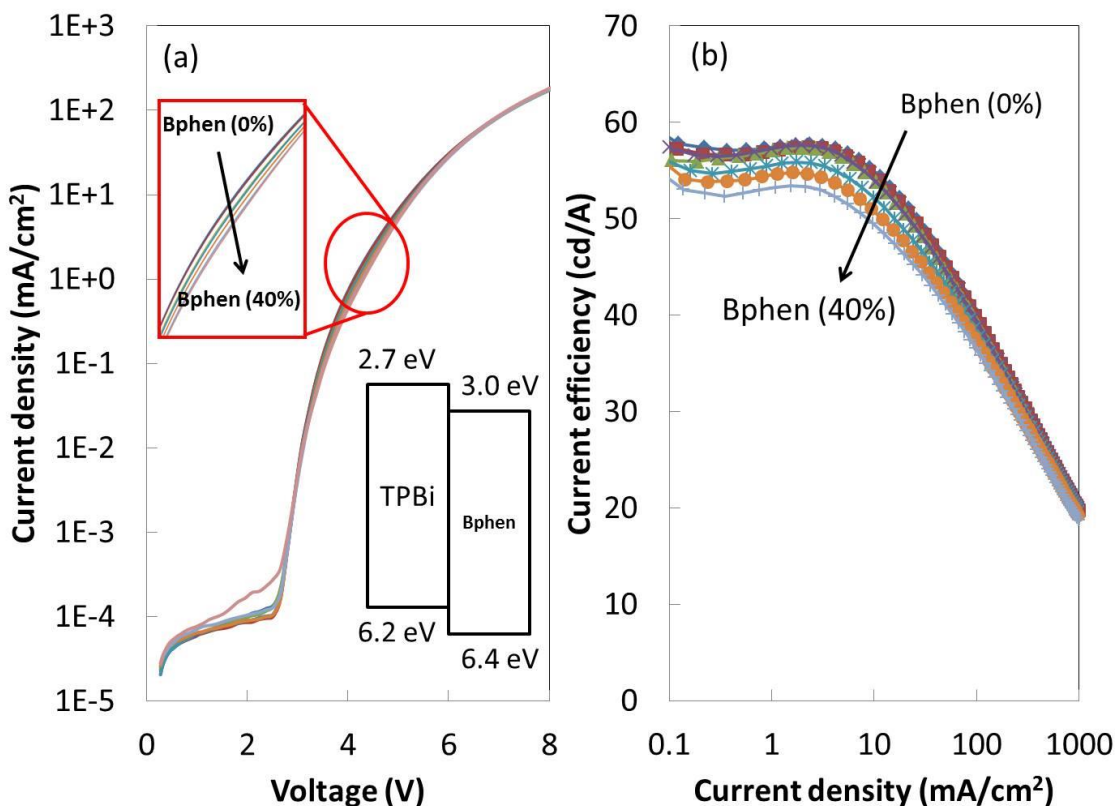


Figure 3.6 (a) Current density vs. voltage and (b) current efficiency vs. current density characteristics of devices with various Bphen doping concentrations in the electron trapping layer. (a) Inset: energy level diagram for TPBi and Bphen.

3.2 Approaches for Improving Charge Balance

Clearly, it can be seen that the simplified PHOLED architecture is generally hole-rich, and with non-optimal charge balance. As such, impeding hole transport would increase efficiency. However, due to the bi-polar transport nature of the HTL used, impeding hole transport would also result in an inevitable increase in electron leakage current. To overcome these two competing factors, a hole transport material that has a lower hole mobility than that of CBP, yet with negligible electron mobility (in order to effectively block electron leakage) would be beneficial for improving charge

balance and efficiency. TCTA is therefore chosen to be used as the HTL since it fulfills these conditions [69]. To illustrate the effectiveness of using such HTL on efficiency, four devices with the following HTL/EML structures are fabricated: A – CBP (30 nm)/CBP:Ir(ppy)₃ (5%) (15 nm); B - TCTA (30 nm)/TCTA:Ir(ppy)₃ (5%) (15 nm); C - TCTA (30 nm)/CBP:Ir(ppy)₃ (5%) (15 nm); and D - TCTA (30 nm)/CBP:Ir(ppy)₃(acac) (5%) (15 nm). Figure 3.7 shows the current efficiency vs. luminance characteristics of these devices. It can be seen that by simply replacing the CBP HTL with TCTA (device C vs. device A), the efficiency of the device can be increased by 25%. Using TCTA as both HTL and host instead of CBP, thus still keeping the number of organic materials limited to 3, a 10% enhancement in current efficiency can be achieved (device B vs. device A). Finally, replacing Ir(ppy)₃ with Ir(ppy)₂(acac) [18], the device efficiency improved by another 18% (device D vs. device C). This current efficiency represents the highest reported for a simplified PHOLED. Figure 3.8 presents the delayed EL signals of device D under 0 and 0.74 MV/cm reverse electric field. Unlike device A (shown in Figure 3.2 (a)), there is no observable spike at the start of the reverse bias, confirming that electron leakage in device D is minimal, and that good charge balance is achieved.

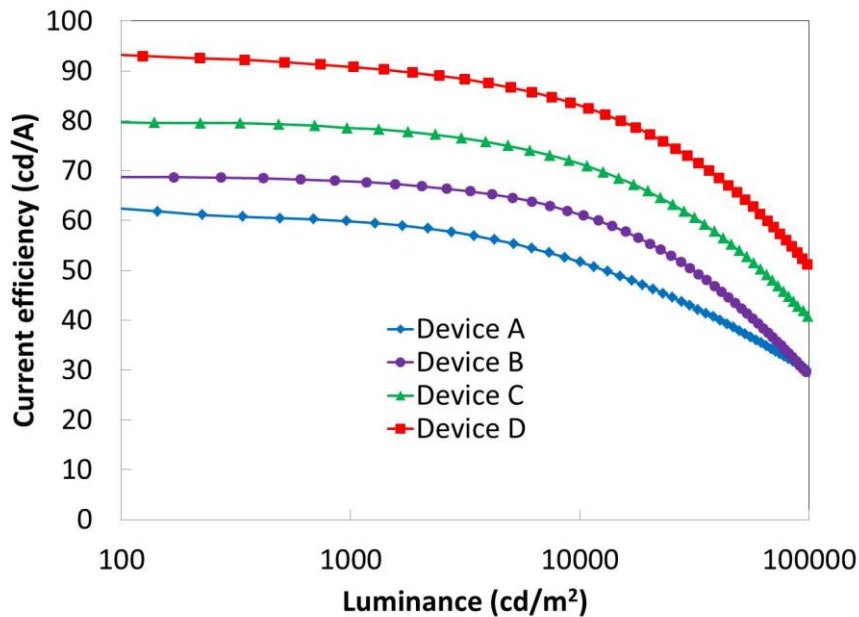


Figure 3.7 Current efficiency vs. luminance characteristics of devices with 45 nm BmPyPhB ETL and various HTL/EML structures: Device A – CBP (30 nm)/CBP:Ir(ppy)₃ (5%) (15 nm); Device B - TCTA (30 nm)/TCTA:Ir(ppy)₃ (5%) (15 nm); Device C - TCTA (30 nm)/CBP:Ir(ppy)₃ (5%) (15 nm); and Device D - TCTA (30 nm)/CBP:Ir(ppy)₃(acac) (5%) (15 nm).

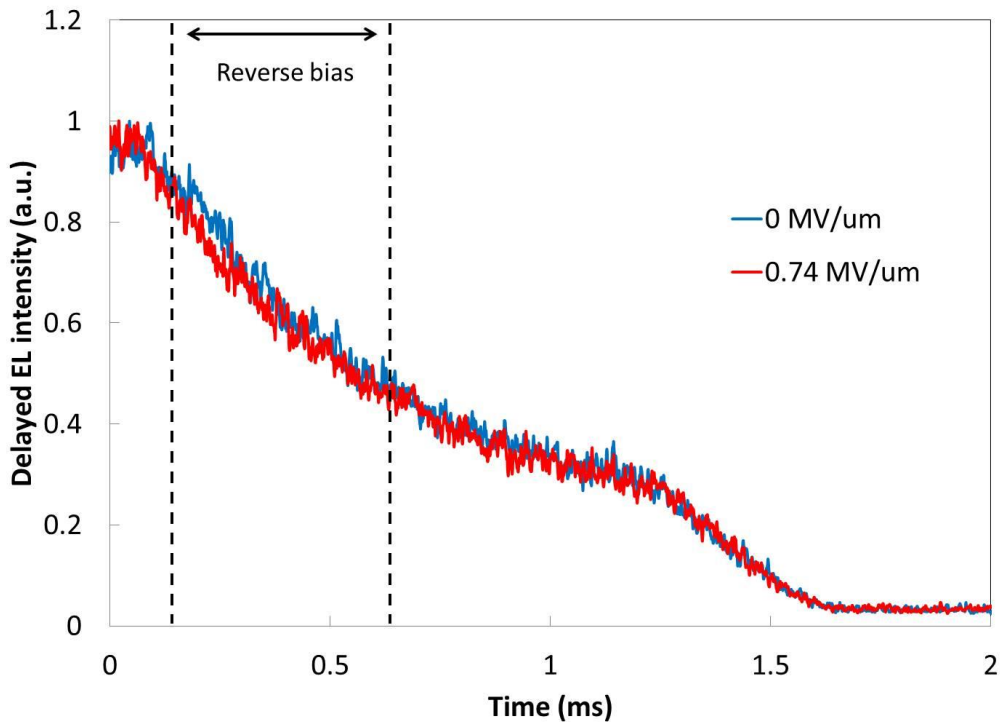


Figure 3.8 Delayed EL signals of device D under 0 and 0.74 MV/cm reverse electric field.

3.3 Conclusions

In summary, the charge balance limitations in simplified PHOLED is studied, particularly through means of changing layer thickness in the organic stack and doping hole and electron traps in the HTL and ETL, respectively. The results show that when using high carrier mobility charge transport materials, changing layer thickness does not impact charge balance appreciably. On the other hand, introducing charge traps in a thin layer within the HTL or ETL can, in comparison, influence charge balance more significantly, and proves to be a more effective approach for studying the factors limiting charge balance in these devices. The results reveal that simplified PHOLEDs are generally hole-rich, and that the leakage of electrons to the counter electrode is also a major mechanism behind the poor charge balance and efficiency loss in these devices. In order to optimize charge balance in simplified PHOLED, it is important to reduce hole transport in the device so that e^-/h^+ ratio can be brought closer to unity, as well as eliminate electron leakage. Finally, it is shown that by simply using an electron blocking HTL, the efficiency of the device can be enhanced by as much as 25%, representing the highest reported for simplified PHOLED.

Chapter 4

Light Outcoupling in Simplified PHOLEDs

The material presented in this chapter was published in Appl. Phys. Lett., vol. 105, no. 1, p. 013305, 2014 and Proc. SPIE 9566, Organic Light Emitting Materials and Devices XIX, 2015, vol. 9566, p. 95661R. It is reproduced here with the permission from the publishers.

In this chapter, two approaches that can increase the light outcoupling in simplified PHOLEDs are demonstrated. First, by increasing the roughness of the ITO, extraction of the light trapped in the ITO/organic wave-guided mode can be greatly improved. An efficiency enhancement of as much as 40% can be achieved when the ITO roughness is increased from 3.3 nm to 8.5 nm, without negative impact on device stability. Moreover, it is shown that changing the ITO thickness can alter OLED efficiency by 25%.

4.1 Approaches for Improving Light Outcoupling

To study the effect of ITO roughness on OLED efficiency, two types of substrates with the same ITO thickness (130 nm) but two different ITO roughness (root-mean-square, R_{rms}), 3.3 nm and 8.5 nm, denoted as ITO_{130/3.3} and ITO_{130/8.5}, respectively, are used. ITO_{130/3.3} is purchased from commercial vendors, whereas ITO_{130/8.5} is prepared by etching commercially available ITO_{150/3.3} in HCl:HNO₃:H₂O (10:1:10) solution for 3 minutes. Simplified PHOLEDs with the structure ITO/MoO₃ (5 nm)/CBP (25 nm)/CBP:Ir(ppy)₃ (5%) (15 nm)/TPBi (40 nm)/LiF (1 nm)/Al (80 nm) (shown in Figure 4.1 (a)) are then fabricated on these substrates and the efficiencies are compared. It is important to point out that although the work function and surface energy of the ITO could change after etching, [17], [81] the insertion of 5 nm MoO₃ anode interfacial layer would eliminate possible difference in charge injection. As can be seen in Figure 4.1 (b), both devices have very similar current-voltage characteristics, indicating that charge injection, hence also charge balance and IQE in both devices are very similar. However, the current efficiency vs. luminance characteristics presented in Figure 4.2 shows that the device made on the rougher ITO exhibits 40% higher efficiency than the device made on the smoother ITO. Considering that the only difference between the two devices is the surface roughness of the ITO, the difference in current efficiency (hence EQE) can be attributed to the ITO roughness, likely due to different extents of light outcoupling. AFM is used to examine the

morphological differences between the two ITO substrates. As can be seen in Figure 4.3, the smoother ITO (Figure 4.3 (a)) has the typical flake-like morphology [82]. The size of the flakes is ~ 500 nm. On the other hand, the rougher ITO (Figure 4.3 (b)) has high density of spikes of ~ 100 nm average size. One can expect that the spikes are able to act as light scattering centers, and thus to out scatter light trapped in the ITO/organic wave-guided mode more efficiently than the smoother flake-like ITO morphology. To test this hypothesis, intensities of OLED EL components that get trapped in wave-guided modes within the ITO and/or the organic stack but subsequently get out-scattered at the ITO/glass interface of other neighboring devices on the same glass substrate, and hence exit the substrate at the locations of these neighboring devices are compared. In order to test for this, an OLED is operated at a constant current to produce a luminance of 10^4 cd/m². The intensity of out-scattered light at neighboring devices (these devices themselves being under no electrical bias and therefore produce no EL themselves) is then measured. Figure 4.4 presents images of rows of OLEDs on two different substrates, ITO_{130/8.5} and ITO_{130/3.3} in the left and right images, respectively, showing this effect. In each case, only the device in the middle is under electrical bias and thus produces EL (the device itself is covered by black tape for enhancing contrast). The faint light observed at the neighboring devices is entirely due to out-scattering effect. The intensity of this out-scattered light is measured and recorded below the images for the corresponding locations, where the numbers represent the intensity in cd/m². It is clear that light extraction from the rougher ITO (ITO_{130/8.5}) is more than 10 times higher. This observation agrees with the notion that the rougher ITO enables higher light extraction.

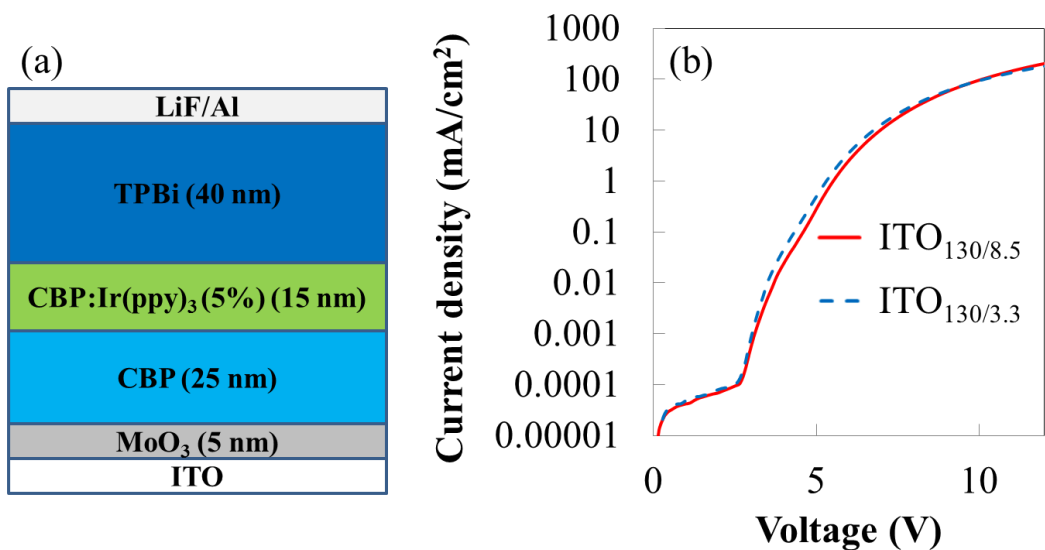


Figure 4.1 (a) Simplified PHOLED structure. (b) Current density vs. voltage characteristics of devices fabricated on ITO_{130/3.3} and ITO_{130/8.5}.

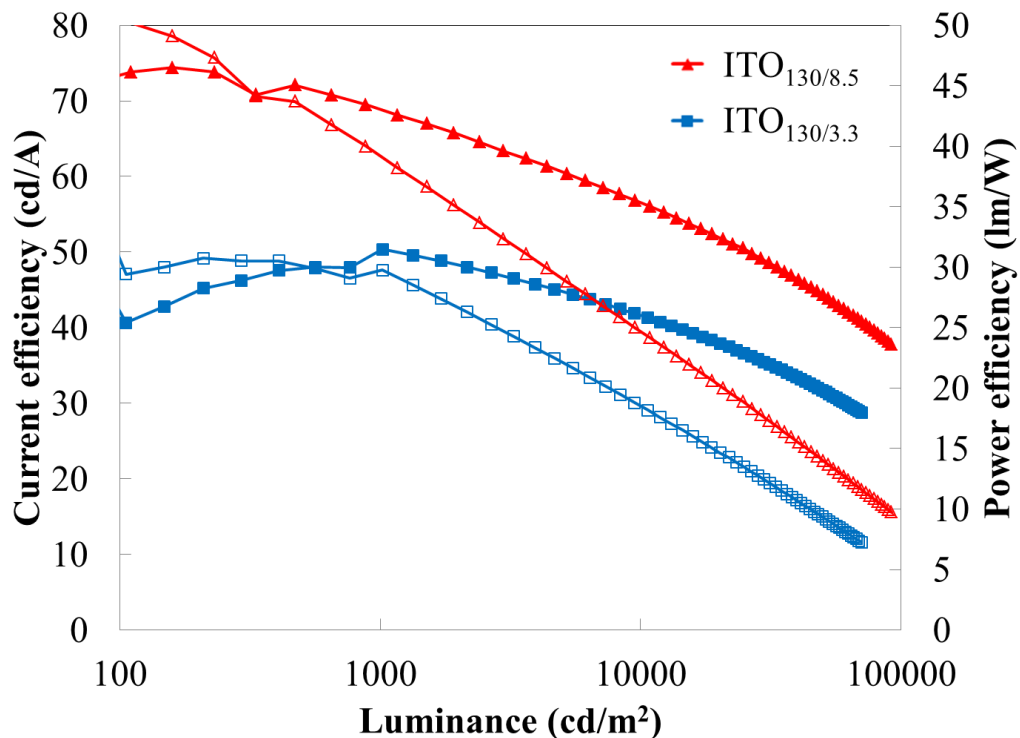


Figure 4.2 Current efficiency (solid symbols) and power efficiency (open symbols) vs. luminance of devices fabricated on ITO_{130/3.3} and ITO_{130/8.5}.

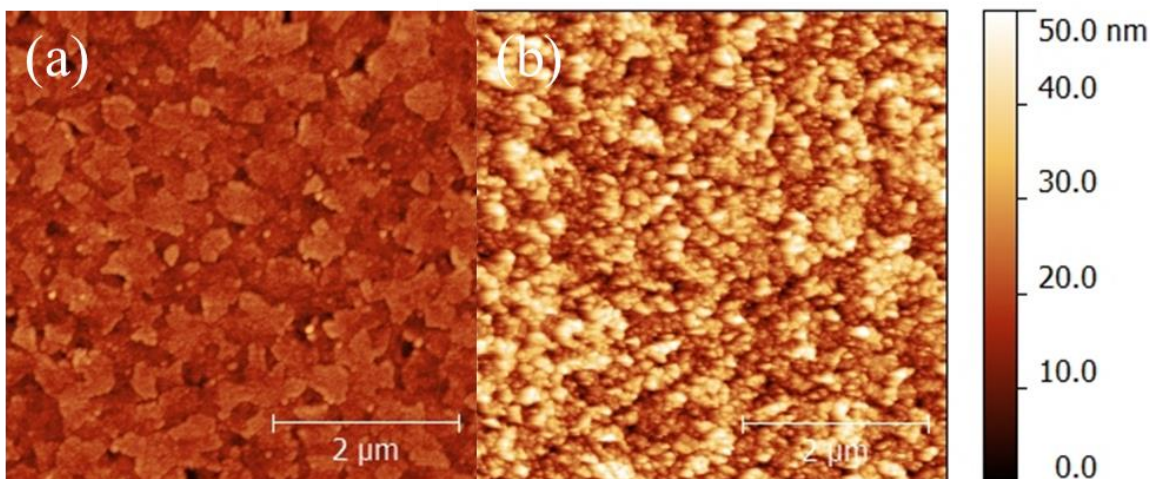


Figure 4.3 AFM images of (a) ITO_{130/3.3} and (b) ITO_{130/8.5}.

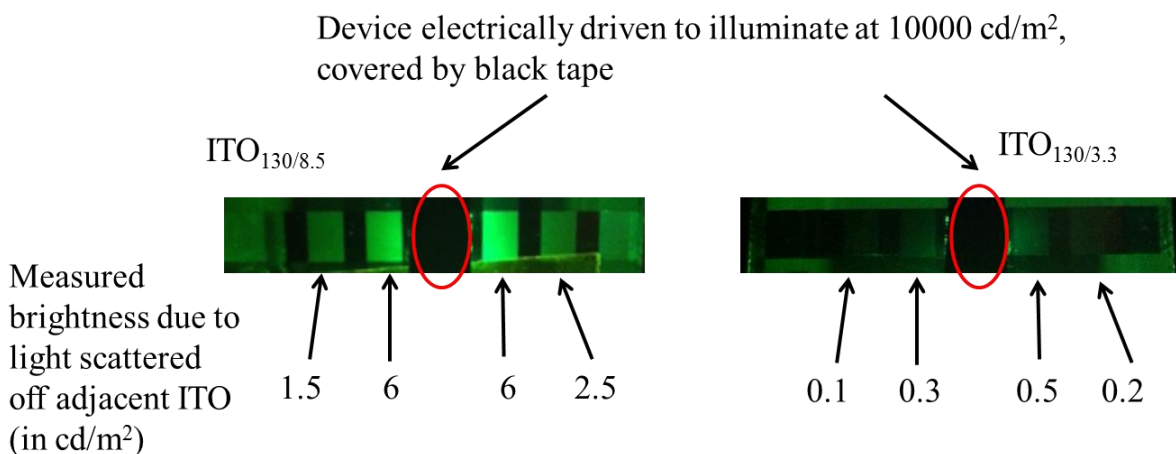


Figure 4.4 Measured brightness due to light scattered off the neighboring ITOs on ITO_{130/3.3} and ITO_{130/8.5}.

Finding that using rougher ITO improves OLED efficiency, a question about its effect on device stability naturally arises. The question is particularly important given the wide presumption in the community that increasing ITO roughness would increase morphological defects, hence expectedly results in a faster deterioration in EL efficiency with driving time (i.e. shorter device lifetime) due to the creation of “hot spots” [83], [84]. Therefore, the stability of devices made on ITO_{100/3.3} and ITO_{130/8.5} are compared. Figure 4.5 shows the changes in EL and driving voltage with

time under electrical bias to maintain a constant current flow of 20 mA/cm² current density. In this figure, the changes in EL are represented in the form of normalized luminance (luminance/initial luminance). The initial EL intensities of the devices are 8330 and 8820 cd/m² for devices made on ITO_{100/3.3} and ITO_{130/8.5}, respectively. As can be seen from the figures, both devices exhibit essentially identical trends, suggesting that the device lifetime is not altered by the change in ITO surface roughness. The morphologies of various layers of the two devices after each deposition step are also compared. Figure 4.6 presents the AFM images of the ITO_{130/3.3} and ITO_{130/8.5} substrates (Figure 4.6 (a) and (e), respectively), MoO₃ deposited on these substrates ((b) and (f)), CBP deposited on the previous layers ((c) and (g)), and the entire organic stacks ((d) and (h)). It can be seen that for both substrates, the surface morphology does not change much after MoO₃ deposition. However, after the CBP layer is deposited, the surface becomes significantly smoother. Particularly, in the case of ITO_{130/8.5}, the surface roughness is reduced from 7.5 nm (Figure 4.6 (f)) to 4.4 nm (Figure 4.6 (g)) and the peak-to-valley roughness (R_{pv}) decreased from 61 nm to 30 nm. More importantly, after the entire device fabrication, both R_{rms} and R_{pv} remain the same (Figure 4.6 (h)). This indicates that the spikes from the ITO substrate are fully covered by the CBP organic layer, and do not penetrate into the other organic layers. Considering that the thickness of the CBP layer accounts for only 30% of the thickness of the entire organic stack, it is therefore unlikely for the rougher ITO_{130/8.5} to cause shorting in the devices. This perhaps explains the similar stability trends of the two devices in Figure 4.5.

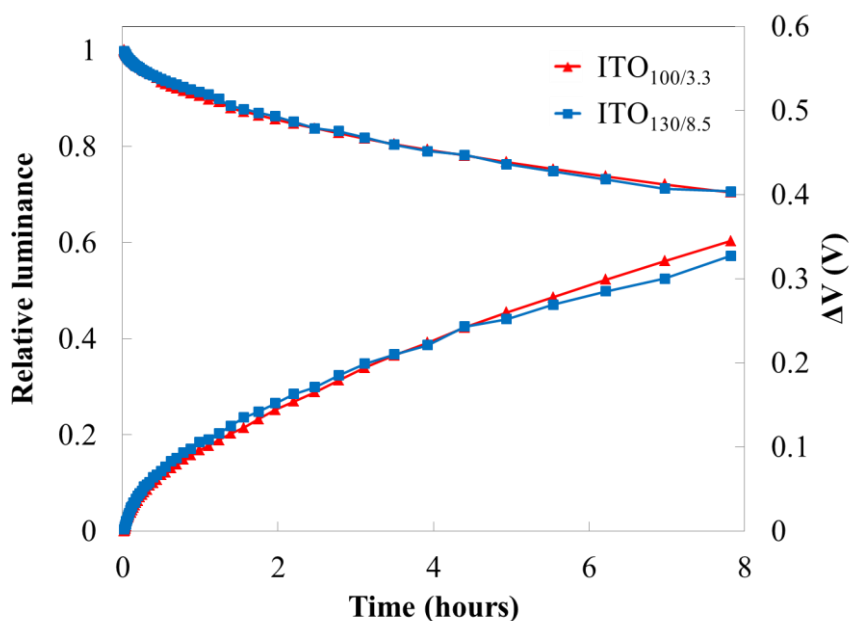


Figure 4.5 Changes in EL and driving voltage with time under 20 mA/cm² current density for devices fabricated on ITO_{130/3.3} and ITO_{130/8.5}.

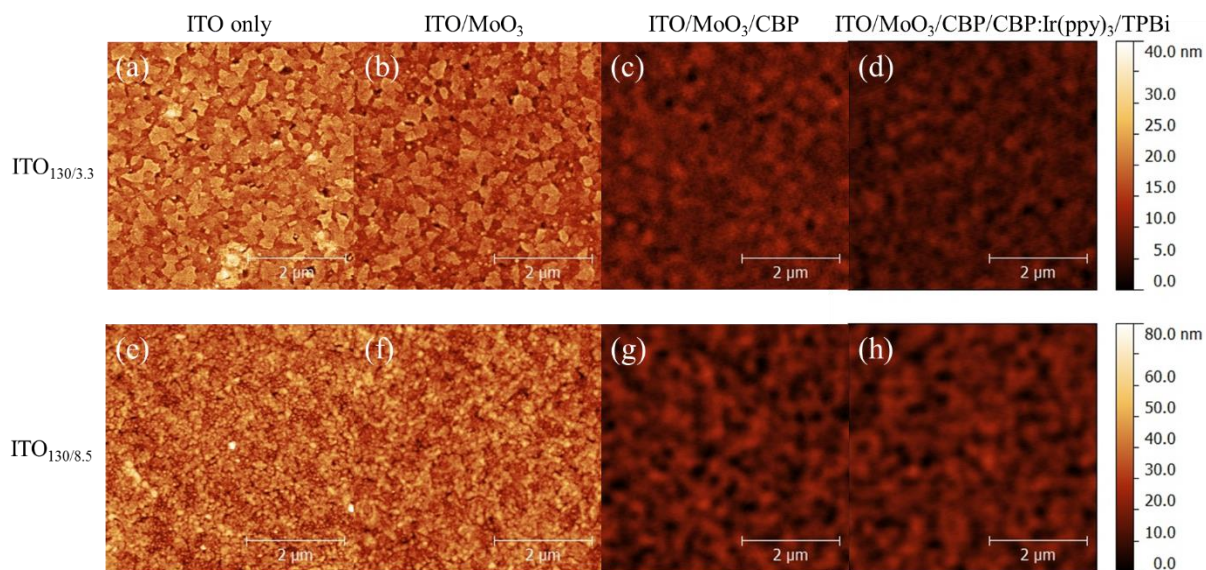


Figure 4.6 AFM images of (a) ITO_{130/3.3}, (b) MoO₃ on ITO_{130/3.3}, (c) CBP on MoO₃ and ITO_{130/3.3}, (d) entire organic stack on ITO_{130/3.3}, (e) ITO_{130/8.5}, (f) MoO₃ on ITO_{130/8.5}, (g) CBP on MoO₃ and ITO_{130/8.5} and (h) entire organic stack on ITO_{130/8.5}. Notice the difference in color scale.

It is important to point out that the increase in light extraction by increasing ITO roughness is also influenced by the ITO thickness. For example, when using thinner ITO, only 100 nm thick instead of 130 nm thick, increasing the ITO roughness from 3.3 nm to 9.9 nm brings about an increase in efficiency of only 10%, as shown in Figure 4.7, smaller than the difference observed for the thicker ITO. Since it has been simulated by Kim et al. [24] that light outcoupling strongly depends on ITO thickness due to optical interference of reflected light within the ITO layer, the transmittance of the ITO substrates, which are directly affected by interference, are then used to further examine the difference between the smooth and the rough ITO. Figure 4.8 presents the transmittance of the four used ITO substrates, $ITO_{130/3.3}$, $ITO_{130/8.5}$, $ITO_{100/3.3}$ and $ITO_{100/9.9}$. It is clear that the transmittance of the ITO is changed when the ITO roughness is increased. Therefore, the improvement in device efficiency when using rougher ITO comes from both more efficient light scattering and changes in optical interference. Light scattering when using rougher ITO is always more efficient, however, on the other hand, changes in optical interference can have a negative impact on light outcoupling. As a result, the efficiency improvement when using $ITO_{130/8.5}$ over $ITO_{130/3.3}$ is more pronounced than when $ITO_{100/9.9}$ is used over $ITO_{100/3.3}$.

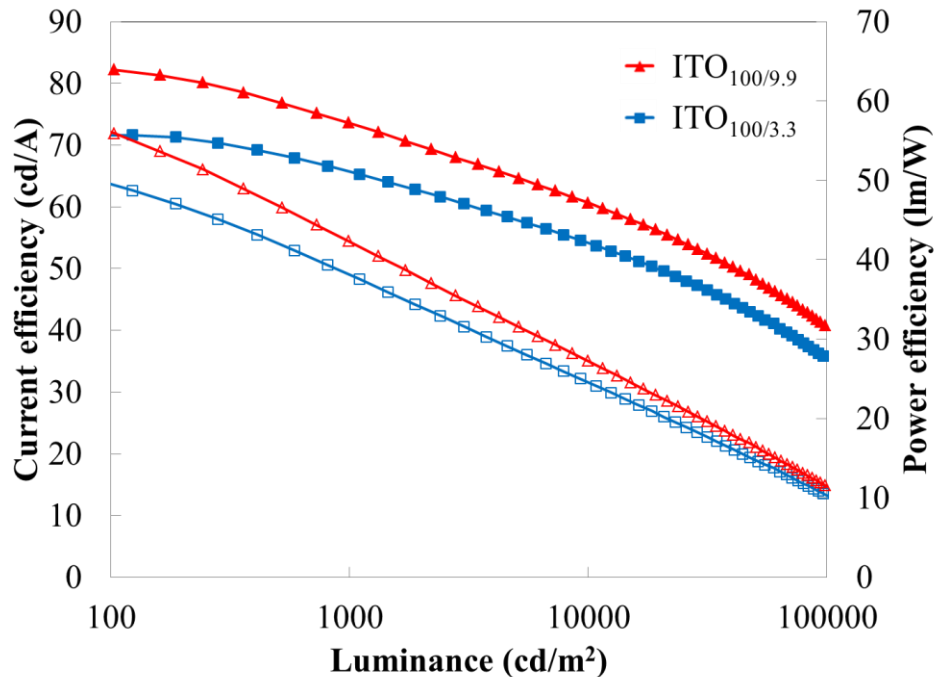


Figure 4.7 Current efficiency (solid symbols) and power efficiency (open symbols) vs. luminance characteristics of devices fabricated on $ITO_{100/3.3}$ and $ITO_{100/9.9}$.

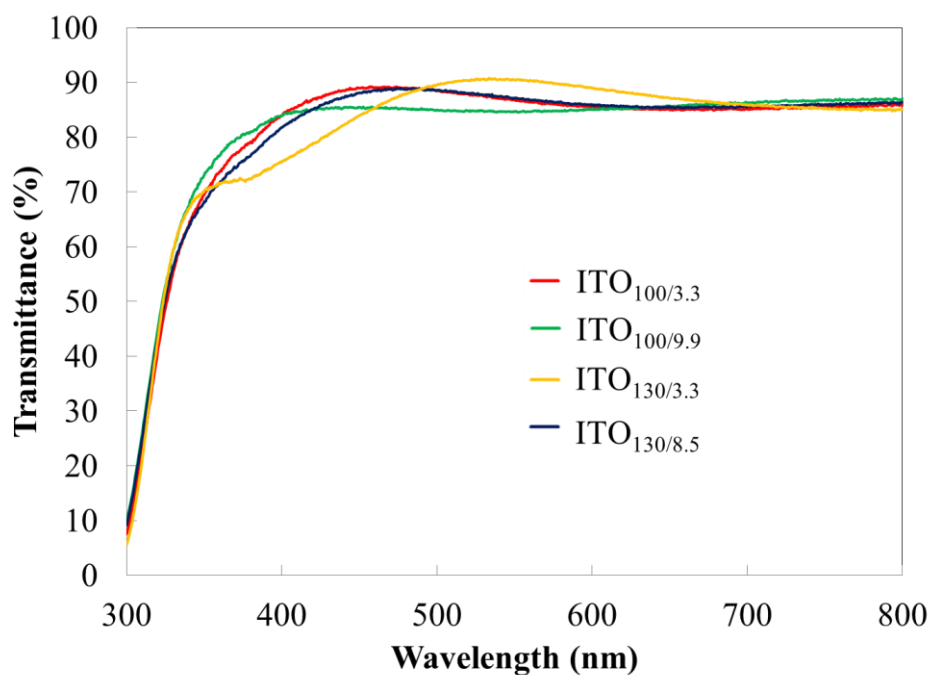


Figure 4.8 Transmittance of ITO_{100/3.3}, ITO_{100/9.9}, ITO_{130/3.3} and ITO_{130/8.5} substrates.

Next, ITO_{130/3.3} and ITO_{130/8.5} are utilized in OLEDs of the structure ITO/26DCzPPy (5 nm)/CBP (25 nm)/CBP: Ir(ppy)₂(acac) (8%) (15 nm)/BmPyPhB (30 nm)/LiF (1 nm)/Al (80 nm), as shown in Figure 4.9 inset. In these device, 26DCzPPy, Ir(ppy)₂(acac) and BmPyPhB replace MoO₃, Ir(ppy)₃ and TPBi used in the original structure in order to optimize efficiency. The current efficiency vs. luminance characteristics of the devices are shown in Figure 4.9. Once again, it can be seen that the device made on the rougher ITO is 40% more efficient, exhibiting very high efficiency at a remarkably high brightness, demonstrating 56 cd/A at 10⁵ cd/m². This represents the highest efficiency at such high brightness to date for an OLED utilizing an ITO anode without external light outcoupling techniques.

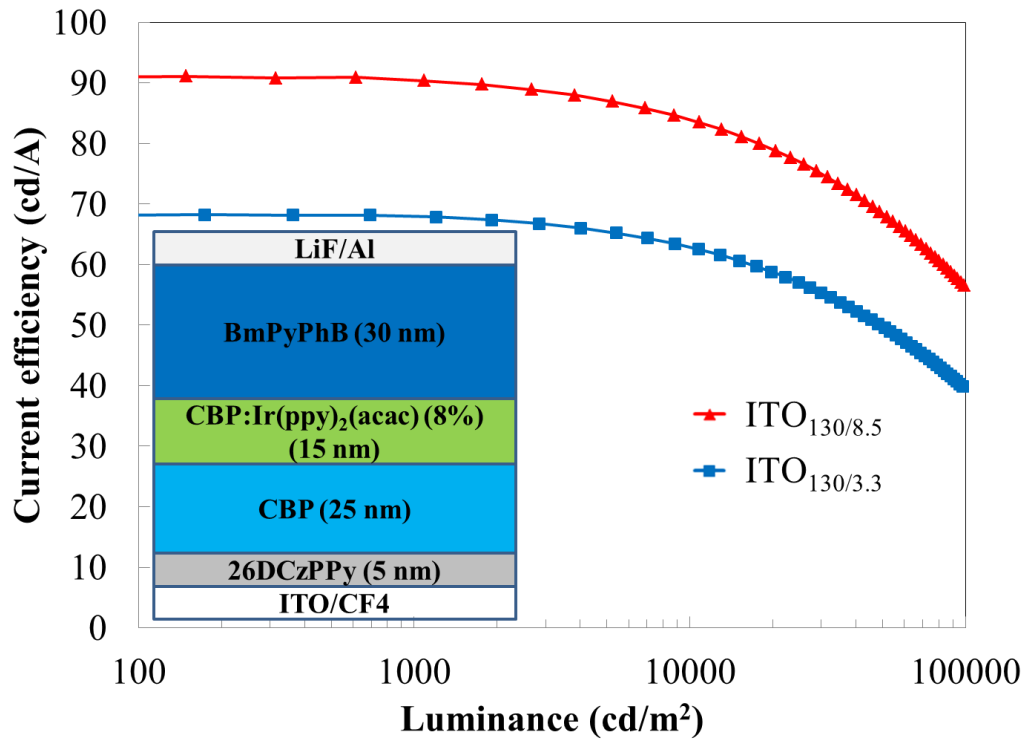


Figure 4.9 Current efficiency vs. luminance characteristics of the device with structure (inset) fabricated on ITO_{130/8.5} and ITO_{130/3.3}.

In order to test the effects of changing ITO thickness alone on efficiency, substrates with the same surface roughness but different ITO thickness, ITO_{130/3.3} and ITO_{100/3.3}, are used. Figure 4.10 shows the current efficiency vs. luminance characteristics of devices fabricated on these substrates. It can be seen that the device made on the thinner ITO (ITO_{100/3.3}) exhibits 25% higher efficiency. Figure 4.10 (inset) shows the transmittance spectra of the two ITO substrates. Although it may be expected that the thinner ITO would have a higher transmittance, possibly leading to lower optical losses and better light outcoupling, the spectra, however, show that the thinner ITO has lower transmittance in the green region where most OLED emission occurs. Microcavity effects in the ITO can be used to explain the lower transmittance of the thinner ITO. Due to the refractive index mismatches at the air/ITO and ITO/glass interfaces, a small portion of light is reflected at each interface. The overall intensity of transmitted light depends on optical interference between the forward transmitted component and forward reflected components resulting from multiple reflections between the two ITO surfaces. The interference pattern will naturally depend on the ITO thickness and the emission wavelength. In this case, when ITO thickness is 130 nm (which represents a travel

distance of 260 nm for light to get reflected off the ITO/glass and then the air/ITO interface) and the emission is at 520 nm (or 260 nm inside ITO, given its ~ 2 refractive index [85]), total constructive interference is expected. When ITO thickness is only 100 nm, partial destructive interference will, in contrast, occur. The lower transmittance in the green region of the thinner ITO_{100/3.3} can therefore be attributed to this effect. For the same reason, it can be expected the total reflectance of the ITO_{100/3.3} substrate to be lower, leading to weaker microcavity effects in the organic stack of the OLED. For the device on the thinner ITO to have a higher light outcoupling efficiency (as suggested from the higher current efficiency), it can be concluded that the weaker microcavity effects in this device result in less losses from destructive interference in the organic stack. Even though the ITO transmittance is lower in this device, the overall light outcoupling efficiency is still higher.

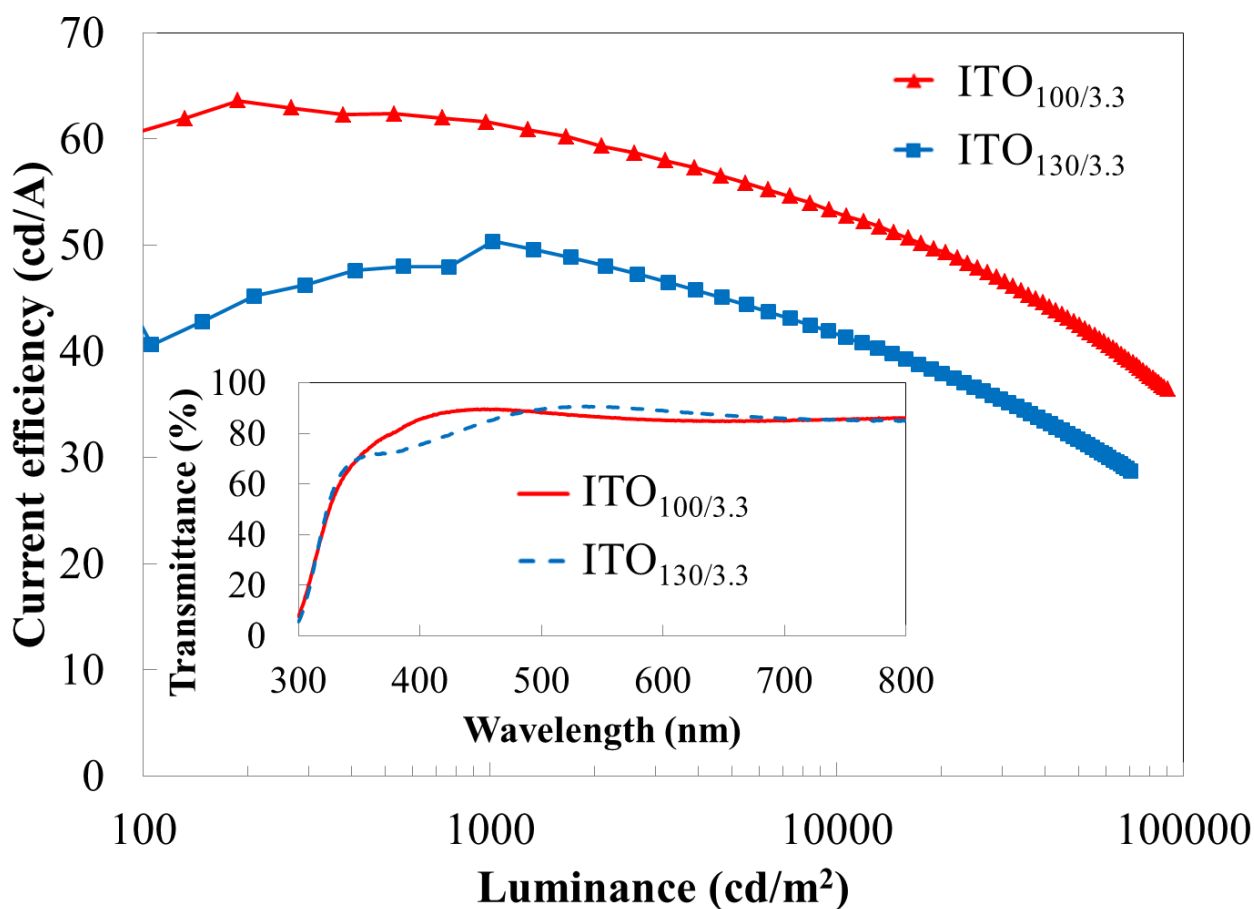


Figure 4.10 Measured transmittance of ITO_{100/3.3} and ITO_{130/8.5}. (b) Current efficiency vs. luminance of devices fabricated on ITO_{100/3.3} and ITO_{130/8.5}.

Knowing that the ITO transmittance affects light outcoupling significantly, it is then important to study the effects of changing ITO roughness while maintaining the ITO transmittance on device efficiency. In order to examine this, two types of substrates $\text{ITO}_{100/3.3}$ and $\text{ITO}_{130/8.5}$ are used. It can be seen in Figure 4.11 (a) that the two substrates indeed have similar transmittance, especially in the green region. This suggests that the transmittance is affected not only by ITO thickness, but also its roughness. The similar current density vs. voltage characteristics of devices made on these substrates, shown in Figure 4.11 (b), suggests they also have very similar charge balance ratios, hence also similar IQE. Quite remarkably, however, the device made on the rougher ITO exhibits 10% higher current efficiency, as illustrated in Figure 4.12. This higher efficiency is attributed to the aforementioned fact that the rougher ITO is able to out scatter trapped light within the ITO and/or the organic stack [86].

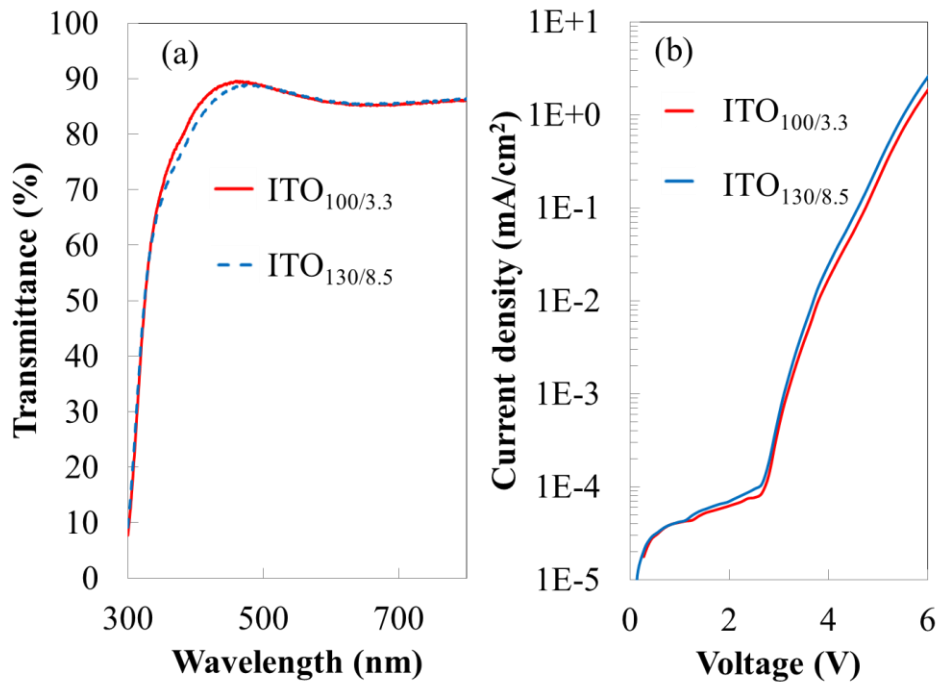


Figure 4.11 (a) Measured transmittance of $\text{ITO}_{100/3.3}$ and $\text{ITO}_{130/8.5}$. (b) Current efficiency vs. luminance of devices fabricated on $\text{ITO}_{100/3.3}$ and $\text{ITO}_{130/8.5}$.

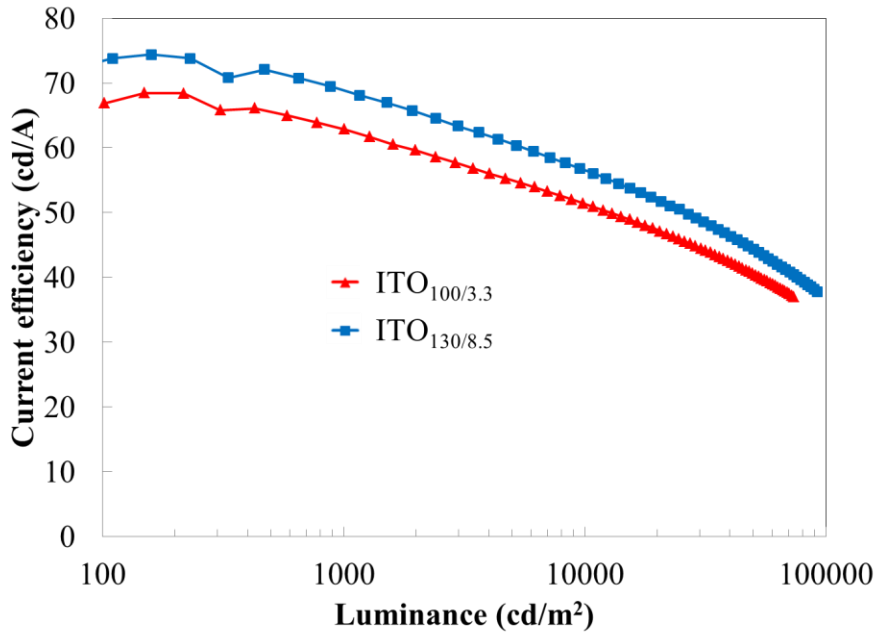


Figure 4.12 Current density vs. voltage characteristics of devices fabricated on ITO_{100/3.3} and ITO_{130/8.5}.

4.2 Conclusions

It is experimentally shown that ITO thickness and roughness both have an effect on the light outcoupling of OLEDs. The transmittance of ITO, which is related to both ITO thickness and roughness, affects the efficiency via microcavity effects. On the other hand, rougher ITO is shown to improve the external efficiency by out scattering light trapped inside the ITO and/or the organic stack. Changes in ITO thickness and roughness are found to be able to alter the light outcoupling efficiency by more than 25% and 10%, respectively. These results clearly demonstrate the significant efficiency benefits of using ITO with optimal thicknesses and higher roughness in OLEDs.

Chapter 5

Exciton-induced Degradation at the ITO/Organic interface

The material presented in this chapter was published in Appl. Phys. Lett., vol. 103, no. 6, p. 063307, 2013². It is reproduced here with the permission from the publisher.

Despite the high initial efficiency, simplified PHOLEDs suffer shorter EL lifetime when the devices are under electrical bias [19], [20]. It has been observed that different treatments on ITO surface lead to different lifetimes of the devices [19], [20]. This suggests that the shorter lifetime of the simplified PHOLEDs may be due to additional degradation phenomena that occur at the ITO/organic interface, besides those known to occur in the EML of the devices, such as chemical instability of organic molecules [50] or polaron induced degradation [56], [87], [88].

It has been recently discovered that ITO/organic interfaces are susceptible to degradation by excitons and that the phenomenon can play a role in limiting the EL stability of OLEDs [57]. By exposing the devices to external illumination, charge injection at the ITO/organic interface suffers a gradual deterioration. A correlation between the OLED operational stability and the interfacial photo stability was also established. Knowing that the shorter lifetime of the simplified PHOLEDs may be associated with degradation phenomena at the ITO/organic interface, the question of whether excitons play a role in the limited EL stability arises.

In this chapter, the effects of electrical driving and external illumination on the EL stability of simplified PHOLEDs are compared. The results show that the shorter lifetime is indeed caused by exciton-induced degradation of the ITO/organic interface. It is also determined that the underlying excitons are created by the recombination of electrons leaked from the EML with holes injected from the ITO. Approaches for controlling this degradation mechanism and increasing device stability are also described.

5.1 Degradation Mechanism

To investigate the possibility that the shorter lifetime of simplified PHOLEDs may be associated with excitons at the ITO/organic interface, devices where CBP is used as both hole

² All work presented in this chapter were done by the author with helpful discussions from the co-authors Mina M. A. Abdelmalek and Qi Wang.

transport and emitter host following Helander et al. [17] are studied. The general device structure is ITO/CBP (30 nm)/CBP:Ir(ppy)₃ (5%) (10 nm)/TPBi (40 nm)/LiF (0.8nm)/Al (80 nm). First, the effect of exposing the device to external illumination is studied. In this experiment, the devices are exposed to illumination at a wavelength of 350 nm, where CBP significantly absorbs, with ~0.5 mW/cm² power density for 12 hours without any electrical bias. Table 5.1 shows the luminance and driving voltage (at 20 mA/cm²) recorded from the device before and after the exposure to illumination. As can be seen, the device exhibits a ~20% decrease in luminance and 1 volt increase in driving voltage after the illumination step, pointing to photo-induced changes. The changes are similar to those observed in other OLEDs and can be generally attributed to exciton-induced degradation phenomena [57]. Next, the EL stability of this device under electrical bias is tested. If the nature of the device EL degradation under bias is exciton-induced, it can be expected that the electrical-induced changes to continue on the changes already produced by illumination. On the other hand, if the electrical degradation is not due to excitons, there would be no correlation between changes produced by electrical driving and those produced by illumination. Therefore, the device would have degradation trends under bias that resemble those of a pristine (i.e. not subjected to illumination before) PHOLED. Figure 5.1 (a) and (b) shows the changes in EL and the driving voltage, respectively, with time under electrical bias to maintain a constant current flow of 20mA/cm² for the device that was subjected to illumination before (denoted to by “illuminated”) and for an identical control device that was not subjected to the illumination (denoted to by “pristine”). In this figure, the EL changes are represented in the form of normalized luminance (luminance/initial luminance) which in case of the illuminated device refers to its pre-illumination luminance, thus the initial point of 0.8. It can be seen from Figure 5.1 (a) that the illuminated device does not exhibit the rapid decay of the pristine sample, indicating that the illumination had an effect on the EL decay trend under electrical bias. Quite interestingly, if the illuminated curve is shifted along the time axis so that the initial point (i.e. 0.8) matches the 0.8 point of the pristine one (shown in Figure 5.1 (a) as the illuminated shifted), the two curves would follow closely. Considering that the illuminated device is subjected two stress processes (illumination and then electrical), whereas the pristine device is subjected to only the electrical stress, for them to have the same EL decay trend, it indicates that the illumination-induced degradation must have something in common with the electrical-induced degradation. Since the illumination only creates excitons in CBP, the common factor here is exciton. Therefore, it can be concluded that electrical degradation process in simplified PHOLEDs is most likely exciton-induced which could be at the ITO/CBP interface. The same can also be observed in changes in driving voltage ($\Delta V = V_t - V_0$,

of which the illuminated device again refers to the changes with respect to the pre-illumination state, hence an initial point of 1 shown in Figure 5.1 (b). If the same shifting scheme is applied, the two voltage curves would also follow closely. Clearly, this rise in voltage over time indicates a deterioration in hole injection.

Table 5.1 Driving voltages and luminance at 20mA/cm² for devices without and with MoO₃ before and after external illumination

	Before illumination		After illumination	
	V (V)	L (cd/m ²)	V (V)	L (cd/m ²)
Without MoO ₃	6.52	7580	7.60	6020
With MoO ₃	6.89	7080	7.11	6910

To test whether the degradation is at the ITO/CBP interface, devices that include a 5 nm MoO₃ layer at the interface are fabricated and tested under the same conditions. The use of MoO₃ at the ITO/organic interface has been recently found to substantially reduce interfacial exciton-induced degradation [57]. The luminance and driving voltage of the sample at 20 mA/cm² measured before and after illumination are listed in Table 5.1. Contrary to the device without MoO₃, external illumination changes the device performance only marginally. This verifies that almost all the photo-induced damage in the device without MoO₃ layer is at the ITO/CBP interface. Therefore, in simplified PHOLEDs, the shorter EL lifetime under electrical bias arises from additional degradation processes at the ITO/CBP interface that are caused by excitons. This argument is also supported by the degradation results shown in Figure 5.1 (c), where EL decay trends of the illuminated and the pristine closely follow each other.

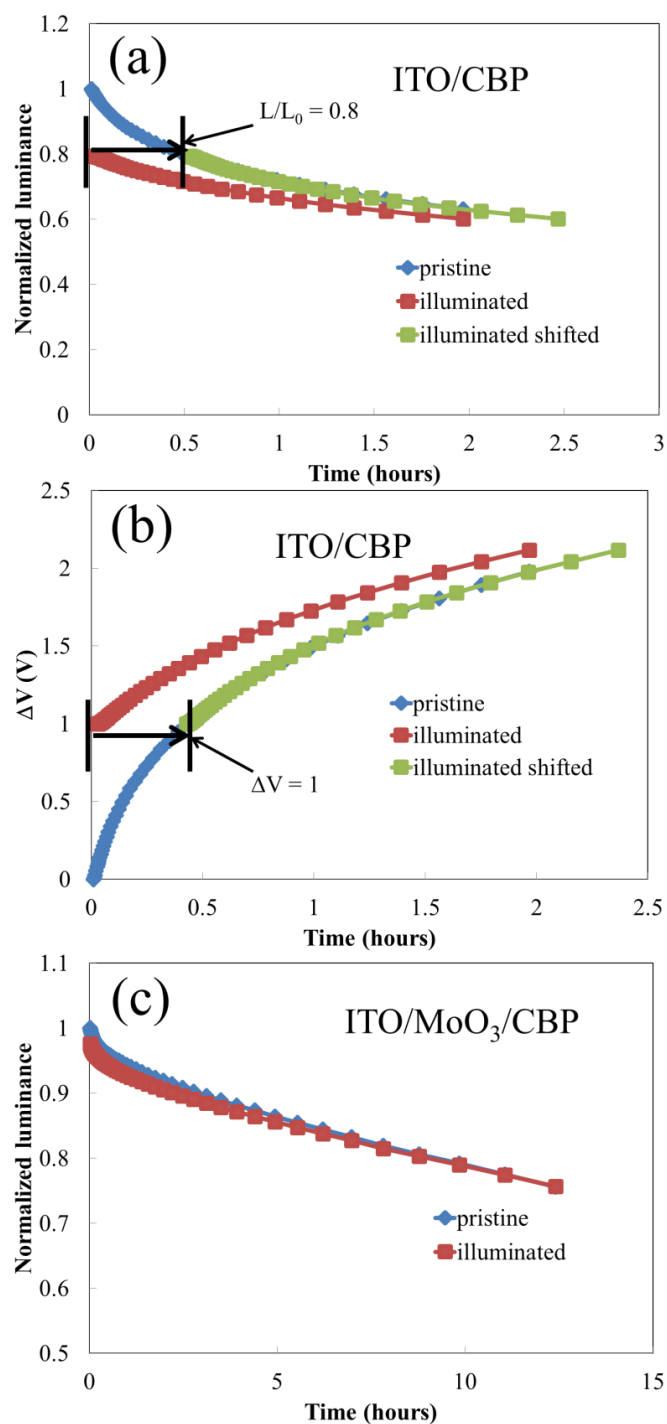


Figure 5.1 Changes in (a) EL and (b) driving voltage with time under 20 mA/cm² current density for pristine and illuminated devices without MoO₃. (c) Changes in EL with time for pristine and illuminated devices with MoO₃.

To further verify that excitons at the ITO/CBP interface lead to the shorter lifetime, the effect of reducing exciton concentration at the interface on device EL stability is studied. In general, there are two mechanisms by which excitons can exist at the ITO/CBP interface: (1) exciton diffusion from the EML, and (2) the formation of excitons near the interface due to the recombination of electrons, which might drift from the EML and reach the interface due to the bipolar charge transport nature of CBP [89], and holes injected from the ITO. Introducing a material that can trap both excitons and electrons as a dopant in the HTL can therefore be expected to reduce the exciton concentration at the ITO/CBP interface. In order to satisfy these requirements, the material needs to have a LUMO level that is significantly deeper than that of CBP (2.8 eV) to be able to efficiently trap excitons and electrons, and a HOMO level similar to that of CBP (6.1 eV) to not significantly alter hole transport across the HTL, hence charge balance. FIrpic, which has a deep LUMO level of 3.47 eV and a HOMO level of 6.15 eV is used for this purpose. Therefore, a series of simplified PHOLEDs of the same structure as before but further contain FIrpic as a dopant in a thin slice (5nm) of the HTL at various concentrations (0-20% by volume) are fabricated and tested. The device structure is ITO/CBP (10 nm)/CBP:FIrpic (x %) (5 nm)/CBP (15 nm)/ CBP:Ir(ppy)₃ (5%) (10 nm)/TPBi (40 nm)/LiF (0.8nm)/Al (80 nm). An examination of the JV characteristics of these devices (Figure 5.2 (a)) shows that changing the FIrpic concentration does not significantly affect the driving voltages of the devices, suggesting that FIrpic does not strongly block holes, as expected. It is also important to note that all devices have very similar current efficiencies, as illustrated in Figure 5.2 (b), suggesting that introducing FIrpic does not significantly alter the charge balance in the devices. The EL stabilities of the devices with different FIrpic concentrations are shown in Figure 5.2 (c). It is clear that devices with higher FIrpic concentrations have longer lifetimes. Because a higher FIrpic concentration results in increased exciton and electron trapping, hence a lower exciton concentration at the ITO/CBP interface, the results are fully consistent with the conclusion that excitons at the ITO/CBP interface are the cause of the fast EL degradation in simplified PHOLEDs. It is noteworthy to point out that the fact that all devices still contain neat (un-doped) CBP at the ITO contact indicates that the stability differences among the devices cannot be a result of easier hole injection or due to changes in the morphological or wetting characteristics of CBP at the ITO contact due to the presence of FIrpic. This conclusion rules out morphological instabilities at the contact from being behind a dominant factor in the short lifetime of the simplified OLEDs.

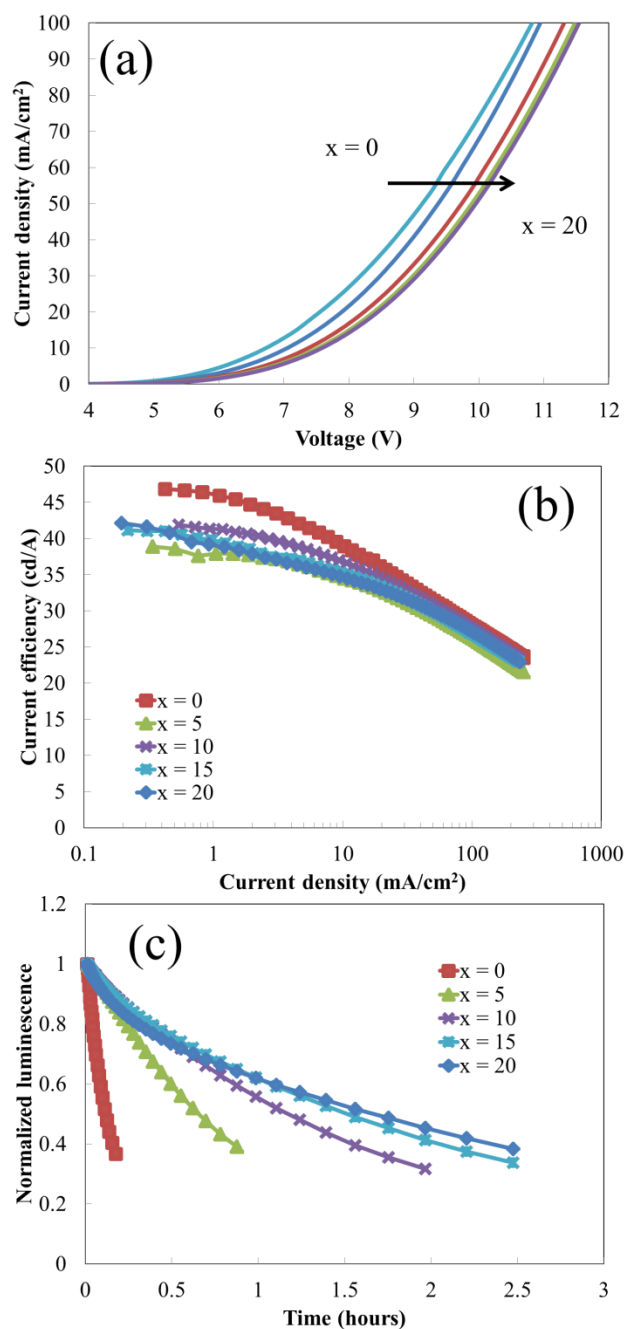


Figure 5.2 (a) JV characteristics of devices with x% FIrpic doping concentrations. x = 0, 5, 10, 15, 20. (b) Current efficiency vs. current density characteristics. (c) Changes in EL with time under 20 mA/cm² current density.

Although the above results show that the presence of excitons in the vicinity of the ITO/CBP interface plays a significant role in limiting the stability of the simplified PHIOLEDs and that

reducing their concentration at the interface, such as by means of introducing FIrpic in the HTL, results in an increase in device stability, they do not indicate whether the excitons exist at the interface due to diffusion from the EML or the result of e-h recombination near the interface. To help answer this question, the effect of increasing the thickness of the CBP HTL in these devices is studied. As the exciton diffusion length in CBP is relatively short (~16.8 nm) [78], it can be expected that varying the thickness of the CBP layer between 20 nm and 100 nm to significantly affects exciton concentration near the ITO interface should their presence in this area be primarily the result of diffusion from the EML, and thus would influence the device lifetime. On the other hand, as CBP is a bipolar material and can transport electrons efficiently [89], increasing the CBP thickness will not significantly hamper the drift of electrons across the CBP layer to reach the ITO under the external bias, and thus would less significantly impact the concentration of excitons near the interface should they be primarily the result of e-h recombination there. The EL stability measurements on 5 different devices with 20, 40, 60, 80 and 100 nm thick CBP HTL reveal they all have essentially the same lifetime, as can be seen in Figure 5.3. This proves that the exciton creation at ITO/CBP interface is primarily the result of e-h recombination in the CBP layer near the ITO interface due to electrons that drift past the EML and into the HTL (i.e. leakage current) which recombine with holes injected from the ITO. In this context, the success of using FIrpic as a dopant in the HTL in increasing device stability must be arising from its role in trapping electrons, thus reducing their arrival to the ITO hence reducing exciton formation near the ITO interface.

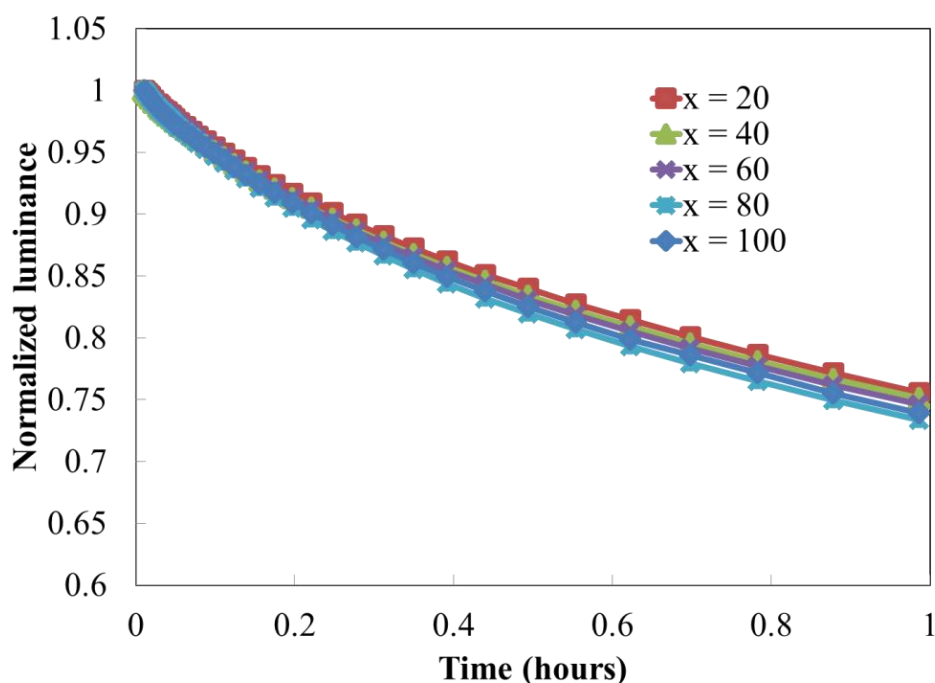


Figure 5.3 Changes in EL with time under 20 mA/cm² current density for devices with x nm thick CBP HTL, where x = 20, 40, 60, 80, 100.

5.2 Approaches to Suppress Degradation

From the findings that (1) excitons at the ITO/CBP interface result in short lifetime in simplified PHOLEDs, (2) excitons are created from electrons leaked from the EML with holes injected from the ITO, and (3) using an electron trapping material as a dopant in the HTL can extend the PHOLED lifetime, it can be expected that introducing a material with a shallower LUMO level than that of CBP yet a similar HOMO level as that of CBP can block electrons from reaching the ITO/CBP interface, thus increase the device stability without undermining efficiency. Therefore, a layer of 26DCzPPy between ITO and CBP is introduced. The device structure is then ITO/26DCzPPy (5 nm)/CBP (25 nm)/ CBP:Ir(ppy)₃ (5%) (10 nm)/TPBi (40 nm)/LiF (0.8nm)/Al (80 nm). Because 26DCzPPy and CBP have similar HOMO levels (6.05 eV and 6.1 eV), hole injection and transport, hence charge balance in both cases, are almost the same. This is evident from Figure 5.4 (a) and (b), which illustrate the characteristics of the devices with the 26DCzPPy layer, showing very similar driving voltages and current efficiencies to those without the layer. Figure 5.4 (c) shows that the lifetime of the PHOLED with 26DCzPPy layer is longer by one order of magnitude. Since 26DCzPPy has a shallower LUMO level than that of CBP (2.56 eV vs. 2.8 eV), electrons leaking from the EML

are blocked at the 26DCzPPy/CBP interface, which prevents exciton formation, hence the exciton-induced degradation at the ITO/26DCzPPy interface. Due to the similarity in HOMO levels, 26DCzPPy in principle can always be used in conjunction with CBP regardless of the work function modification treatment on ITO to increase the lifetime of the simplified PHOLEDs.

It is also important to emphasize that 26DCzPPy provides protection against exciton-induced degradation by blocking leaked electrons from reaching the ITO interface, thus preventing the formation of excitons thereby. However, it is also shown that if excitons are created on 26DCzPPy (e.g. via external illumination), the ITO/26DCzPPy interface would still degrade, similarly to the ITO/CBP interface. For example, a PHOLED with a structure ITO/26DCzPPy (20 nm)/ CBP:Ir(ppy)₃ (5%) (10 nm)/TPBi (40 nm)/LiF (0.8nm)/Al (80 nm) would lose 15% of its initial luminance after 25 hours of exposure at a wavelength of 300 nm (where 26DCzPPy absorbs). As shown in Figure 5.5, when the illuminated device is subjected to electrical bias, the EL decay trend highly resembles that of a pristine device. This can be seen more clearly when the illuminated curve is overlaid on top of the pristine one. If the degradation at the ITO/CBP interface in simplified PHOLEDs was not exciton-induced, the devices in Figure 5.1 would have shown similar results.

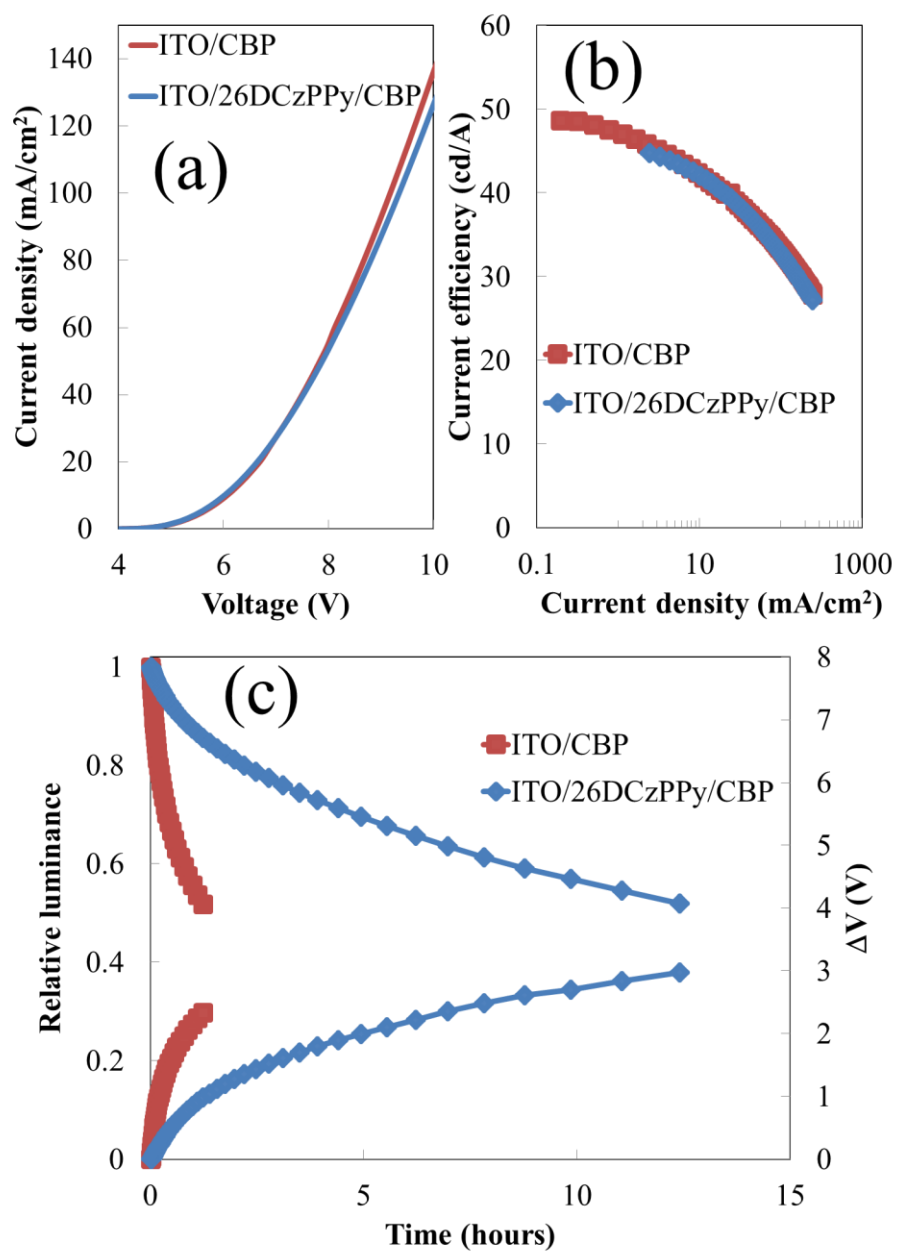


Figure 5.4 (a) JV and (b) current efficiency vs. current density characteristics of devices with ITO/CBP and ITO/26DCzPPy/CBP interfaces. (c) Changes in EL with time of devices with ITO/CBP and ITO/26DCzPPy/CBP interfaces under 20 mA/cm² current density.

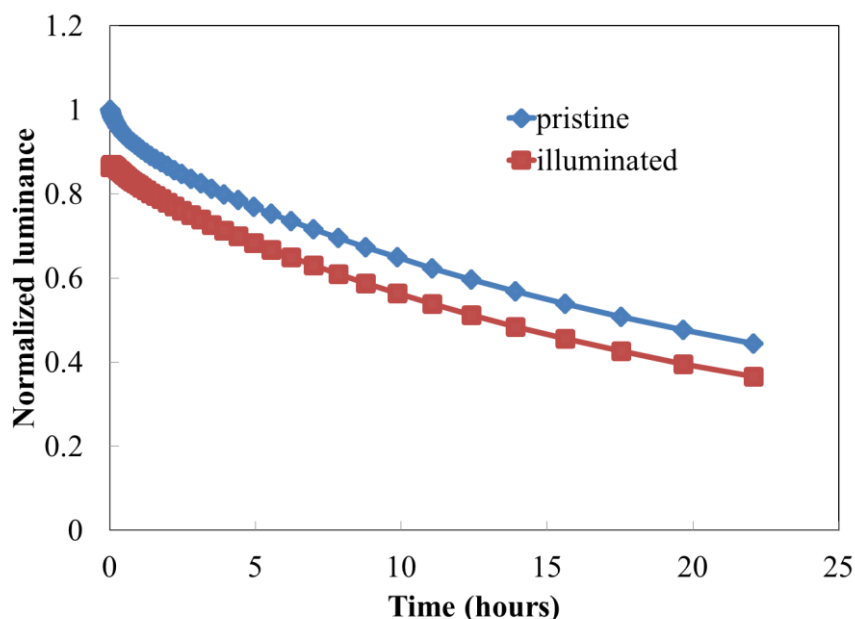


Figure 5.5 Changes in EL with time of pristine and illuminated devices under 20 mA/cm² current density.

It is important to realize that simplified PHOLEDs, which utilize one material for hole transport and emitter host, would in general be prone to this exciton-induced degradation of the ITO/organic interface. This is because the material is required to have bipolar property to be an efficient emitter host, thus the transport of electrons to the ITO will not be insignificant. Conventional PHOLEDs with HTL/EML interfaces can usually limit electrons from reaching the ITO/organic interface hence the creation of excitons nearby, and therefore are less susceptible to this degradation mechanism.

5.3 Conclusions

In conclusion, it has been shown that the shorter lifetime in simplified PHOLEDs is due to exciton-induced degradation near the ITO/organic interface. The excitons are created from recombination of electrons leaked from the EML with holes injected from the ITO. Introducing an electron trapping dopant (e.g. Flrpic) in the HTL or an electron blocking layer (e.g. 26DCzPPy) can prevent electrons from reaching the interface, hence increase the lifetime of the PHOLEDs. Having similar HOMO level to that of CBP makes 26DCzPPy a very useful HTM. Using 26DCzPPy in conjunction with CBP with any ITO treatment can potentially enhance the lifetime of the simplified PHOLEDs.

Chapter 6

Exciton-polaron Induced Degradation at the Organic/Organic Interface

Due to their advantages in contrast, viewing angle and color quality, displays utilizing OLEDs, especially the more efficient PHOLEDs [90], [91], now account for the second largest shipments in display industry, after liquid crystal displays [92]. The relatively lower stability of OLEDs has however been a long-standing issue that limits their wider adoption. In particular, the different stability of devices that produce different colors results in differential color aging in OLED displays. Over the past decade, much research has focused on uncovering the degradation mechanisms in PHOLEDs, and several degradation mechanisms have been proposed. Those include interactions between host anions and guest excitons [55], [56], chemical processes that occurs during device operation [50]–[54], buildup of hole space charge in the emission layer (EML) [88], [93], and exciton induced degradation of the ITO/organic [71], organic/organic [61], [75] and organic/metal interfaces [60].

It is recently found that interactions between excitons and positive polarons result in aggregation of host materials, especially in the vicinity of the organic/organic inter-layer interfaces of the device. Moreover, a correlation between device EL lifetime and the rate by which this aggregation behavior occurs in a given host material [62] has been shown. Quite interestingly, the investigations also revealed a clear correlation between the rate of aggregation and the width of the energy band-gap of the material where materials with wider energy band-gap tend to aggregate faster. These new findings help explain, for the very first time, the generally lower stability of blue and other wide band-gap based OLEDs. One phenomenon that this theory, however, still does not explain is why devices utilizing the same host material but different guest materials can sometimes have very different lifetimes [65]. In view of this phenomenon, a better understanding of the main factors governing device stability requires answering the following two questions (1) Is it the host or the guest that plays a more dominant role in governing device stability? (2) If the host plays a more dominant role, then how does the guest affect the stability of the host?

The answers to these questions are provided in section 6.1. Investigations show that the device lifetime is determined by the host aggregation rate, confirming that the host plays a more influential role on OLED stability. They also show that the aggregation rate of a host material can

vary significantly depending on the choice of the guest material introduced in it. Finally, phase segregation between the host and the guest is found to be an important aspect of the morphological changes that take place in those material systems. Because of this phase separation, transfer of excitons from the host to the guest becomes increasingly less efficient in the devices, resulting in the loss in EL efficiency over time.

Knowing that the aggregation of the host caused by exciton-polaron interactions is the key to device degradation, approaches to suppress this degradation can include reducing (a) exciton and (b) polaron concentrations at the organic/organic interface, and (c) using pre-aggregated neat emitting layer. The approaches are described in details in section 6.2.

6.1 Degradation Mechanism

Reprinted with permission from ACS Appl. Mater. Interfaces, 2016. Copyright 2016 American Chemical Society.

In order to determine whether it is the host or the guest that plays a more dominant role in governing device stability, the change in EL with electrical driving time of OLEDs comprising the same host material but different guest materials is investigated. For this purpose, OLEDs with the structure ITO/MoO₃ (5 nm)/ CBP (30 nm)/CBP:guest (15 nm)/ TPBi (45 nm)/LiF (1 nm)/Al (80 nm) are fabricated and tested. In these devices CBP is used as the host material whereas Ir(ppy)₃, Ir(ppy)₂(acac) or Ir(piq)₃ is used as a guest material [94] doped into the host at 0.25% doping concentration. Such low guest concentration is used so that complete energy transfer from the host to the guest can be avoided. This allows us to obtain EL from both the host and the guest, and thus offers an opportunity to study changes in their relative EL intensities with time under electrical stress. Figure 6.1 (a) presents normalized EL spectra collected from the Ir(ppy)₃-doped device after electrical driving at 20mA/cm² for various times. As can be seen, device EL is dominated by Ir(ppy)₃ emission. A close examination of the spectra, however, reveals the presence of an additional emission band with peak around 400nm, which corresponds to emission from the CBP host, as expected. An enlarged view of the host EL spectral characteristics in this range are shown in Figure 6.1 (b). The spectra in this figure are normalized to the guest EL peak height so that the change in the host EL relative to the guest EL can be better illustrated. As can be seen, in addition to the typical 400 nm CBP EL band, the spectra reveal the emergence of a new EL band at 480 nm with time. This band can be attributed to emission from CBP aggregates [62]. The intensity of this new band increases with

time whereas that of the 400nm band, which will be referred to hereinafter as the CBP “monomer” band, decreases. The trends point to a possible gradual increase in CBP aggregates accompanied with a decrease in the number of CBP monomer molecules in the device with time. This behavior can be more clearly seen if the guest EL band is removed (i.e. mathematically subtracted) from the overall spectrum, as shown in Figure 6.1 (c). Tests on devices with Ir(ppy)₂(acac) and Ir(piq)₃ as guest materials in place of Ir(ppy)₃ exhibit the same host aggregation trends. The results from those devices are shown in Figure 6.1 (d), (e) and (f) for Ir(ppy)₂(acac), and in Figure 6.1 (g), (h) and (i) for Ir(ppy)₂(acac).

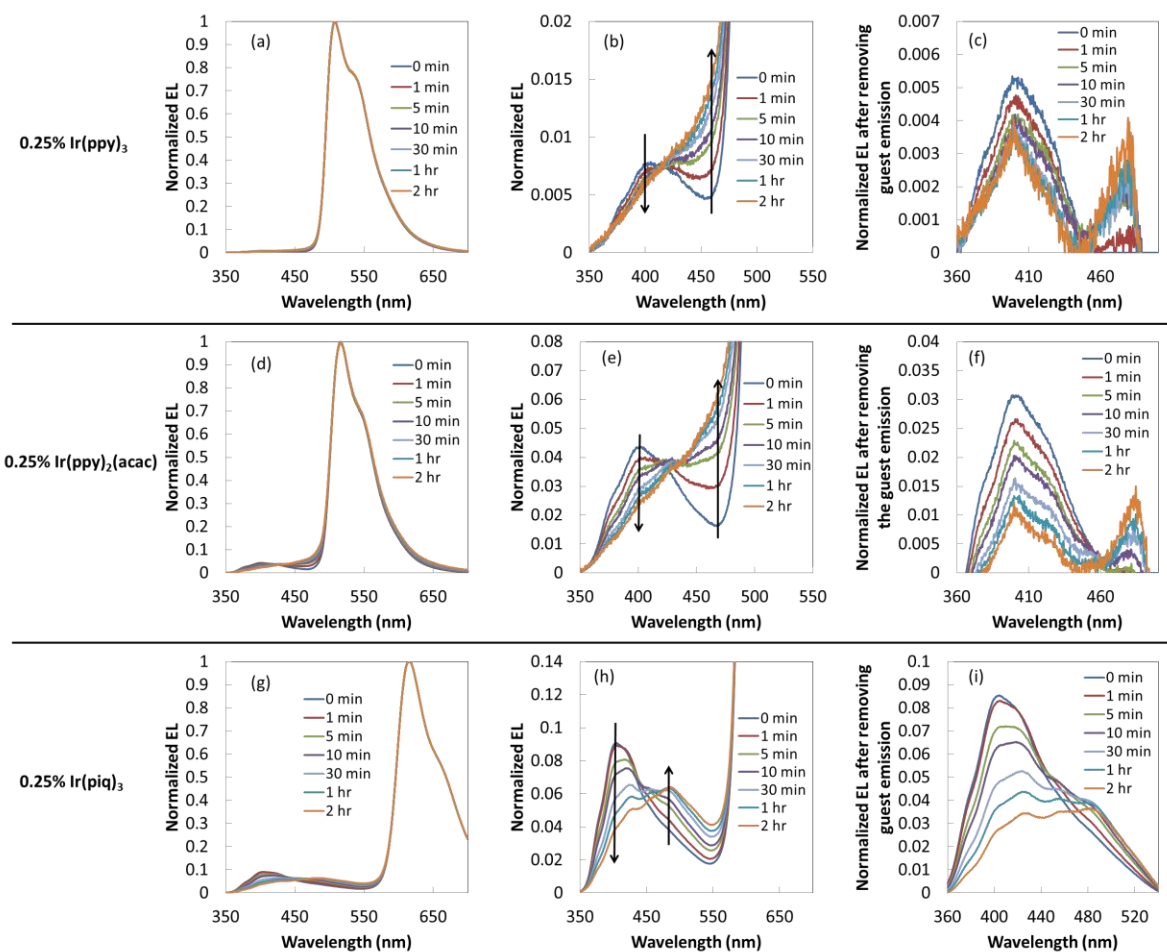


Figure 6.1 EL spectra (normalized to the guest emission peak intensity) of devices with (a) 0.25% Ir(ppy)₃, (d) 0.25% Ir(ppy)₂(acac) and (g) 0.25% Ir(piq)₃ as dopant, collected before and after electrical driving at 20mA/cm² for certain periods of time. (b), (e) and (h) The enlarged views of (a), (d) and (g) centered around the host emission peaks, respectively. The arrows

highlight the direction of changes in the CBP monomer and aggregate peaks relative to the guest emission peaks. (e), (f) and (i) Normalized EL spectra from (a), (d) and (g), respectively, after removing the guest emission peaks.

To investigate if device lifetime correlates with the CBP aggregation rate, similar measurements were carried out on OLEDs with various guest concentrations. Figure 6.2 (a) presents changes in device total luminance (presented in the form of luminance at the given time relative to the initial luminance) and in CBP monomer emission intensity (from the height of the 400 nm CBP EL band at the given time relative to its initial height) from a device with 1.5% Ir(ppy)₂(acac) over time. During this test, the device is subjected to a constant electrical driving at 20 mA/cm². Clearly, the two quantities follow the same trend, suggesting a strong correlation between device lifetime and CBP aggregation rate exists. Figure 6.2 (b) presents an enlarged view of EL spectra from the same device (the view is limited to the 350-550nm range where CBP emission occurs) at the given times. Like in Figure 6.1 (b), the spectra are normalized to the guest EL peak in order to better illustrate relative changes in host versus guest EL intensities. Clearly, the intensity of EL from the CBP monomer molecules (i.e. the 400 nm band) does not change relative to the guest EL band with driving time in this case (which agrees with the observation in Figure 6.2 (a)). Yet, once again, a gradual increase in CBP aggregate emission with time is observed. The fact that the intensities of both guest EL and the host monomer EL decrease at the same rate suggests that the two effects are inter-related. This is not unexpected and can be readily explained in terms of the well-established notion that guest excitation in phosphorescent OLEDs occurs primarily via energy transfer from the host [95]. In this regard, the equal degradation rates suggest that the decrease in guest EL with time (and hence also the device overall EL degradation rate considering that guest EL constitutes the majority of device EL) arises from a decrease in energy transfer from the host to guest and is associated with the decrease in the host monomer EL. The equal rates also suggest that only excitons on the CBP monomer molecules, but not those on the aggregated molecules, can be transferred and cause excitation to the guest molecules and thus produce EL from the guest. Similar results are also observed in devices using Ir(ppy)₂(acac) (Figure 6.2 (c) and (d)) and Ir(piq)₃ (Figure 6.2 (e) and (f)) emitters.

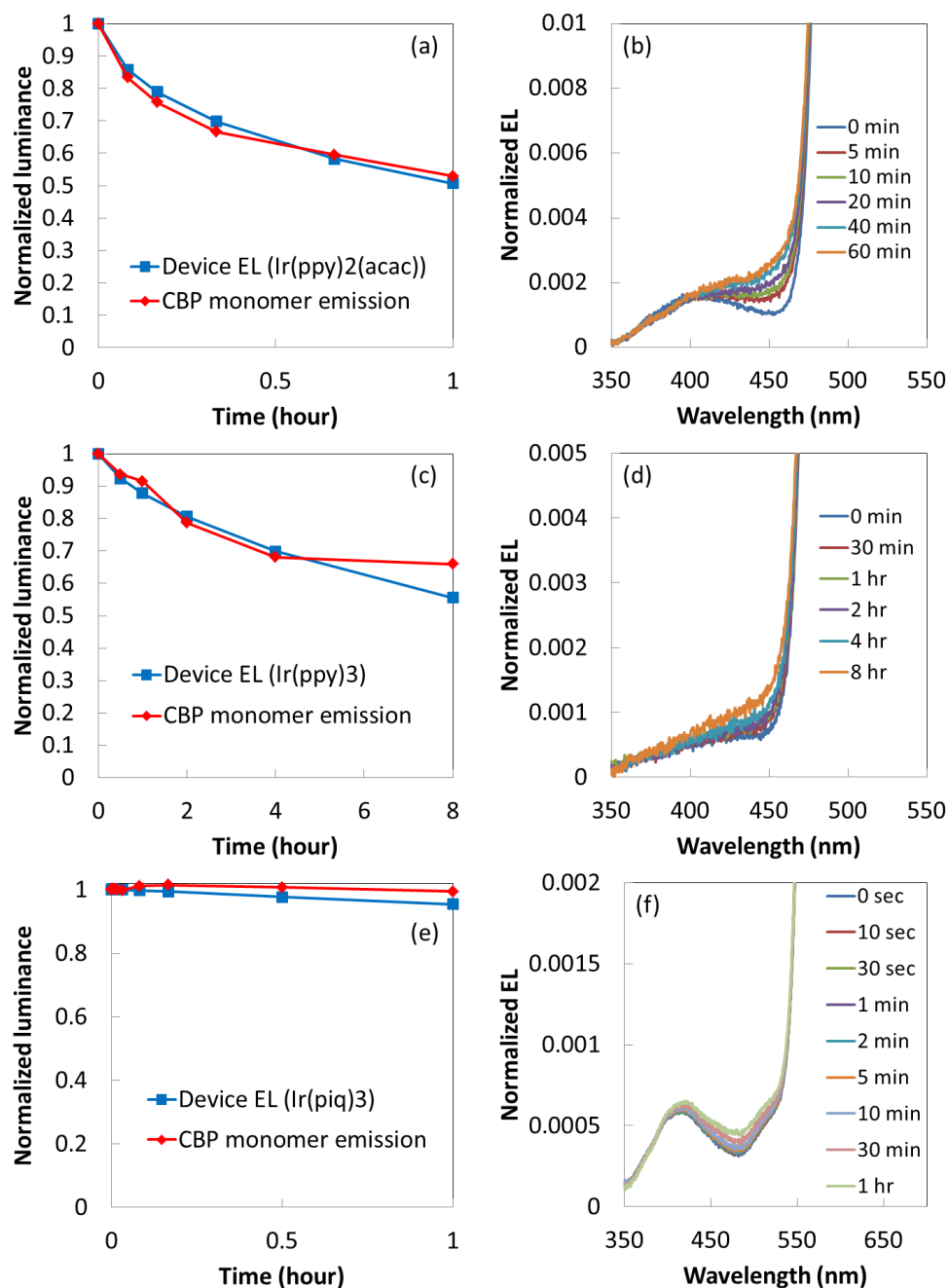


Figure 6.2 Changes in device EL and CBP monomer emission over time of devices using (a) 1.5% Ir(ppy)₃, (c) 1.5% Ir(ppy)₂(acac) and (e) 1.5% Ir(piq)₃ as dopant, under electrical driving at 20 mA/cm². EL spectra (normalized to the guest emission peak intensity) of devices with (b) 1.5% Ir(ppy)₃, (d) 1.5% Ir(ppy)₂(acac) and (f) 1.5% Ir(piq)₃ as dopant, collected before and after electrical driving at 20mA/cm² for certain periods of time.

Devices with the three guest materials doped in other concentrations were also studied. Figure 6.3 (a) summarizes the results from those devices, presenting them in the form of the ratio of CBP monomer EL-to-guest EL intensity (i.e. the ratio of the 400nm peak height to the guest EL peak height) versus electrical driving time. As can be seen from the figure, in devices with low guest concentrations (< 0.5%) EL from CBP monomer molecules decreases faster with time than EL from the guest molecules. This may be due to the fact that, at such low concentrations, a significant fraction of host molecules will not be in close proximity to guest molecules, and thus will not be able to dissipate their excitation energy as quickly. These host molecules will therefore be more susceptible to aggregation due to exciton-polaron interactions [62], causing the fast degradation in CBP monomer EL. In contrast, in devices with sufficiently high guest concentrations (and thus most host molecules are within a few angstroms from a guest molecule and can therefore transfer energy efficiently to the guest via both Forster and Dexter processes), the degradation rates of the guest EL and the host EL become essentially equal. This scenario occurs at a concentration of 1.5% in case of Ir(ppy)₃, where, as evident from the figure, the CBP monomer-to-guest ratio remains at unity. Similar results are also observed in devices with Ir(ppy)₂(acac) (Figure 6.3 (b)) and Ir(piq)₃ (Figure 6.3 (c)) emitters, with that threshold concentration being between 0.5% and 1.5%, and around 1.5%, respectively. In view of these results, it can be concluded that in commonly used PHOLEDs where guest concentrations are typically above 1.5%, the deterioration in device EL is governed mainly by the stability of the host material, and the changes in its ability to transfer the energy to the guest³. This indicates that the host plays a more dominant role than the guest in device stability.

³ It is noted that conducting similar experiments on devices with doping concentration exceeding 4% is not feasible due to complete energy transfer from the host to the guest, hence the difficulty of detecting host EL.

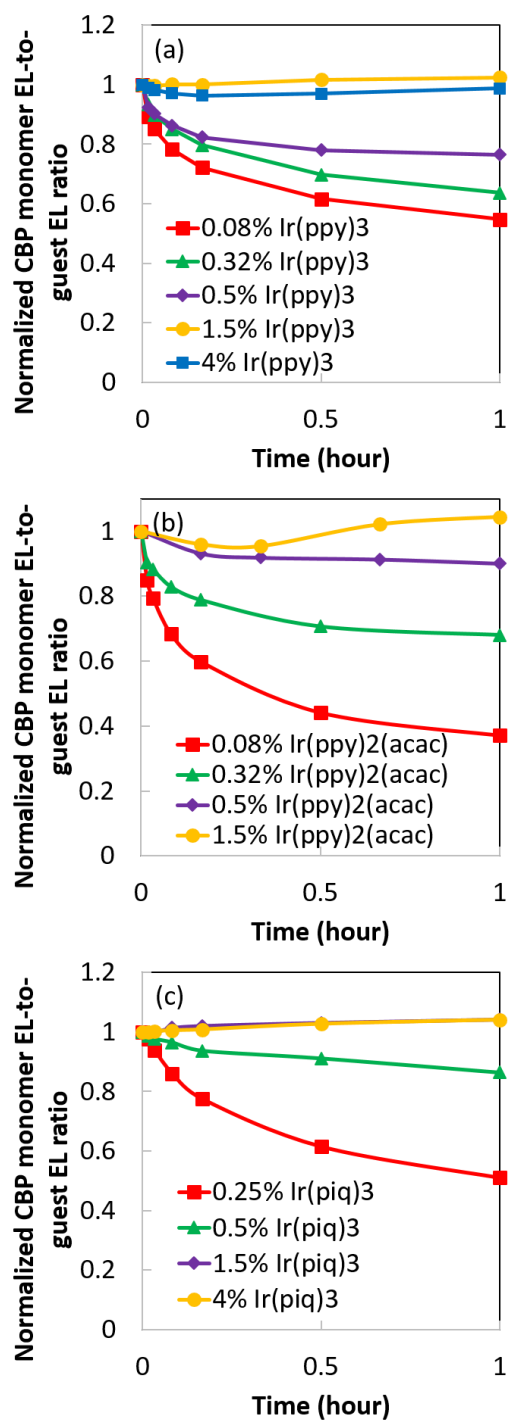


Figure 6.3 Changes in CBP-to-dopant EL peak ratio over time for devices using (a) Ir(ppy)₃, (b) Ir(ppy)₂(acac) and (c) Ir(piq)₃ as dopant with various doping concentrations, under constant electrical driving at 20 mA/cm².

The above results therefore lead to the conclusion that the aggregation rate of the host is what governs the rate of decrease in device EL with time. Furthermore, they show that the decay rate of CBP monomer EL varies among the devices depending on the choice of the guest material and its concentration. The question whether the morphological stability of the host is affected by both the guest material species and its concentration therefore arises.

To investigate the dependence of the morphological stability of the host on the guest material and its concentration, the effects of subjecting CBP films doped with various guest materials and concentrations to heating on their morphology are tested. The use of thermal stress as a way to induce the same aggregation behavior as that induced by exciton-polaron interactions during electrical driving of the device has been established previously [62]. The films are 30 nm thick, with either 0.25% or 5% dopant concentration. The same set of dopants - Ir(ppy)₃ or Ir(ppy)₂(acac) or Ir(piq)₃ are again compared. Figure 6.5 shows images of these films taken under UV irradiation (i.e. PL images) before (top half of the figure) and after (bottom half) heating @ 120°C for 6 minutes (heating of films is performed on a hotplate inside a glove box where both oxygen and moisture levels are kept below 1 ppm). This temperature exceeds the glass transition temperature T_g of CBP, which is 62 °C [96]. The compositions of these films from left to right are: CBP (30 nm), CBP:Ir(piq)₃ (5%) (30 nm), CBP:Ir(piq)₃ (0.25%) (30 nm), CBP:Ir(ppy)₂(acac) (5%) (30 nm), CBP:Ir(ppy)₂(acac) (0.25%) (30 nm), CBP:Ir(ppy)₃ (5%) (30 nm) and CBP:Ir(ppy)₃ (0.25%) (30 nm). It can be clearly seen that the 5% doped films show no visible signs of crystallization. On the other hand, the neat CBP film and the 0.25% doped films exhibit signs of significant crystallization. The average size of the crystallites in these films increases from smallest to largest in the order: Ir(ppy)₃ → Ir(ppy)₂(acac) → Ir(piq)₃ → CBP. It is interesting to note that the lifetime of devices with the same guests and concentrations also follow the same order⁴. A similar trend can also be observed in the 5% doped films after heating for 30 mins (with one exception that the film with 5% Ir(piq)₃ now has the least amount of crystallization, as shown in Figure 6.5). Once again, the lifetime of devices using the same guests and concentrations follow the same order. The clear correlation between the morphological stability of the host and its dependence on the guest supports the hypothesis that both the choice of the guest species and its concentration affects the morphological stability of the host.

⁴ The Ir(piq)₃-doped device indeed has a shorter lifetime than the Ir(ppy)₂(acac)-doped device at low doping concentration of 0.25%. However, this behavior is reversed at high guest concentrations.

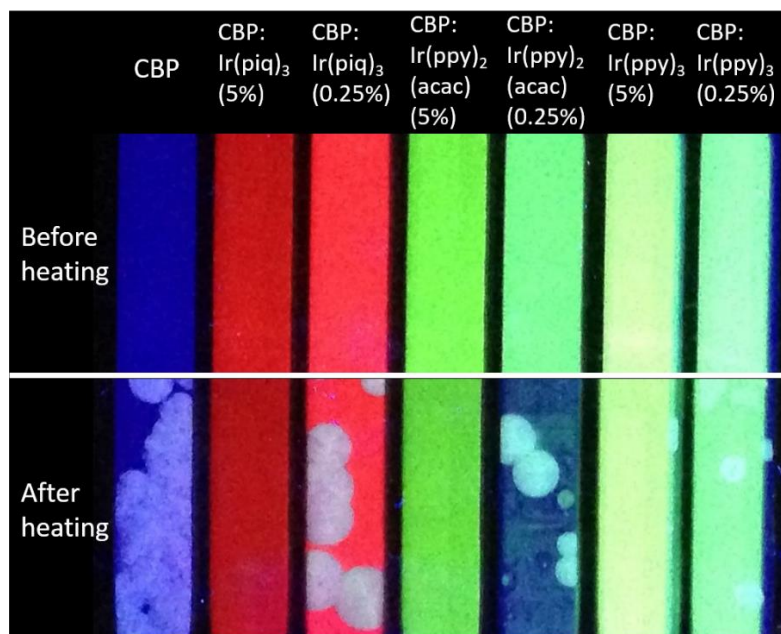


Figure 6.4 Image of films (top) before and (bottom) after heating at 120°C for 6 minutes, taken under UV irradiation. The film compositions from left to right are: CBP (30 nm), CBP:Ir(piq)₃ (5%) (30 nm), CBP:Ir(piq)₃ (0.25%) (30 nm), CBP:Ir(ppy)₂(acac) (5%) (30 nm), CBP:Ir(ppy)₂(acac) (0.25%) (30 nm), CBP:Ir(ppy)₃ (5%) (30 nm) and CBP:Ir(ppy)₃ (0.25%) (30 nm).

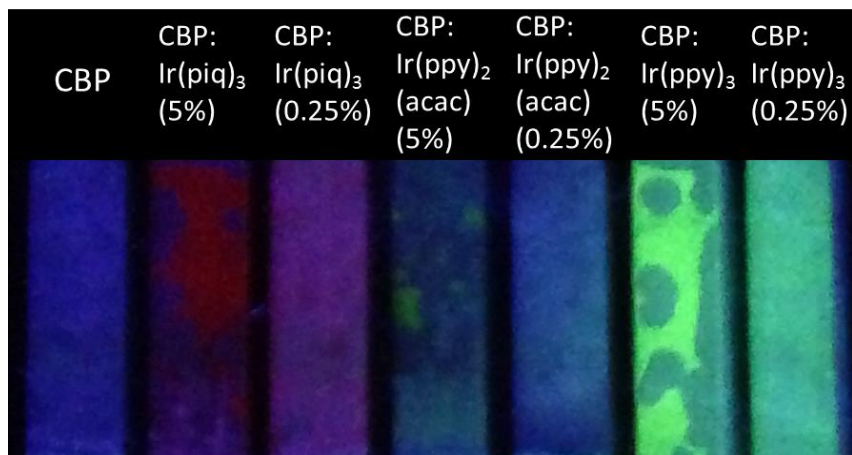


Figure 6.5 Image of films after heating at 120°C for 30 minutes, under UV irradiation. The film compositions from left to right are: CBP (30 nm), CBP:Ir(piq)₃ (5%) (30 nm), CBP:Ir(piq)₃ (0.25%) (30 nm), CBP:Ir(ppy)₂(acac) (5%) (30 nm), CBP:Ir(ppy)₂(acac) (0.25%) (30 nm), CBP:Ir(ppy)₃ (5%) (30 nm) and CBP:Ir(ppy)₃ (0.25%) (30 nm).

In order to better understand how the guest material and its concentration can affect the morphological stability of the host, the PL spectra of the films in Figure 6.4 are collected. Figure 6.6 (a) present the PL spectra collected from the neat (i.e. undoped) CBP films before and after heating. Interestingly, the PL spectrum of the neat CBP after heating shows clear vibronic bands, indicating the CBP molecules become more highly ordered, which is consistent with the earlier conclusion that molecular aggregation occurs and also with the observed crystallization. Furthermore, when comparing results from the 0.25% Ir(ppy)₃-doped film before and after heating, shown in Figure 6.6 (b), the following can be observed (1) The heated films show significant PL in the 350-450 nm range, typical of that of CBP, indicating that energy transfer from CBP to the guest becomes less efficient after heating. (2) This PL has the same vibronic features seen in the spectrum of the heated neat CBP film, indicating that molecular reorganization and aggregation of CBP molecules occurs here as well despite the presence of the guest molecule. (3) Unlike the CBP PL peak, the shape of the guest PL peak remains essentially unchanged after heating, suggesting that, unlike the host, the guest does not undergo significant aggregation. The first two observations indicate that the thermal stress brings about phase segregation between the host and the guest. The implications of this phase segregation are (a) The host and guest molecules form separate domains which results in a decrease in host-to-guest energy transfer and thus allows fluorescence from the CBP to appear. (b) The CBP molecules, now present in essentially guest-free domains, are offered a better opportunity to organize and attain more ordered morphologies, which leads to the appearance of clear vibronic features in the PL spectrum. In contrast, the guest molecules do not seem to aggregate appreciably during the same time frame, possibly due to their presence in much smaller numbers. The 0.25% Ir(ppy)₂(acac)-doped films were similarly tested. The results are presented in Figure 6.6 (c) and show a very similar behavior to that observed in the 0.25% Ir(ppy)₃-doped films.

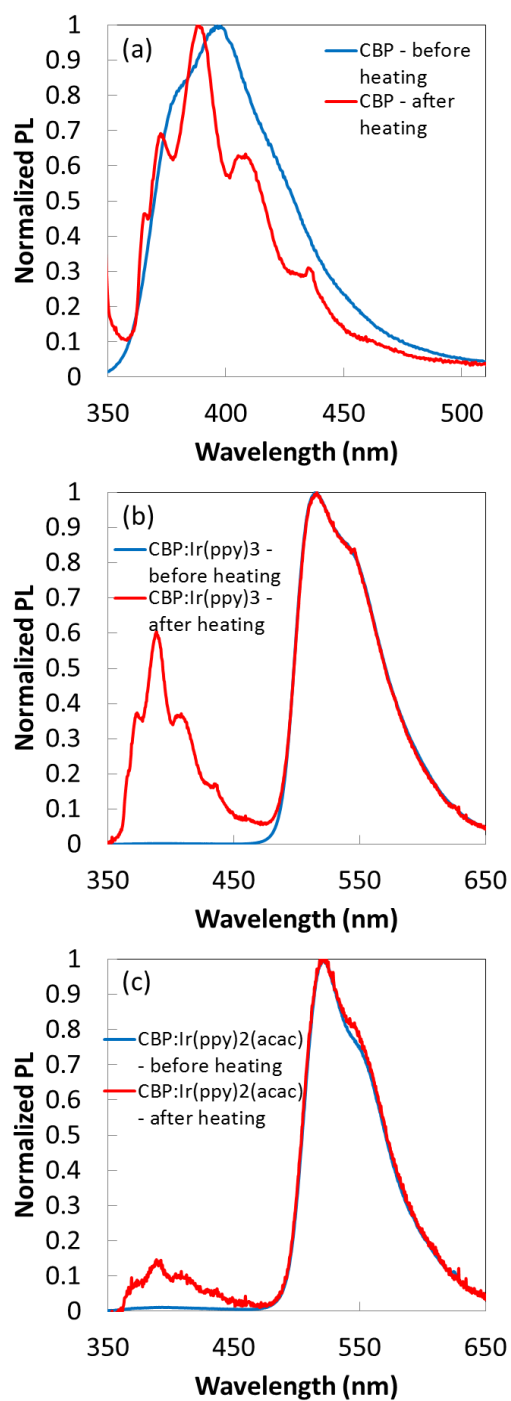


Figure 6.6 PL spectra of (a) CBP (30 nm), (b) CBP:Ir(ppy)₃ (0.25%) (30 nm) and (c) CBP:Ir(ppy)₂(acac) (0.25%) (30 nm) films before and after heating at 120°C for 30 minutes, respectively.

From Figure 6.4 it can also be seen that the films with higher guest concentration (e.g. 5%) are generally much more stable morphologically and show only negligible (if any) crystallization after heating. The increased morphological stability with higher guest concentration may be attributed to more sluggish host/guest phase segregation due to the presence of a larger number of guest molecules dispersed within the host. It can also be seen from the same figure that films doped with different guest materials, but at the same concentration show crystallization to various extents, indicating that they have different morphological stabilities. The dependence of the morphological stability of the films on the guest species points to a possible influence of the guest molecular structure on the host/guest phase segregation. This may explain why using a different guest material in an otherwise identical OLED structure can alter device stability. For example, Ir(ppy)₂(acac), the guest material utilized in the least morphologically stable doped films, has the least symmetric molecular structure, which can be expected to make it more polar, and thus a stronger tendency to segregate from the less polar CBP host. Ir(ppy)₃, in contrast, has the most symmetric molecular structure. Therefore CBP:Ir(ppy)₃ host:guest system may be the least susceptible to this phase segregation. This perhaps sheds light on why devices in which Ir(ppy)₂(acac) is used instead of Ir(ppy)₃ generally have a much lower EL stability [65].

In order to further understand and verify the connection between the morphological changes and the deterioration in device EL with time, time-resolved fluorescence measurements are carried out on the films shown in Figure 6.4. Figure 6.7 (a) presents the CBP fluorescence decay characteristics at 389 nm, 407 nm and 436 nm collected from the neat CBP films before heating. These three wavelengths are selected because they correspond to the three vibronic bands observed in the PL spectra in figure 6. As expected, the fluorescence at longer wavelengths exhibits a slower decay rate, indicating that singlet exciton lifetime becomes longer, in agreement with predictions from basic theory that the oscillator strength decreases as the wavelength of the transition increases [15]. Measurements on the heated neat films (Figure 6.7 (b)) again show the same trend. However, in this case, the fluorescence decay rates are significantly shorter, especially for the 389 nm transition. The decrease in exciton lifetime with heating points to the formation of additional pathways by which excitons can now lose their energy non-radiatively, and is fully consistent with the occurrence of molecular aggregation. Due to increased intermolecular interactions in aggregate morphologies, new quenching pathways become efficient, and compete with the radiative fluorescence process, resulting in a decrease in the fluorescence quantum yield of the material (an effect commonly known as

“concentration quenching” [15]). Since the shorter wavelength excitons are the most efficient players in the host-to-guest energy transfer process (due to their larger oscillator strength), quenching of these excitons will result in significant reductions in energy transfer to the guest. To see this effect more clearly, the exciton lifetime at 389 nm in films with various dopants and doping concentrations are measured and the results are shown in Figure 6.8 (a). It can be seen that as the doping concentration increases, the exciton lifetime decreases, reflecting the expected increase in energy transfer from the host to the guest as the concentration of the latter increases. More interestingly however, the exciton lifetimes in all films (regardless of their guest content) after heating become similar to that of the heated neat CBP as shown in Figure 6.8 (b). This verifies that phase segregation between the host and the guest indeed occurs in all films by heating, and that CBP becomes aggregated. These results also confirm that the deterioration in device EL results from a decrease in the quantum yield of the host due to its aggregation, which in turn can lead to a decrease in energy transfer from host to guest with time, causing the observed gradual decrease in guest EL. It is also noteworthy to point out that the data also shows that CBP excitons exhibit very similar lifetimes in case of films doped with Ir(ppy)₃ and Ir(ppy)₂(acac), indicating that energy transfer rates from the host to either guest is comparable. This suggests that the difference in device lifetime when these two guests are used is primarily governed by the differences in the morphological stability of the two host:guest systems as noted above, and is less dependent on the rate of exciton quenching on the host [62].

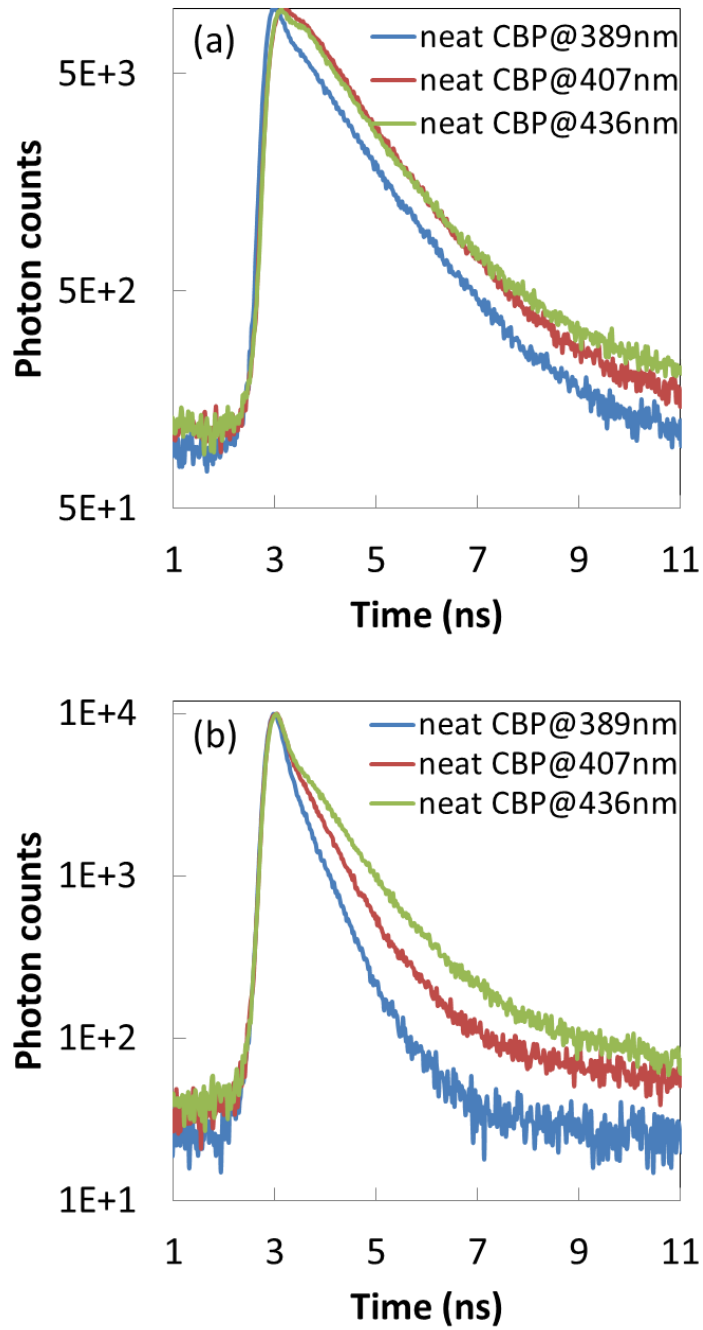


Figure 6.7 Exciton lifetime in neat CBP films measured at various detection wavelength (a) before and (b) after heating at 120°C for 6 minutes.

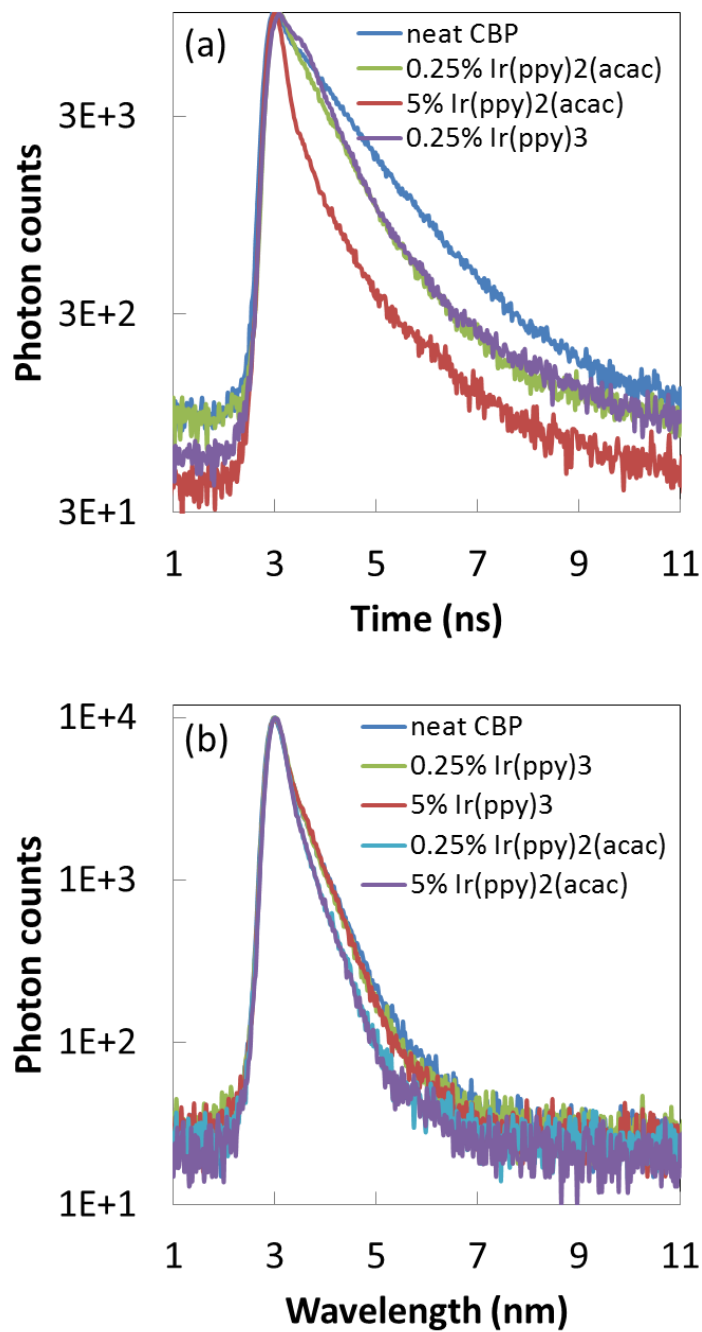


Figure 6.8 Exciton lifetime of CBP films with various doping conditions measured at 389nm detection wavelength (a) before and (b) after heating at 120°C for 6 minutes.

In order to establish that the above phenomena occur in other host:guest systems, and are not limited to ones utilizing CBP as a host, similar investigations are conducted on systems in which

26DCzPPy ($T_g = 102\text{ °C}$ [97]) and TAPC ($T_g = 78\text{ °C}$ [98]), two other widely used host materials in OLEDs, are utilized. 26DCzPPy is selected because it is commonly used as a host material for blue emitting phosphorescent guest materials [99], whereas TAPC is selected because, unlike CBP and 26DCzPPy, it is not a carbazole but rather a tertiary aromatic amine and thus represents a different class of materials from a molecular structure standpoint. As before, a range of typical guest materials is used with each of these hosts.

Figure 6.9 presents PL images of 26DCzPPy films doped with various guest materials and at various concentrations, before and after heating at 160 °C for 1 mins. The film compositions from left to right are: 26DCzPPy:Ir(ppy)₃ (0.25%) (30 nm), 26DCzPPy:Ir(ppy)₃ (5%) (30 nm), 26DCzPPy:Ir(ppy)₂(acac) (0.25%) (30 nm), 26DCzPPy:Ir(ppy)₂(acac) (5%) (30 nm), 26DCzPPy:FIrpic (0.25%) (30 nm), 26DCzPPy:FIrpic (5%) (30 nm) and 26DCzPPy (30 nm). A comparison of these images with those in Figure 6.4 clearly shows that the same trends occur in the 26DCzPPy films. Although it is difficult to compare the size of the crystallites in this figure by the naked eye, microscopic examination (images shown in Figure 6.10) reveals that films with lower guest concentration levels indeed have more aggregates. Once again, the film containing Ir(ppy)₂(acac) shows more aggregation than that containing Ir(ppy)₃, which shows that using Ir(ppy)₂(acac) as a dopant brings about only modest levels of morphological stability enhancements to host materials in comparison to Ir(ppy)₃. Furthermore, it can also be seen that the film doped with FIrpic shows the most significant aggregation, consistent with the widely known behavior that devices using FIrpic as the emitter generally have a much shorter EL lifetime in comparison to their green emitter-doped counterparts. The close correlation between the changes in the morphological stability of the films with the dopant material and its concentration on one hand, and the well-known EL stability trends (shown in Figure 6.11, devices subjected to constant electrical driving at 20 mA/cm^2) of devices using these dopants on the other hand show that device EL stability is indeed primarily governed by the morphological stability of the host material, and how it is influenced by the presence of the dopant.

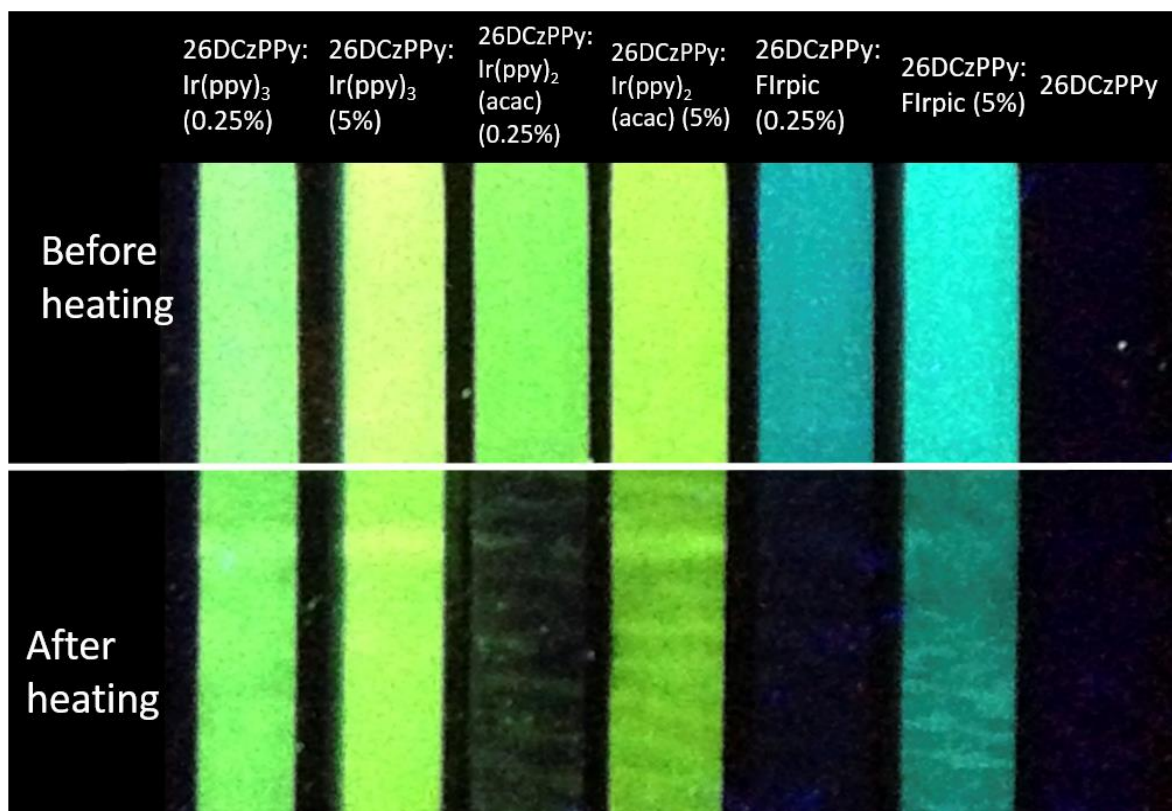


Figure 6.9 Image of films (top) before and (bottom) after heating at 160°C for 1 minute, taken under UV irradiation. The film compositions from left to right are: 26DCzPPy:Ir(ppy)₃ (0.25%) (30 nm), 26DCzPPy:Ir(ppy)₃ (5%) (30 nm), 26DCzPPy:Ir(ppy)₂(acac) (0.25%) (30 nm), 26DCzPPy:Ir(ppy)₂(acac) (5%) (30 nm), 26DCzPPy:FIrpic (0.25%) (30 nm), 26DCzPPy:FIrpic (5%) (30 nm) and 26DCzPPy (30 nm).

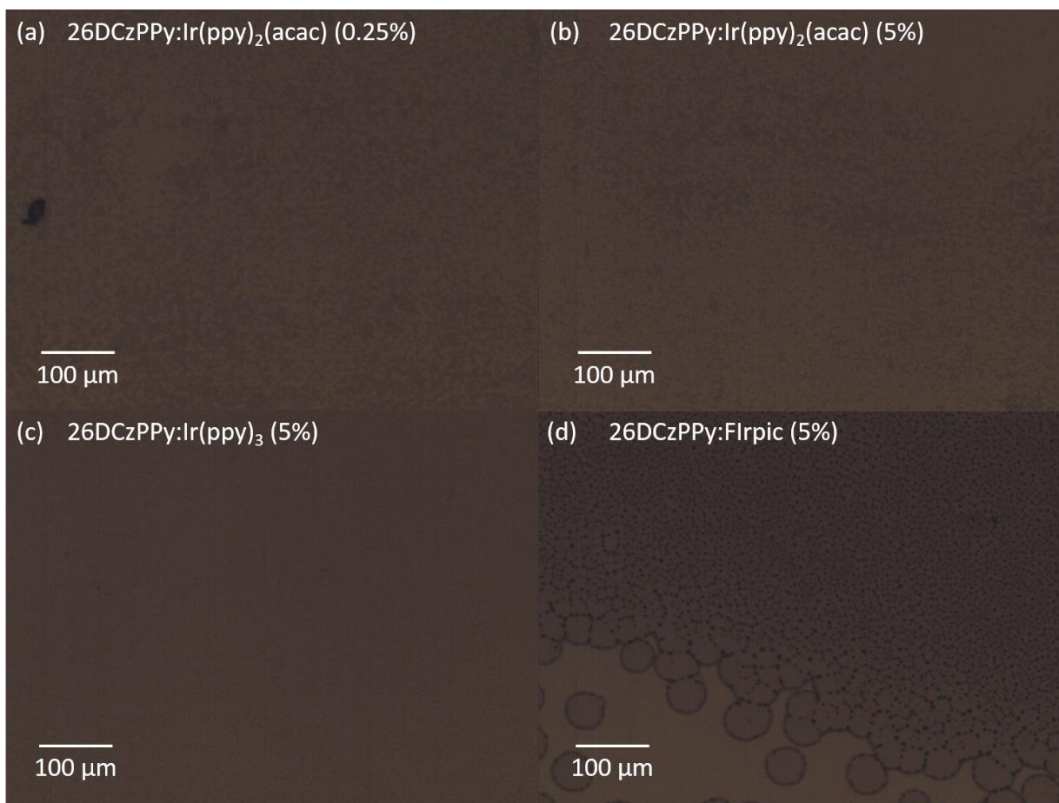


Figure 6.10 Microscope images of (a) 26DCzPPy:Ir(ppy)₂(acac) (0.25%) (30 nm), (b) 26DCzPPy:Ir(ppy)₂(acac) (5%) (30 nm), (c) 26DCzPPy:Ir(ppy)₃ (5%) (30 nm) and (d) 26DCzPPy:FIrpic (5%) (30 nm) films after heating at 160°C for 1 minute.

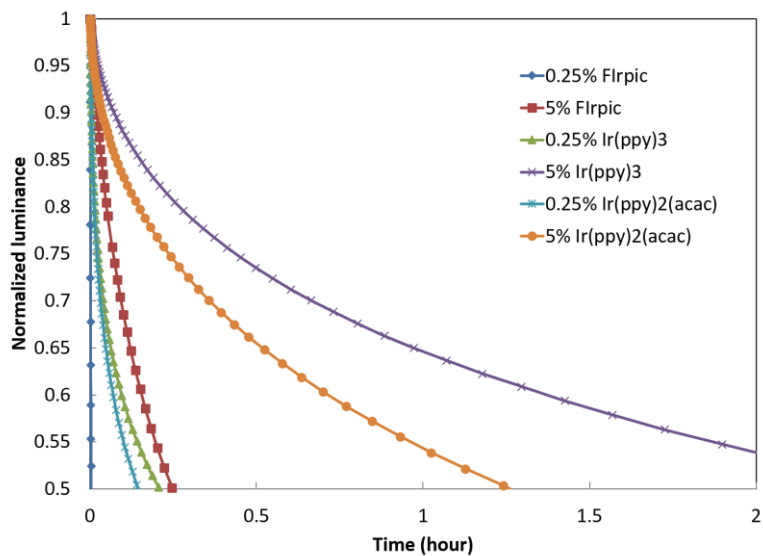


Figure 6.11 Changes in device EL over time of devices with various dopant materials and concentrations under electrical driving at 20 mA/cm².

Figure 6.12 presents PL images of TAPC films doped with various guest materials and at various concentrations, before and after heating at 140 °C for 2 mins. The film compositions from left to right are: TAPC:Ir(ppy)₃ (0.25%) (30 nm), TAPC:Ir(ppy)₃ (5%) (30 nm), TAPC:Ir(ppy)₂(acac) (0.25%) (30 nm) and TAPC:Ir(ppy)₂(acac) (5%) (30 nm). Once again, microscope images (shown in Figure 6.13) show the same general behavior. These results indeed suggest that the phenomena observed here are not limited to a specific material or a host:guest system, but rather have a universal presence.

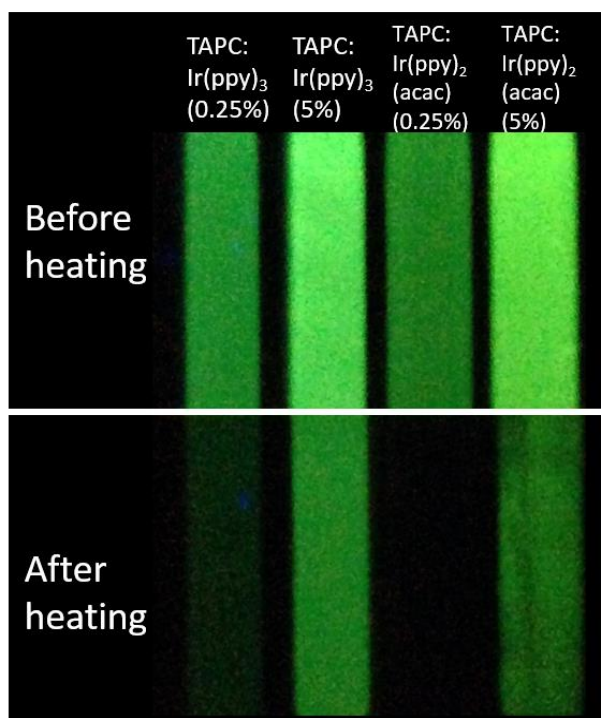


Figure 6.12 Image of films (top) before and (bottom) after heating at 140°C for 2 minutes, taken under UV irradiation. The film compositions from left to right are: TAPC:Ir(ppy)₃ (0.25%) (30 nm), TAPC:Ir(ppy)₃ (5%) (30 nm), TAPC:Ir(ppy)₂(acac) (0.25%) (30 nm), TAPC:Ir(ppy)₂(acac) (5%) (30 nm).

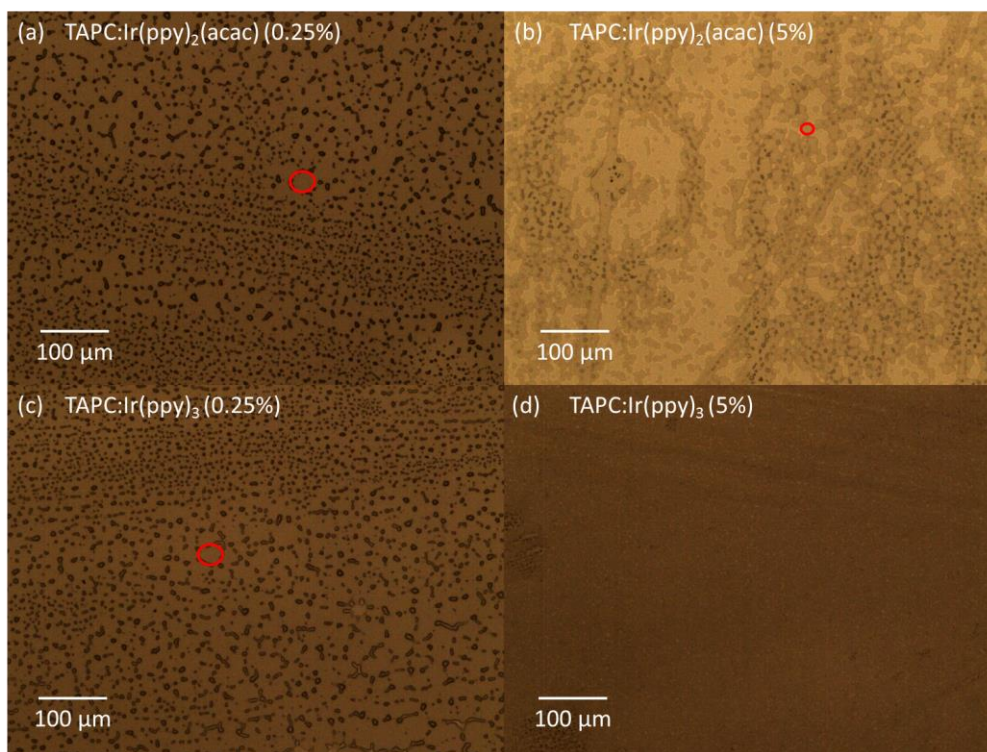


Figure 6.13 Microscope images of (a) TAPC:Ir(ppy)₂(acac) (0.25%) (30 nm), (b) TAPC:Ir(ppy)₂(acac) (5%) (30 nm), (c) TAPC:Ir(ppy)₃ (0.25%) (30 nm) and (d) TAPC:Ir(ppy)₃ (5%) (30 nm) films after heating at 140°C for 2 minutes. Red circles indicate the average sizes of the crystallites.

The root causes of the differences in EL stability among PHOLEDs utilizing different emitter guests are studied. The results show that the host plays a more influential role in limiting device stability. During the electrical driving of a PHOLED, the host undergoes aggregation due to the interactions between the excitons and positive polarons. The rate of this aggregation is found to be the limiting factor for device lifetime. Moreover, the aggregation rate of the host is affected by the choice of the guest material and its concentration. Finally, it is shown that phase segregation between the host and the guest is an important aspect of these morphological changes. Because of this segregation, transfer of excitons from the host to the guest becomes increasingly less efficient in the devices, resulting in the loss in EL efficiency over time. The findings explain why PHOLEDs utilizing different guest materials but otherwise identical material systems can have significantly different lifetimes.

Knowing that the aggregation of the host caused by exciton-polaron interactions is the key to device degradation, approaches to suppress this degradation can include reducing (a) exciton and (b) polaron concentrations at the organic/organic interface.

6.2 Approaches for Suppressing Degradation

6.2.1 Reducing Exciton Concentration at the Organic/Organic Interface

Reprinted with permission from ACS Appl. Mater. Interfaces, vol. 6, no. 3, pp. 1697–701, 2014⁵. Copyright 2014 American Chemical Society.

In order to study the influence of reducing excitons concentration at the organic/organic interface on PHOLED stability, the effect of increasing the thickness of the EML is studied. A thicker EML can be expected to lead to a wider and less confined e-h recombination zone, thus a lower exciton concentration at the EML/ETL interface. Therefore, devices are fabricated with the following structure: ITO/MoO₃ (5 nm)/CBP (30 nm)/CBP:Ir(ppy)₃ (5%) (x nm)/TPBi (40 nm)/LiF (0.8 nm)/Al (80 nm), where x = 10, 20 and 30, as shown in Figure 6.14 inset. Figure 6.14 shows the changes in EL with respect to time under electrical bias to maintain constant current flows of 20 mA/cm² for devices with 10, 20 and 30 nm EML. In this figure, the change in EL is represented in the form of normalized luminance, i.e. luminance/initial luminance, where the initial luminance for these devices with 10, 20 and 30 nm EML are 6720, 6840 and 5640 cd/m², respectively. It clearly shows that increasing the thickness of the EML leads to a longer device lifetime. To verify if a thicker EML indeed leads to a broader recombination zone, hence a lower exciton concentration at the organic/organic interface, a neat layer of the host material – CBP, is inserted between the EML and the ETL in the devices, to be employed as a marking layer. Figure 6.15 inset (a) shows the EL spectra for devices with and without the neat CBP layer. The device structures for these devices are ITO/MoO₃ (5 nm)/CBP (20 nm)/CBP:Ir(ppy)₃ (5%) (15 nm)/ CBP (10 nm)/TPBi (1 nm)/LiF/Al and ITO/MoO₃ (5 nm)/CBP (25 nm)/CBP:Ir(ppy)₃ (5%) (15 nm)/TPBi (40 nm)/LiF/Al, respectively. Since only the device with the neat CBP marking layer shows emission from CBP, it is clear that significant e-h recombination occurs in the neat CBP layer, suggesting that charge transport in it is primarily bipolar, and is therefore not limited to electron transport. The intensity of the CBP

⁵ All work presented in this sub-section were done by the author with helpful discussions from the co-author Qi Wang.

emission is used to probe the exciton concentration at the CBP/TPBi interface. Figure 6.15 shows the EL spectra of the devices with the neat CBP marking layer and with different CBP:Ir(ppy)₃ layer thickness x (where, $x = 10, 15, 20, 25$ and 30), normalized to the Ir(ppy)₃ intensity. The EL spectra of these devices without normalization are provided in inset (b). As the thickness x increases, the emission from CBP is seen to decrease, indicating a decrease in exciton density. This observation verifies that increasing the thickness of the EML indeed leads to a lower exciton density in the vicinity of the CBP/TPBi interface.

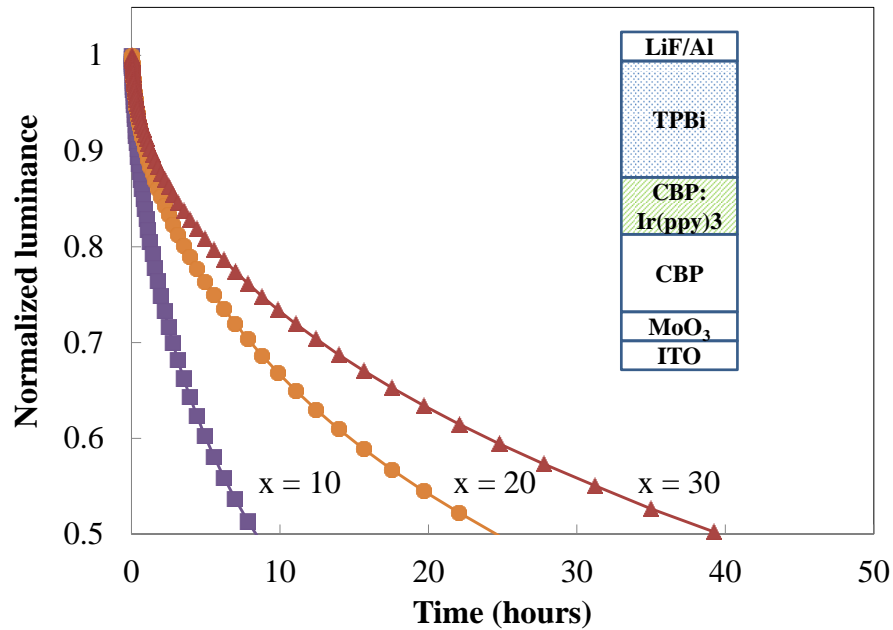


Figure 6.14 Changes in EL with time under 20 mA/cm² current density for devices with 10, 20 and 30 nm EML all utilizing 30 nm CBP HTL and 40 nm TPBi ETL. (Inset) The structures of these devices.

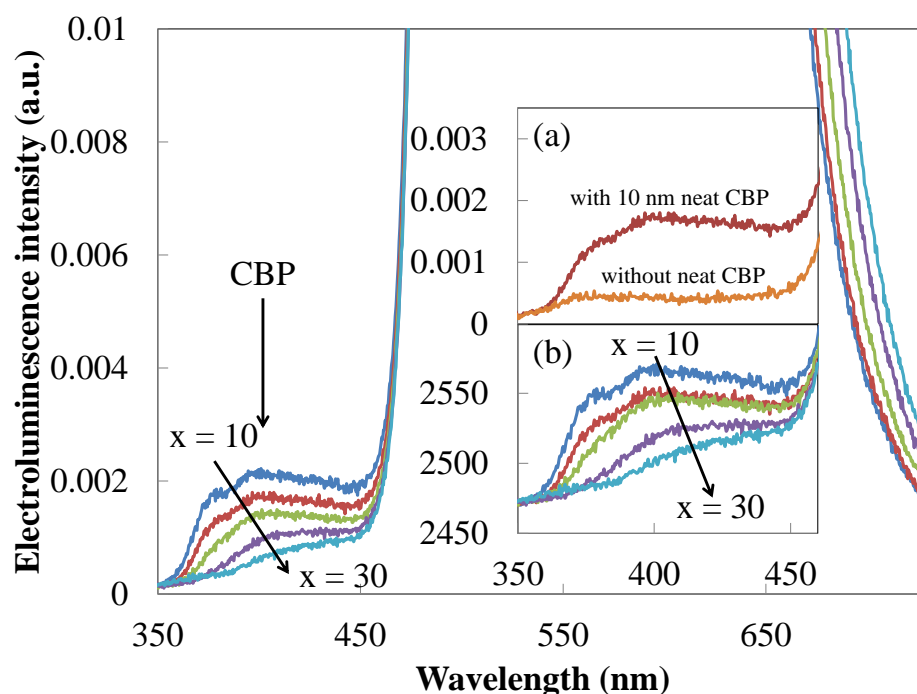


Figure 6.15 Inset (a) EL spectra for devices with and without the 10 nm neat CBP layer. EL spectra for devices with 10, 15, 20, 25 and 30 nm EML and with 10 nm neat CBP marking layer, normalized to Ir(ppy)₃ emission. Inset (b) EL spectra of these devices without normalization.

Although the lifetime of a simplified PHOLED can be increased by increasing the thickness of the EML, the charge balance, hence the device efficiency is also altered. Figure 6.16 shows the current efficiency versus current density of devices with various organic layer structures. The current density versus voltage (J-V) characteristics of these devices are also shown in the inset. It can be seen that the current efficiency of a device with 30 nm EML is significantly lower than that of a device with 10 nm EML (denoted as device A), both utilizing a 30 nm CBP HTL and a 40 nm TPBi ETL. Changing the ETL thickness from 40 nm to 2 nm in this device (i.e. with 30 nm EML) results in a significant efficiency improvement (denoted as device B). Further improvement can be achieved by removing the Ir(ppy)₃ dopant for the 10 nm of the EML adjacent to the EML/ETL interface, thereby having only a neat CBP layer. Using 1 nm of BmPyPhB [100] instead of 2 nm of TPBi is found to benefit the efficiency even further (denoted as device C). It is important to point out that although device C has relatively high efficiency, it is still slightly less efficient than device A. This may be due to the smaller distance between the EML and the reflective cathode, which can lead to less optimal

optical interference. Optical modeling of OLEDs with the ultrathin ETLs can provide invaluable guidance in this regard, and will therefore be pursued in the future. Despite less optimal optical interference, it is still quite surprising that a device with an ETL as thin as only 1 nm can have such comparable efficiency. Figure 6.17 shows the changes in EL over time under constant 20 mA/cm² current density for devices A, B and C. The device structures are also shown in Figure 6.17 inset. The initial brightness for device A, B and C are 5640, 6960 and 7870 cd/m², respectively. It can be seen that the device with 1 nm BmPyPhB (device C) has roughly the same lifetime (i.e. the extended lifetime) as the device with 30 nm EML (device B). Therefore, by using this structure with only 1 nm BmPyPhB ETL, higher efficiency and stability can be simultaneously achieved. Another benefit is the significant reduction in device thickness. The structure with the ultrathin ETL has around 50 nm thick organic materials in total, i.e. only half the thickness of typical PHOLEDs. This thinner structure can be expected to offer advantages in lowering fabrication cost by reducing material consumption and processing time.

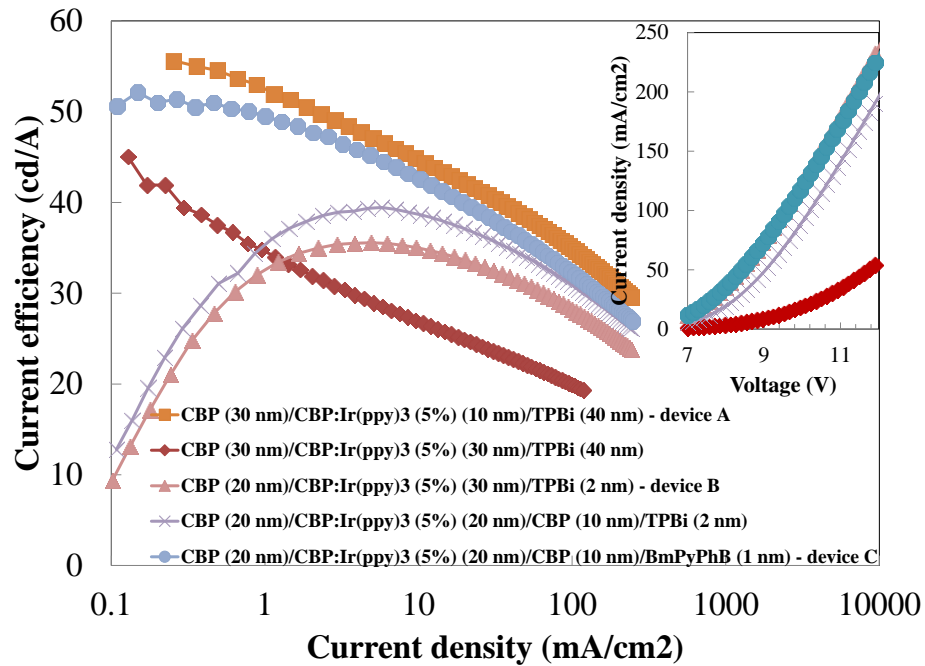


Figure 6.16 Current efficiency vs. current density characteristics of selected devices. (Inset) Current density vs. voltage characteristics of these devices.

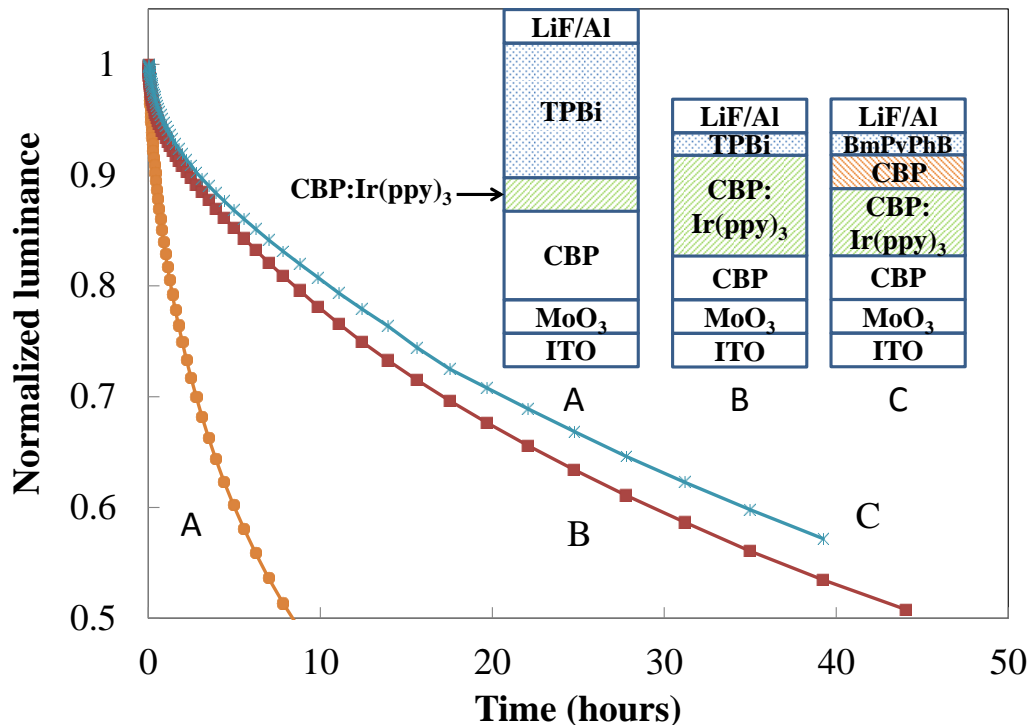


Figure 6.17 Changes in EL with time of devices A, B and C. (Inset) The structures of these devices.

It is noteworthy to point out that in the tests on various ETL/EIL configurations, it is found that only a few electron transport materials can be used in this ultrathin structure to obtain high device efficiencies. Figure 6.18 shows the current efficiency versus current density of devices with selected ETL/EIL configurations. The “simplified reference” device refers to the device with the CBP (30 nm)/CBP:Ir(ppy)₃ (5%) (10 nm)/TPBi (40 nm)/LiF (0.8 nm) structure. All other devices use the common CBP (20 nm)/CBP:Ir(ppy)₃ (5%) (20 nm)/CBP (10 nm) stack, followed by an ultrathin ETL and/or EIL. All devices with only an EIL (but no ETL) have poor efficiencies, regardless of the EIL material (LiF, Cs₂CO₃ or Ca). Surprisingly, despite being very thin, different ETLs (i.e. TPBi, BmPyPhB, BAlq and Alq₃) can lead to vastly different efficiencies, with only TPBi and BmPyPhB giving the highest efficiencies. Considering an ETL as thin as 1 nm can have such a major impact on device current efficiency, what roles this ETL plays in the device becomes an interesting question.

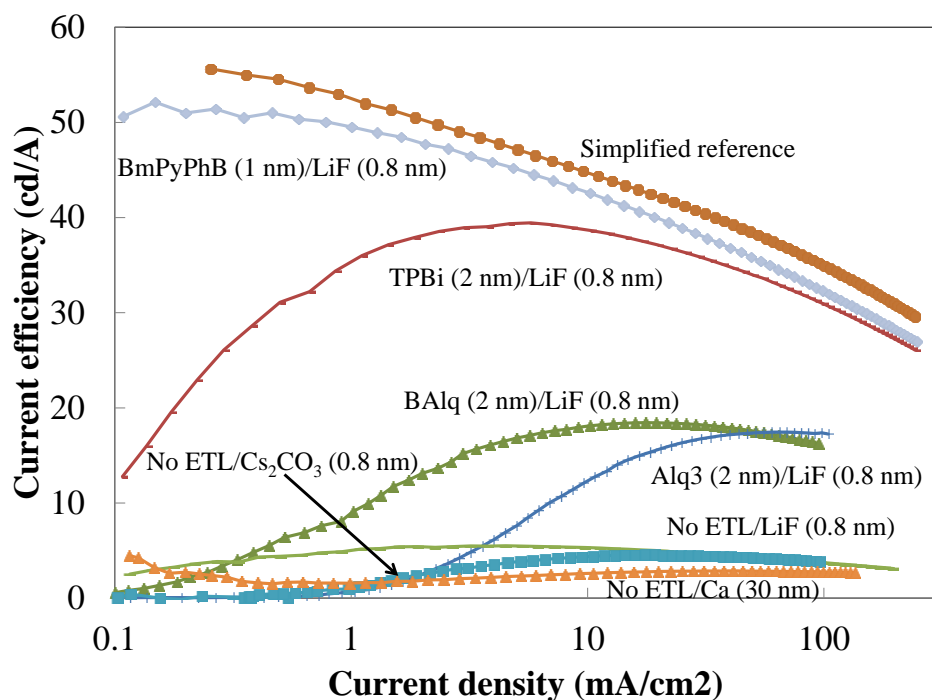


Figure 6.18 Current efficiency vs. current density characteristics of selected devices with different ETL/EIL configurations.

In addressing the roles of these ETLs, it is important to first examine layer coverage and whether continuous layers of these materials at these thicknesses (~ 1 nm) are formed. For this purpose, devices with the common CBP (20 nm)/CBP:Ir(ppy)₃ (5%) (20 nm)/CBP (10 nm) structure followed by the specific ETL listed are studied. An EIL consisting of 0.8 nm LiF and a cathode of 80 nm Al is used in all devices. Figure 6.19 (a) shows the J-V characteristics of devices in which BCP is used as the ETL, of various thicknesses. It is important to note that the driving voltage first decreased as the thickness of the BCP layer is increased from 0.8 nm to 3 nm, and then increased on further increasing the thickness to 10 nm. This trend suggests that a complete coverage of the CBP layer by the BCP layer is achieved at a minimum BCP thickness of 3 nm, below which the coverage is only partial and leads to non-efficient electron injection. Thus, as the BCP thickness is increased to 3 nm, the driving voltage gradually decreases. On the other hand, an increase in film thickness beyond 3 nm results in a longer electron transport pathway, hence the increase in driving voltage. Therefore, the coverage of the ETL appears to play an important role in the J-V characteristics behavior of the device.

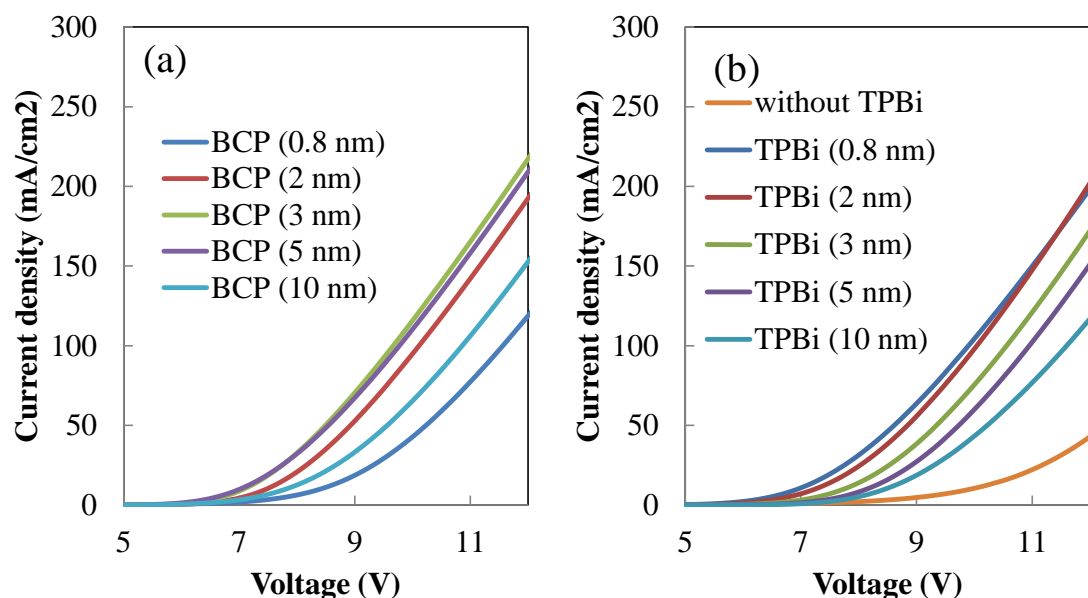


Figure 6.19 Current density vs. voltage characteristics of devices with various (a) BCP and (b) TPBi ETL thicknesses.

The roles of the ultrathin ETL in increasing device efficiency are then examined. In general, ETLs increase device efficiency by the following means: facilitating electron injection/transport, blocking holes and blocking excitons [101]. In the context of devices with ETLs as thin as 1 nm, electron mobility of the ETL cannot play an important role. Moreover, since the cathode is at ~ 1 nm distance of the interface where excitons are created (i.e. EML/ETL interface), the role of the ETL in blocking singlet excitons must be insignificant since quenching by long range Förster transfer to the metal can occur. As a result, only triplet exciton blocking can have an effect on device efficiency. Therefore, the three possible roles of the ultrathin ETL on increasing efficiency are (1) electron injection, (2) hole blocking and (3) triplet exciton blocking.

In order to examine the role of the ultrathin ETL in facilitating electron injection, the driving voltages of the device with and without the ultrathin ETL are studied. Figure 6.19 (b) shows that the driving voltage of the device without a TPBi ETL is significantly higher than that of the device with a 2 nm TPBi ETL, beyond which the coverage of the TPBi film becomes complete, as indicated in the figure. It is clear that the electron injection is facilitated when the ultrathin ETL is present. Since

electron injection significantly affects charge balance, it is natural that electron injection plays an important role in increasing device efficiency.

Next, the hole blocking role of the ETL is examined by studying OLEDs utilizing various ETL materials (BAIq, BmPyPhB and Alq₃) in different thicknesses. At first glance, it seems that the HOMO level of the ETL has an effect on device efficiency, as shown in Figure 5. When the HOMO level of the ETL is shallower than that of the CBP (e.g. 5.9 eV for BAIq and 5.7 eV for Alq₃ versus 6.1 eV for CBP), holes can leak to the ETL, and the devices have low efficiencies. On the other hand, when the HOMO level of the ETL is deeper than that of CBP (e.g. 6.2 eV for TPBi and 6.67 eV for BmPyPhB versus 6.1 eV for CBP), which leads to an injection barrier for holes, the devices exhibit high efficiencies. Considering that BAIq is widely used as an ETL for Ir(ppy)₃-based highly efficient PHOLEDs [102], [103], this finding is very surprising. A closer look at the effect of the ETL thickness on device efficiency, however, reveals that high efficiency can still be achieved in the device with ~ 10 nm BAIq ETL, as shown in Figure 6.20 (a). This result suggests that hole blockage by BAIq is achieved by the low hole mobility of the material [104], hence a relatively thicker ETL is required. On the other hand, hole blocking by TPBi and BmPyPhB is obtained by deeper HOMO levels, thus only a thinner ETL is sufficient in these cases, as indicated in Figure 6.20 (b) that a thicker BmPyPhB does not improve efficiency much. When Alq₃ is used as the ETL in this study, the efficiency of the device increases as the ETL thickness increases but saturates at ~ 25 cd/A (shown in Figure 6.20 (c)). Since hole mobility in Alq₃ is comparable to that in BAIq [73], [104], it is expected that the capacity of hole blocking in both thick films are similar. However, since the triplet energy of Alq₃ is lower than that of BAIq [105], [106], better triplet exciton blocking, and hence higher efficiency is expected in BAIq devices. This is in line with the common understanding that triplet exciton blocking is important in achieving high efficiency in PHOLEDs.

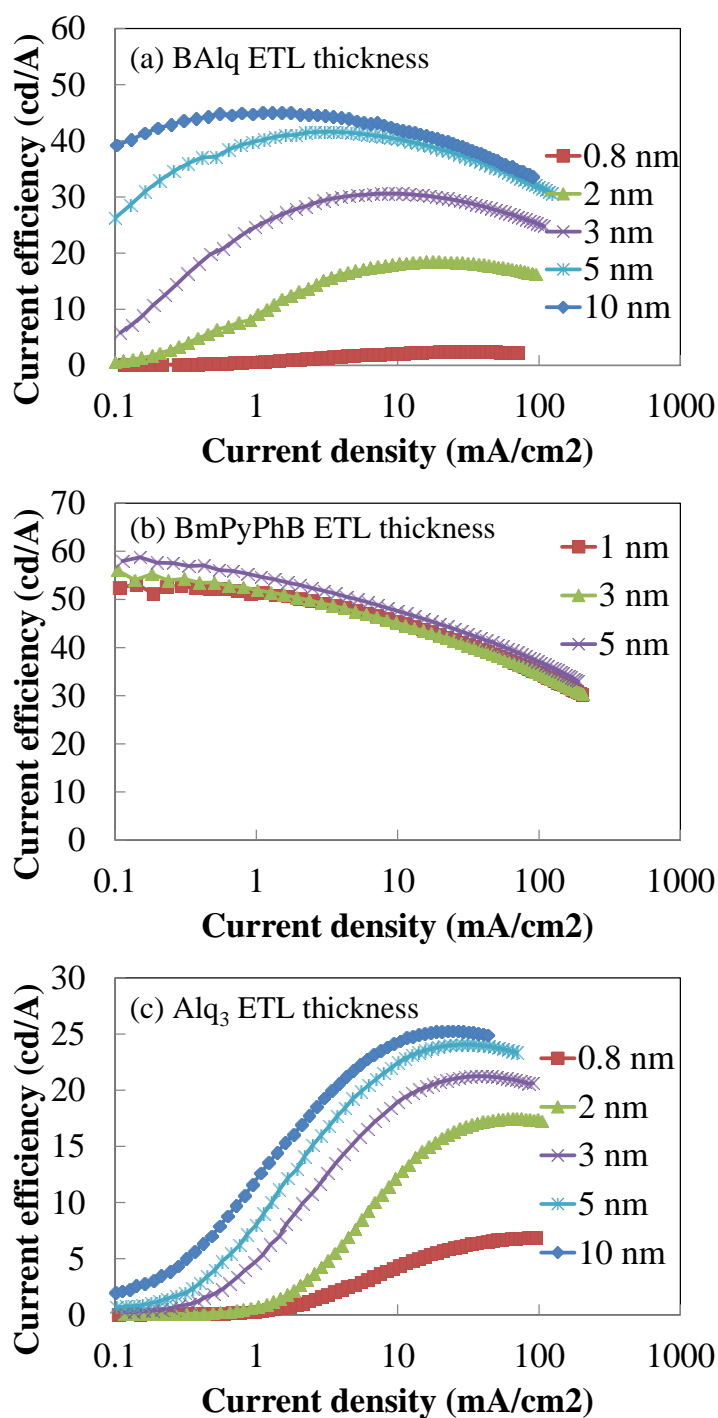


Figure 6.20 Current efficiency vs. current density characteristics of devices with various (a) BA1q, (b) BmPyPhB and (c) Alq₃ ETL thicknesses.

In conclusion, reducing the exciton density near the interface by means of increasing the EML thickness can lead to increased device lifetime. Moreover, it is shown that devices incorporating a BmPyPhB ETL as thin as 1 nm can have both high efficiency and this extended lifetime. The roles of this ultrathin ETL include facilitating electron injection and blocking holes and triplet excitons. In order to utilize this structure with an ultrathin ETL, this layer should satisfy the following requirements: (1) the layer should have complete coverage; (2) it should help lower the electron injection barrier; (3) the HOMO level of the material should be deeper than that of the host to ensure good hole blocking; and (4) the triplet energy of the material should be comparable to or preferably wider than that of the host to have good blocking on triplet excitons. Another benefit of this structure is that the organic stack used is only 50 nm thick, which is more than 50% thinner than the typical PHOLEDs. This opens up opportunities for much shorter processing time and lower fabrication costs in PHOLEDs industry.

6.2.2 Reducing Polaron Concentration at the Organic/Organic Interface

The material presented in this section was published in Org. Electron., vol. 22, pp. 69–73, 2015. It is reproduced here with the permission from the publisher.

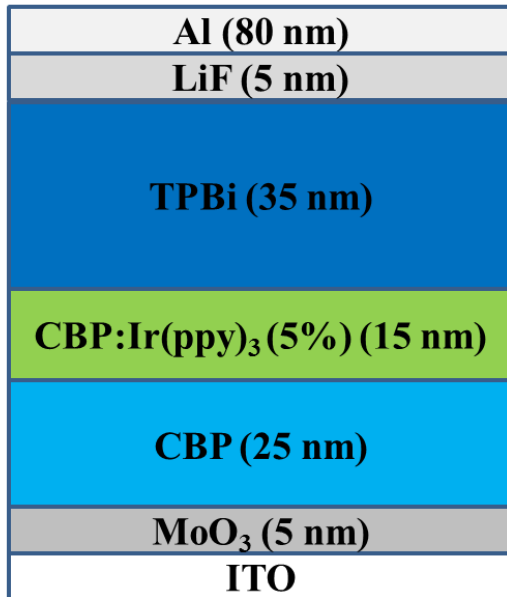
In the vast majority of OLEDs, the bottom electrode (i.e. the one adjacent to the substrate) functions as a hole injection anode with the other electrode functioning as an electron injection cathode. Recently, an inverted device architecture in which the functionality of the electrodes is inverted (i.e. the bottom and top electrodes function as cathode and anode, respectively) has gained much interest in the field. This is motivated by two major advantages that the inverted structure has (i) compatibility with the inexpensive n-channel a-Si thin film transistors (TFTs) used in active matrix displays [107]–[109], and (ii) potentially higher light outcoupling efficiency in top-emitting configuration [40], [41], [110]. As a result, a growing body of research has been focusing on PHOLEDs with inverted architecture recently, with the purpose of improving their efficiency. Surprisingly, the stability of inverted PHOLEDs has not been systematically studied to date, despite being an equally important aspect of OLED performance.

In this section, it is shown that the lifetime of an inverted simplified PHOLED is three times longer than that of a standard simplified PHOLED while having similar current efficiency. The underlying mechanism for the difference in stability is also studied. Results show that inverted

devices have higher electron/hole (e/h) ratio, resulting in less positive polarons at the emission layer/electron transport layer interface, thus reduced interfacial degradation.

First, to compare the performance of simplified PHOLEDs in standard and inverted architectures, devices are fabricated with the structures presented in Figure 6.21: standard device A – ITO/MoO₃ (5 nm)/CBP (25 nm)/CBP:Ir(ppy)₃ (5%) (15 nm)/TPBi (35 nm)/LiF (1nm)/Al (80 nm) and inverted device B - ITO/Mg (5 nm)/TPBi (35 nm)/CBP:Ir(ppy)₃ (15 nm)/CBP (30 nm)/ MoO₃ (5 nm)/Al (80 nm). It is important to point out that several EILs including Mg, LiF, LiNH₂ and CsCO₃ have been tested in the inverted device. Mg is chosen due to its good deposition reproducibility, which gives a more consistent device performance. The use of slightly different CBP layer thicknesses in the two structures is to achieve optimal efficiency in each case. In the standard architecture, optimizing the CBP thickness is mainly for adjusting charge balance; whereas in the inverted architecture, optimizing the CBP thickness is primarily for adjusting microcavity effects since it separates the emission zone from the reflective metal contact [66]. Figure 6.22 (a) presents the current density vs. voltage characteristics of these devices. It can be seen that the inverted device has a higher driving voltage, which can be attributed to the use of a thicker organic stack as well as an EIL with a deeper work function (3.7 eV for Mg vs. 2.6 eV for LiF), hence the presence of a higher injection barrier. Despite the difference in driving voltages, both devices demonstrate similar current efficiency, as shown in Figure 6.22 (b), suggesting that the exciton density in the EMLs of the two devices must be comparable. It is important to note that the efficiency roll-off behavior in these devices is dominated by host-host triplet-triplet annihilation as opposed to triplet polaron quenching [93]. Given the similar exciton density in the EML, it is not surprising that both devices also exhibit similar efficiency roll-off. The EL stability of these devices is tested by measuring luminance over time while the devices are electrically driven at a constant 20 mA/cm² current density. Figure 6.22 (c) presents the normalized luminance (luminance/initial luminance) of these devices over time. Interestingly, despite being made of the same organic materials, it can be seen that the inverted device shows a three times longer lifetime.

(a) Standard – Device A



(b) Inverted – Device B

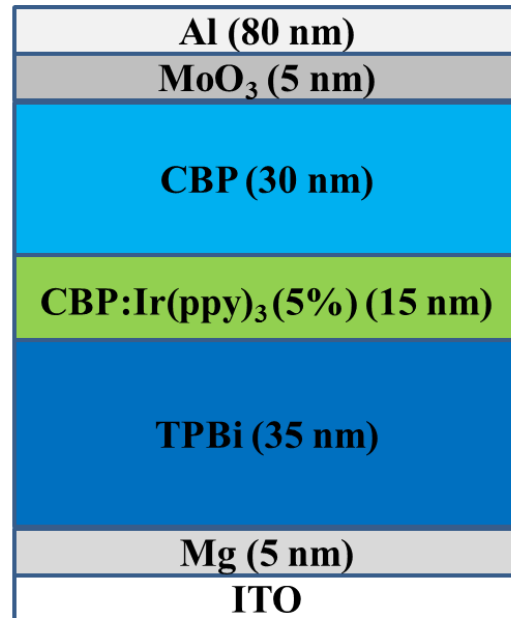


Figure 6.21 Device structures of simplified PHOLEDs in (a) standard and (b) inverted architectures.

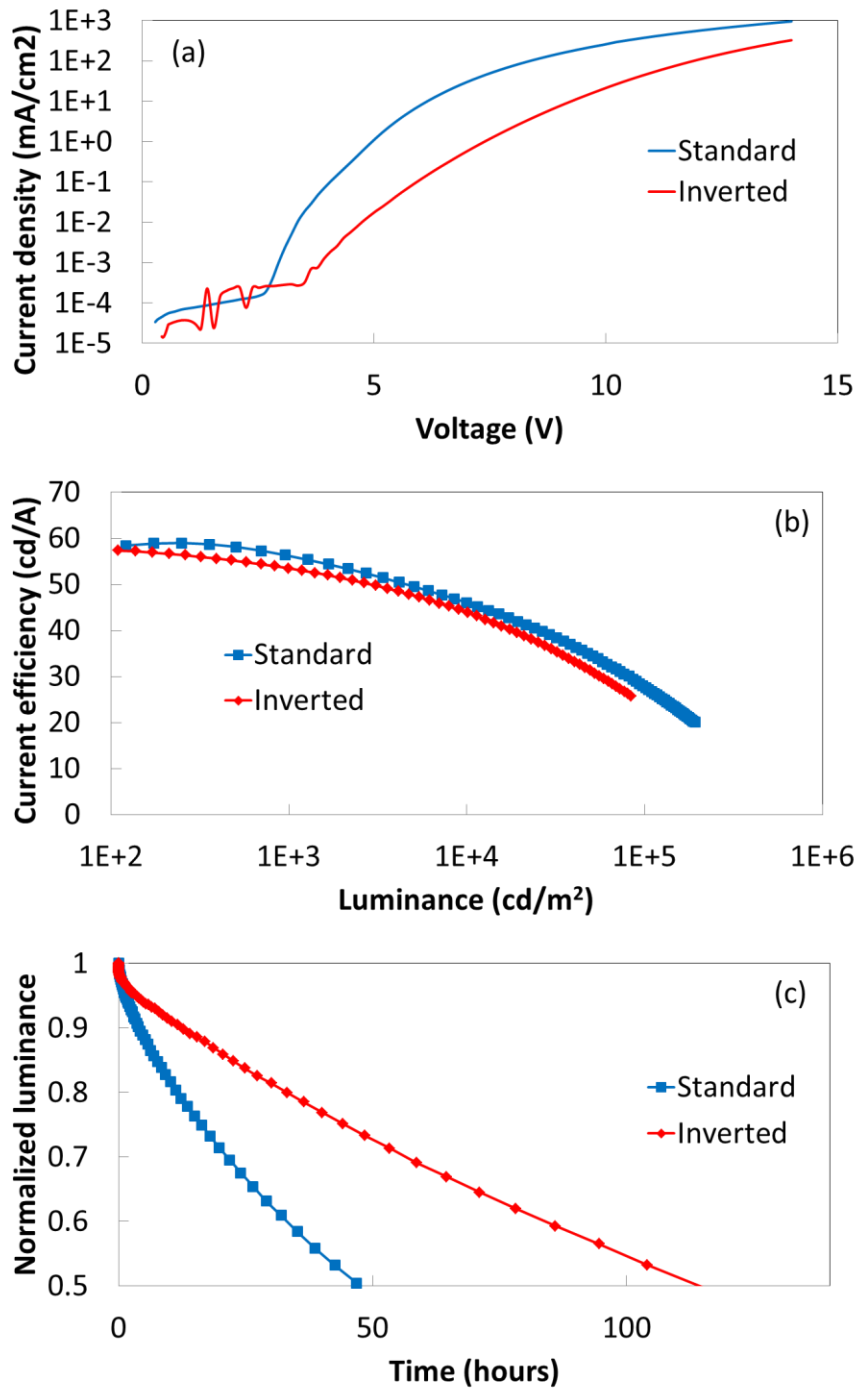
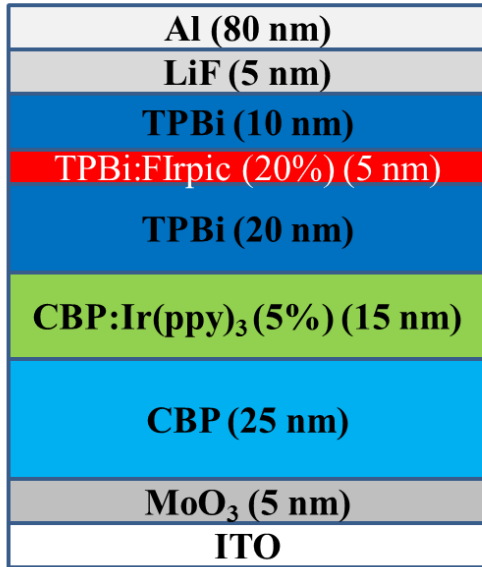


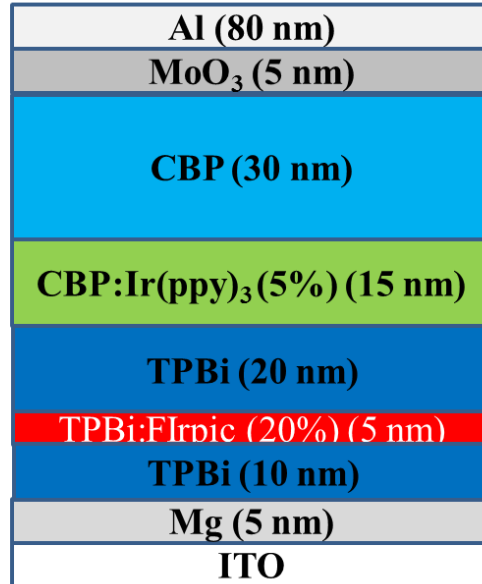
Figure 6.22 (a) JV characteristics, (b) current efficiency and (c) lifetime comparison of standard and inverted simplified PHOLEDs.

Seeing that the inverted device gives higher stability than the standard device despite the use of the same organic molecules, it naturally becomes interesting to identify the root cause of this behavior. It is recently found that excitons near the ITO/organic interface [71] and the organic/organic interface [61], [62], [75] in PHOLEDs play a dominant role in the deterioration of the EL intensity over time. To this end, luminescent marking materials are introduced in different layers of the two devices as a means for probing charge concentrations in them. Specifically, FIrpic is doped into CBP or TPBi as the luminescent marking material. FIrpic is selected due to its sufficiently different emission color from that of Ir(ppy)₃. At the same time, due to the similar energy of the HOMO levels of FIrpic and CBP and of the LUMO levels of FIrpic and TPBi, introducing FIrpic in CBP or TPBi does not significantly alter charge balance in the devices [71]. The structures of these test devices with the marking layers are shown in Figure 6.23. Devices C and D have the marking layers placed in the TPBi ETLs, whereas devices E and F have them in the CBP HTLs. Figure 6.24 presents the EL spectra of these devices, along with spectra from devices A and B, standard and inverted devices without the marking layer as reference. It is clear that standard and inverted devices with marking layers in TPBi show no emission from FIrpic (i.e. C and D), indicating that the transport of holes across the ETL is insignificant. This is likely due to the efficient hole blocking characteristics of the CBP/TPBi interface, which also results in hole accumulation in the vicinity of the interface [61]. On the other hand, strong FIrpic emission can be observed in standard and inverted devices with marking layers in the CBP (i.e. devices E and F), demonstrating that a significant number of electrons is transported across the HTL, hence the possibility for e-h recombination and exciton formation at the marking layer. This result agrees with previous findings that electron leakage currents are significant in simplified PHOLED [71]. Interestingly, it can also be noticed that the FIrpic emission in the inverted device is stronger than that in the standard device, indicating a larger electron leakage current, thus a higher e/h ratio across the HTL and the EML, hence a lower concentration of un-recombined trapped holes (i.e. positive polarons) in both layers. Since the interactions of positive polarons and excitons near the organic/organic interface can result in device degradation [61], [62], by having a bigger electron leakage current and a higher e/h ratio in the HTL and EML, the density of positive polarons, hence also exciton-polaron induced degradation at the EML/ETL interface is expected to be lowered.

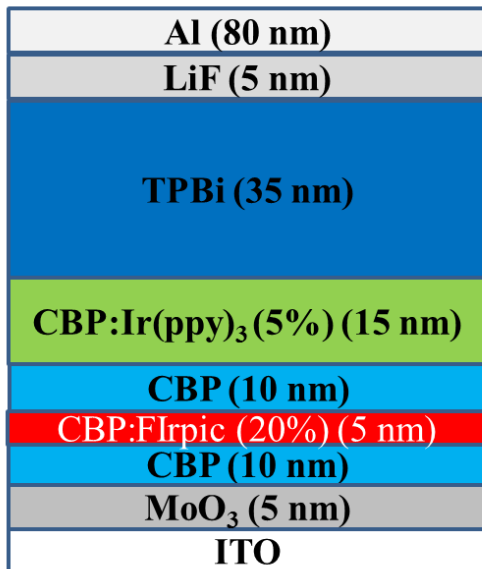
(a) Standard – Device C



(b) Inverted – Device D



(c) Standard – Device E



(d) Inverted – Device F

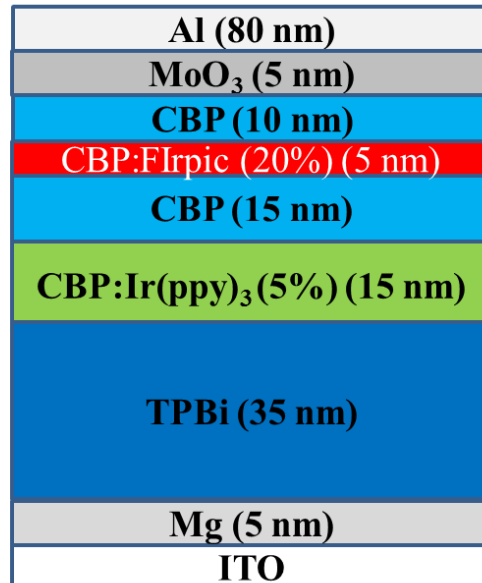


Figure 6.23 Device structures of (a) device C in the standard architecture and (b) device D in the inverted architecture with marking layers in TPBi, (c) device E in the standard architecture and (d) device F in the inverted architecture with marking layers in CBP.

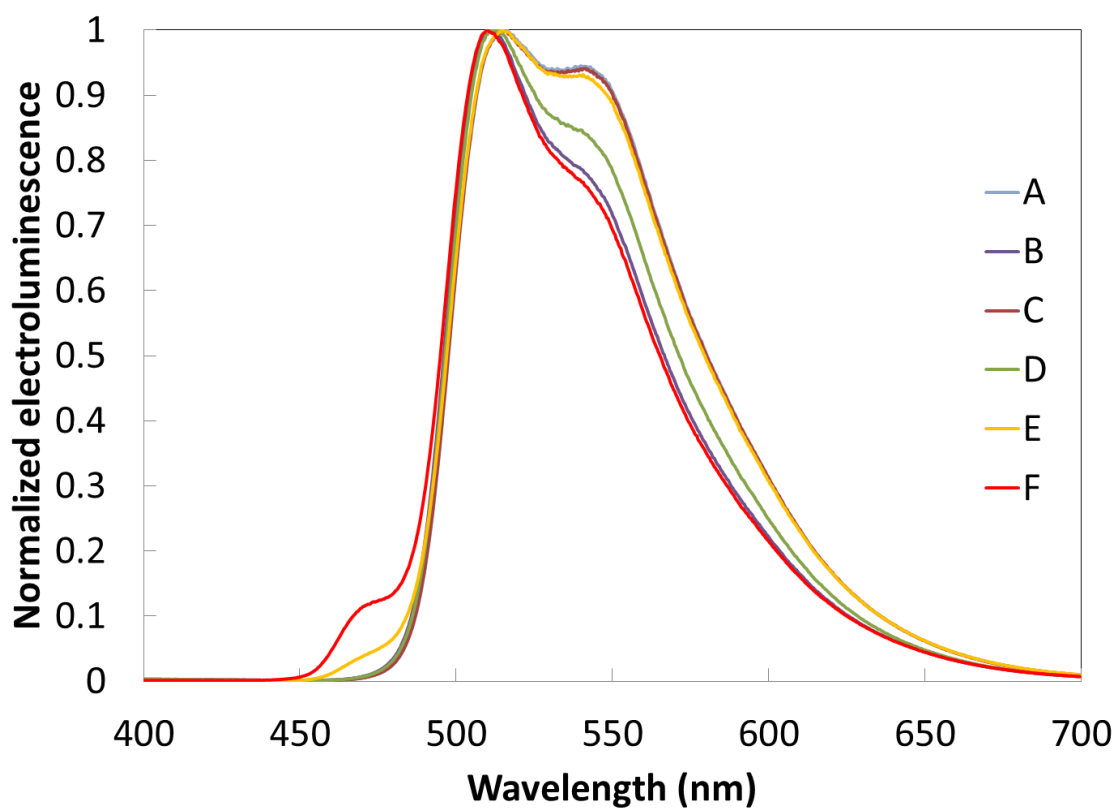


Figure 6.24 EL spectra of devices A, B, C, D, E and F.

To verify that devices with inverted architectures indeed have a lower concentration of positive polarons near the organic/organic interface, delayed EL characteristics of these devices are studied as they provide a direct way to assess difference in charge accumulation and have the advantage of allowing probing charges in the EML specifically. In this technique, a device is driven using a square pulse driving scheme with a pulse width of 0.5 ms (the pulse is sufficiently long enough for prompt EL to reach its steady-state intensity). An optical shutter opens to collect delayed EL 0.3 ms after the end of the forward bias pulse, which is significantly longer than the lifetime of Ir(ppy)₃ triplet state lifetime (<1 μs) to ensure the absence of any contributions from prompt EL in the collected signal. As such, any collected signal will arise from the radiative decay of excitons that are formed after the end of the forward bias pulse. A detailed description of the delayed EL measurement setup and signal detection protocol is reported elsewhere [70], [76], [88]. One common source of delayed EL is the recombination of charges that were initially trapped but are released after the end of the forward bias pulse. In order to identify contributions by this mechanism to the observed delayed EL, a 0.5 ms reverse bias pulse (of magnitude -10 V) is applied on a device during the delayed EL

signal collection, and subsequent changes in delayed EL characteristics are monitored as a means for probing charge redistribution effects. Figure 6.25 (a) and (b) present the delayed EL intensity over time of standard and inverted devices, respectively. Clearly, the response of the delayed EL to the reverse bias pulse is different in the two devices. In case of the standard device, the delayed EL shows a spike at the beginning of the reverse bias, indicating a sudden surge in e-h recombination. Since it has been shown above that the concentration of holes in the ETL is insignificant in these devices, it follows that the holes that are involved in e-h recombination and cause the delayed EL surge must originate from positive polarons that accumulate at the CBP/TPBi interface. On the other hand, the delayed EL of the inverted device shows no spike when the reverse bias is applied, indicating that there is a much lower concentration of positive polarons near the CBP/TPBi interface. Rather, a sudden non-reversible decrease in delayed EL intensity can be seen at the beginning of the reverse bias in this case. This sudden decrease can be attributed to the sweep-out of charges by the reverse electric field. Figure 6.26 illustrates the differences in charge distribution across the standard and inverted structures, depicting the higher concentration of positive polarons at the EML/ETL interface in the first structure. In this case, exciton-polaron interactions in the vicinity of the CBP/TPBi interface are significant, and, as such, lead to faster degradation of the interface hence the lower device stability. In contrast, since the concentration of positive polarons at the CBP/TPBi interface in the inverted device is much lower, the devices are more stable. It is also important to re-emphasize that standard and inverted devices have similar exciton density in the emission layer, as evident from their similar current efficiencies.

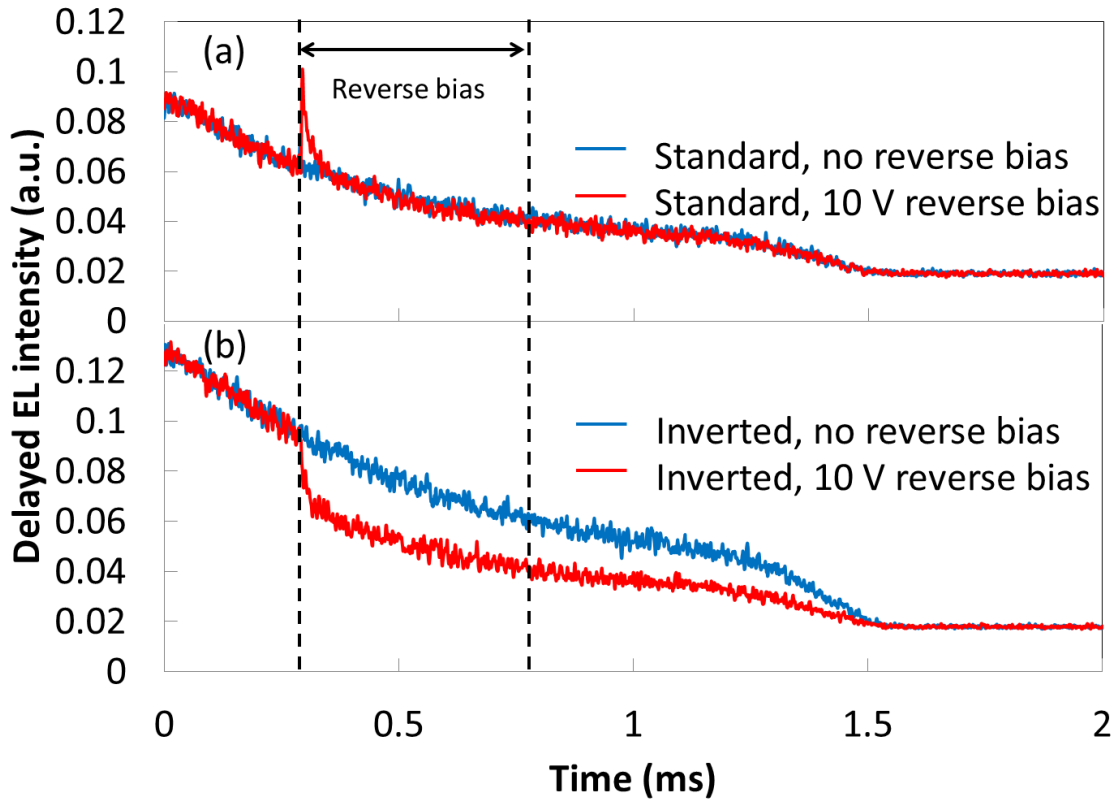


Figure 6.25 Delayed EL measurements of devices with (a) standard and (b) inverted structures with no reverse biases and with 10 V reverse biases.

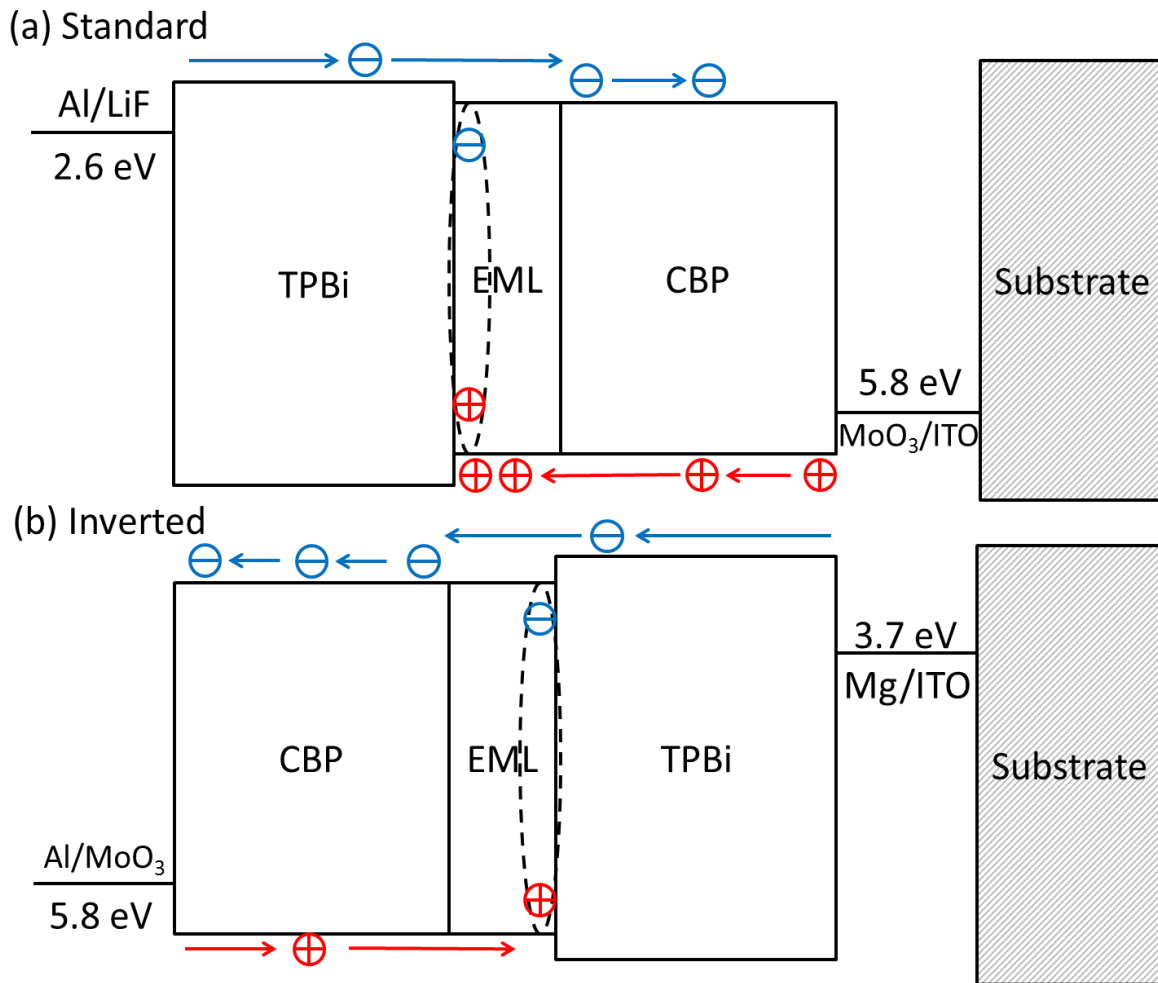


Figure 6.26 Proposed device operating mechanisms in (a) standard and (b) inverted simplified PHOLEDs. Blue and red arrows indicate the movement of electrons and holes in the devices under operation, respectively.

Since standard and inverted devices use the same materials and layer structures with the only one exception being the EIL (Mg in case of the inverted device but LiF in case of the standard device), the question whether the difference in the e/h ratio, and consequently stability may simply be due to the different EIL materials naturally arises. Therefore, standard devices in which Mg instead of LiF is used as EIL are fabricated and tested. These devices show a very short lifetime (< 1 hour), indicating that the higher stability of the inverted device is not simply the result of using Mg EIL.

It is important to point out that the increase in stability when using an inverted structure is not limited to Ir(ppy)₃ devices. Similar tests on devices using Ir(ppy)₂(acac) emitters also show that the inverted architecture gives three times higher stability compared to the standard one, as shown in Figure 6.27.

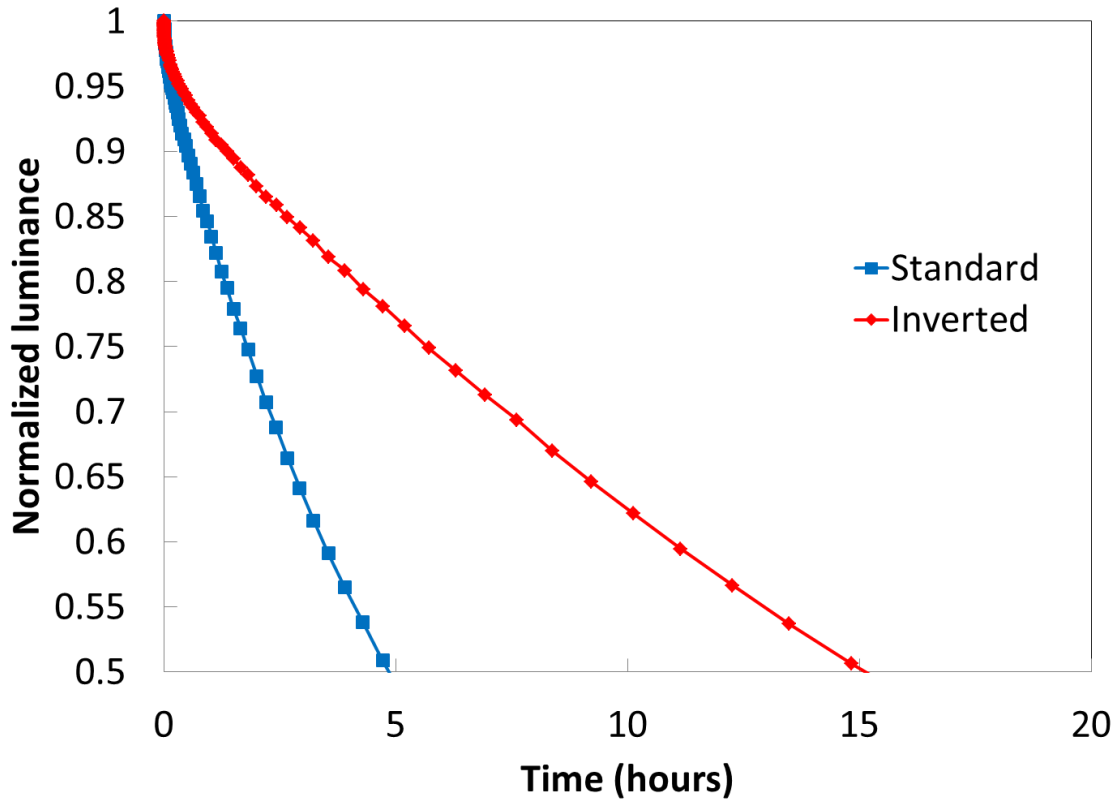


Figure 6.27 Lifetime of simplified PHOLEDs using Ir(ppy)₂(acac) emitters with standard and inverted structures

In conclusion, it has been demonstrated that inverted simplified PHOLEDs are three times more stable than the standard ones, while having the same current efficiency. The underlying mechanisms arise from a higher e/h ratio in the HTL and EML in the inverted devices, resulting in a lower concentration of positive polarons, hence reduced exciton-polaron induced degradations at the CBP/TPBi interface.

6.3 Conclusions

It has been shown that the host in a PHOLED undergoes aggregation due to the interactions between the excitons and positive polarons during device operation. The rate of this aggregation is

found to be the limiting factor for device lifetime. It has also been shown that phase segregation between the host and the guest is an important aspect of these morphological changes. Because of this segregation, transfer of excitons from the host to the guest becomes increasingly less efficient in the devices, resulting in the loss in EL efficiency over time.

To suppress the degradation at the organic/organic interface, two approaches have been successfully demonstrated: (a) reducing exciton concentration near the interface, and (b) reducing the polaron density near the interface.

Chapter 7

Conclusions & Future Work

7.1 Conclusions

The main findings of this work can be summarized as follows:

Investigations of the efficiency behavior of simplified PHOLEDs show that charge balance in these devices is not optimal. Particularly, the devices are generally hole-rich, and that the leakage of electrons to the counter electrode also presents a major mechanism that results in efficiency loss. Using HTLs that can also block electrons is found to further increase device efficiency by 25%. Results also show that by using a rougher ITO, light trapped in the ITO/organic wave-guided mode can be efficiently extracted, and a light outcoupling enhancement as high as 40% is achieved. Furthermore, it is found that the ITO thickness can also influence light outcoupling by 40%. These results demonstrate the significant efficiency benefits of using ITO with optimal thicknesses and higher roughness in OLEDs.

The conclusions about the underlying processes that govern charge balance in simplified PHOLEDs and the means for improving charge balance are derived from the following findings:

1. It is found that the traditional method of probing charge balance via monitoring device efficiency while varying layer thickness is ineffective in devices utilizing high carrier-mobility materials, such as simplified PHOLEDs, due to the strong dependence of device efficiency on microcavity effects.
2. It is found that delayed EL is a sensitive technique for detecting small changes in charge balance without any influence from microcavity effects, and is therefore suitable for studying charge balance in simplified PHOLEDs.
3. It is found that introducing charge traps in a thin layer within the HTL or ETL can influence charge balance significantly, and proves to be another effective approach for studying the factors limiting charge balance in simplified PHOLEDs.

4. It is concluded that simplified PHOLEDs are generally hole-rich. Furthermore, the electron leakage is the other major mechanism behind their suboptimal charge balance.
5. It is shown that by using an electron blocking HTL, thus eliminating electron leakage and also improving the e/h ratio, the efficiency of simplified PHOLEDs can be improved by as much as 25%.

The conclusions about the influence of ITO roughness and thickness on light outcoupling are derived from the following findings:

1. It is found that by using a rougher ITO, a light outcoupling enhancement as high as 40% can be achieved in simplified PHOLEDs.
2. The reasons behind the light outcoupling enhancement from using a rougher ITO is found to be due to more efficient extraction of light trapped in the ITO/organic wave-guided mode via scattering, as well as to changes in optical interference.
3. It is shown that changing ITO thickness can also change optical interference, and thus alter light outcoupling by more than 40%.
4. It is found that changes in interference and light scattering from using a rougher ITO can cause light outcoupling efficiency to be improved by more than 25% and 10%, respectively.
5. It is shown that the lifetime of simplified PHOLEDs is not affected by the ITO roughness.

Investigations of the factors governing device stability show that the exciton-induced degradation of the ITO/organic interface plays an important role in limiting the lifetime of simplified PHOLEDs. It is found that the lack of electron blocking layers in these devices allows electrons to leak from the emission layers and recombine with holes to form excitons near the ITO/organic interface. Furthermore, it is shown that introducing an electron blocking HTL can increase device lifetime by one order of magnitude. The results also show that the interactions between excitons and positive polarons in the host lead to host aggregation followed by the formation of exciton quenchers within. It is found that the rate of host aggregation limits the lifetime of PHOLEDs, and is also influenced by the guest material and concentration. These findings explain why PHOLEDs utilizing different guest materials but otherwise identical material systems can have significantly different lifetimes and provide an answer to a long-lasting question in the field. Finally, it is found that

reducing the exciton and polaron densities within the EML can further improve the lifetime of simplified PHOLEDs by one order of magnitude.

The conclusion about exciton-induced degradation of the ITO/organic interface playing an important role in limiting the lifetime of simplified PHOLEDs is derived from the following findings:

1. It is shown that the ITO/organic interface in simplified PHOLEDs is susceptible to exciton-induced degradation. Furthermore, this degradation mechanism is found to be a major reason behind the relatively shorter lifetime of simplified PHOLEDs.
2. It is found that the excitons near the ITO/organic interface in simplified PHOLEDs are from recombination of electrons leaked from the EML with holes injected from the ITO, and not from the diffusion of excitons created in the EML.
3. It is shown that the lifetime of simplified PHOLEDs can be improved if the electrons leaked from the EML can be constrained so that they do not reach the ITO/organic interface to form excitons by recombining with holes nearby.
4. It is found that introducing an electron trapping dopant in the HTL or inserting an EBL between the ITO and the HTL can stop electrons from reaching the ITO/organic interface, and thus improve device lifetime. In particular, introducing a thin layer of 26DCzPPy can increase the lifetime of the devices by one order of magnitude without any negative effects on device efficiency.

The conclusion about the rate of the aggregation of the host limiting the lifetime of simplified PHOLEDs, and that the aggregation rate is influenced by the guest material and concentration is derived from the following findings:

1. It is shown that the rate of the aggregation of the host due to the interactions between the excitons and positive polarons limits the lifetime of simplified PHOLEDs.
2. It is found that the aggregation rate of the host is affected by the choice of the guest material and concentration.

3. It is found that host-guest phase segregation occurs during the host aggregation process. As a result, energy transfer from the host to the guest is shown to be increasingly less efficient in devices, leading to a gradual loss in EL efficiency over time.
4. These findings explain why PHOLEDs utilizing different guest materials but otherwise identical material systems can have significantly different lifetimes, thus providing an answer to a long-lasting question in the field.

The conclusion about reducing the exciton and polaron densities within the EML can further improve the lifetime of simplified PHOLEDs is derived from the following findings:

1. It is found that reducing the exciton density near the organic/organic interface can lead to an increase in device lifetime.
2. It is shown that the exciton density can be reduced by using a thicker EML or moving the doped layer away from the EML/ETL interface. Both methods are found to be able to increase device lifetime by a factor of four.
3. It is found that reducing the positive polaron density near the organic/organic interface improves device lifetime.
4. It is shown that inverted simplified PHOLEDs, compared to the standard devices, have a higher e/h ratio in the HTL and EML, thus lower positive polaron density near the organic/organic interface. Using the inverted structure is found to improve device lifetime by a factor of three.

Although this work is directed towards simplified PHOLEDs, some of the findings from this work are also applicable to other devices. Specifically, the light outcoupling enhancement technique using rougher ITO can be applied to OLEDs in general. Moreover, the findings on the influence of the guest on the host, and thus device stability, provide new insights into the importance of material design in PHOLEDs. Particularly, additional attention should be paid to the interactions between the host and the guest, i.e. the effects of the guest on the morphological stability of the host.

7.2 Future work

7.2.1 Using Pre-Aggregated Neat Emitting Layer to Suppress Exciton-Polaron Induced Aggregation

Finding that the rate of host aggregation limits the lifetime of PHOLEDs, future work to examine the effects of using pre-aggregated neat emitting layer (i.e. the EML consists of an emitter with high crystallinity) on the extent of exciton-polaron induced aggregation, and hence device lifetime would be beneficial.

In general, emitters with highly preferred molecular orientation [18], [111], [112] exhibit high crystallinity when deposited through PVD. However, due to concentration quenching, devices utilizing these emitters in neat films are often not efficient. Surprisingly, it is found in 2014 that one emitter, Pt(II) bis(3-(trifluoromethyl)-5-(2-pyridyl)pyrazolate) ($\text{Pt}(\text{fppz})_2$) [113] has a quantum yield of nearly unity even when used in neat films [114]. Moreover, the neat film exhibits properties similar to a single crystal [115]. Therefore, it is interesting to study the stability of devices utilizing neat $\text{Pt}(\text{fppz})_2$ EMLs.

Appendix A List of Publications Derived from this Work

- [1] Y. Zhang and H. Aziz, “Insights into charge balance and its limitations in simplified phosphorescent organic light-emitting devices,” *Org. Electron.*, vol. 30, pp. 76–82, 2016.
- [2] Y. Zhang and H. Aziz, “Very high efficiency phosphorescent organic light-emitting devices by using rough indium tin oxide,” *Appl. Phys. Lett.*, vol. 105, no. 1, p. 013305, Jul. 2014.
- [3] Y. Zhang and H. Aziz, “Dependence of light outcoupling in organic light-emitting devices on ITO thickness and roughness,” in *Proc. SPIE 9566, Organic Light Emitting Materials and Devices XIX*, 2015, vol. 9566, p. 95661R.
- [4] Y. Zhang, M. M. A. Abdelmalek, Q. Wang, and H. Aziz, “Degradation mechanism in simplified phosphorescent organic light-emitting devices utilizing one material for hole transport and emitter host,” *Appl. Phys. Lett.*, vol. 103, no. 6, p. 063307, 2013.
- [5] Y. Zhang and H. Aziz, “The influence of the guest on the aggregation of the host by exciton-polaron interactions and its effects on the stability of phosphorescent organic light-emitting devices,” Submitted to *ACS Appl. Mater. Interfaces*.
- [6] Y. Zhang, Q. Wang, and H. Aziz, “Simplified organic light-emitting devices utilizing ultrathin electron transport layers and new insights on their roles,” *ACS Appl. Mater. Interfaces*, vol. 6, no. 3, pp. 1697–701, Feb. 2014.
- [7] Y. Zhang and H. Aziz, “Enhanced stability in inverted simplified phosphorescent organic light-emitting devices and its origins,” *Org. Electron.*, vol. 22, pp. 69–73, 2015.

Bibliography

- [1] M. Pope, H. P. Kallmann, and P. Magnante, "Electroluminescence in Organic Crystals," *J. Chem. Phys.*, vol. 38, no. 8, p. 2042, 1963.
- [2] C. W. Tang and S. A. VanSlyke, "Organic electroluminescent diodes," *Appl. Phys. Lett.*, vol. 51, no. 12, p. 913, 1987.
- [3] W. Brütting, Ed., *Physics of Organic Semiconductors*. Weinheim, FRG: Wiley-VCH Verlag GmbH & Co. KGaA, 2005.
- [4] W. Brütting and C. Adachi, Eds., *Physics of Organic Semiconductors*. Weinheim, Germany: Wiley-VCH Verlag GmbH & Co. KGaA, 2012.
- [5] H. Bässler, "Localized states and electronic transport in single component organic solids with diagonal disorder," *Phys. status solidi*, vol. 107, no. 1, pp. 9–54, Sep. 1981.
- [6] P. M. Borsenberger, L. Pautmeier, and H. Bässler, "Charge transport in disordered molecular solids," *J. Chem. Phys.*, vol. 94, no. 8, p. 5447, 1991.
- [7] S. a Van Slyke, C. H. Chen, and C. W. Tang, "Organic electroluminescent devices with improved stability," *Appl. Phys. Lett.*, vol. 69, no. 15, p. 2160, 1996.
- [8] Y. Kawamura, K. Goushi, J. Brooks, J. J. Brown, H. Sasabe, and C. Adachi, "100% phosphorescence quantum efficiency of Ir(III) complexes in organic semiconductor films," *Appl. Phys. Lett.*, vol. 86, no. 7, p. 071104, 2005.
- [9] J. Huang, M. Pfeiffer, A. Werner, J. Blochwitz, K. Leo, and S. Liu, "Low-voltage organic electroluminescent devices using pin structures," *Appl. Phys. Lett.*, vol. 80, no. 1, p. 139, 2002.
- [10] M. Pfeiffer, S. R. Forrest, K. Leo, and M. E. Thompson, "Electrophosphorescent p-i-n Organic Light-Emitting Devices for Very-High-Efficiency Flat-Panel Displays," *Adv. Mater.*, vol. 14, no. 22, pp. 1633–1636, Nov. 2002.
- [11] G. He, O. Schneider, D. Qin, X. Zhou, M. Pfeiffer, and K. Leo, "Very high-efficiency and low voltage phosphorescent organic light-emitting diodes based on a p-i-n junction," *J. Appl. Phys.*, vol. 95, no. 10, p. 5773, 2004.
- [12] G. He, M. Pfeiffer, K. Leo, M. Hofmann, J. Birnstock, R. Pudzich, and J. Salbeck, "High-efficiency and low-voltage p-i-n electrophosphorescent organic light-emitting diodes with

- double-emission layers,” *Appl. Phys. Lett.*, vol. 85, no. 17, p. 3911, 2004.
- [13] K. Walzer, B. Maennig, M. Pfeiffer, and K. Leo, “Highly efficient organic devices based on electrically doped transport layers.,” *Chem. Rev.*, vol. 107, no. 4, pp. 1233–71, Apr. 2007.
- [14] S.-J. Su, E. Gonmori, H. Sasabe, and J. Kido, “Highly Efficient Organic Blue-and White-Light-Emitting Devices Having a Carrier- and Exciton-Confining Structure for Reduced Efficiency Roll-Off,” *Adv. Mater.*, vol. 20, no. 21, pp. 4189–4194, Oct. 2008.
- [15] J. A. Barltrop and J. D. Coyle, *Principles of Photochemistry*. 1978.
- [16] K. Okumoto, H. Kanno, Y. Hamaa, H. Takahashi, and K. Shibata, “Green fluorescent organic light-emitting device with external quantum efficiency of nearly 10%,” *Appl. Phys. Lett.*, vol. 89, no. 6, pp. 10–13, 2006.
- [17] M. G. Helander, Z. B. Wang, J. Qiu, M. T. Greiner, D. P. Puzzo, Z. W. Liu, and Z. H. Lu, “Chlorinated indium tin oxide electrodes with high work function for organic device compatibility.,” *Science*, vol. 332, no. 6032, pp. 944–7, May 2011.
- [18] K.-H. Kim, C.-K. Moon, J.-H. Lee, S.-Y. Kim, and J.-J. Kim, “Highly efficient organic light-emitting diodes with phosphorescent emitters having high quantum yield and horizontal orientation of transition dipole moments.,” *Adv. Mater.*, vol. 26, no. 23, pp. 3844–7, Jun. 2014.
- [19] C.-H. Gao, S.-D. Cai, W. Gu, D.-Y. Zhou, Z.-K. Wang, and L.-S. Liao, “Enhanced hole injection in phosphorescent organic light-emitting diodes by thermally evaporating a thin indium trichloride layer.,” *ACS Appl. Mater. Interfaces*, vol. 4, no. 10, pp. 5211–6, Oct. 2012.
- [20] X. a. Cao and Y. Q. Zhang, “Performance enhancement of organic light-emitting diodes by chlorine plasma treatment of indium tin oxide,” *Appl. Phys. Lett.*, vol. 100, no. 18, p. 183304, 2012.
- [21] W. Rieb, T. a. Beierlein, and H. Riel, “Optimizing OLED Structures for a-Si Display Applications via Combinatorial Methods and Enhanced Outcoupling,” *Phys. Org. Semicond.*, no. 6, pp. 511–527, 2006.
- [22] G. Gu, D. Z. Garbuzov, P. E. Burrows, S. Venkatesh, S. R. Forrest, and M. E. Thompson, “High-external-quantum-efficiency organic light-emitting devices,” *Opt. Lett.*, vol. 22, no. 6, p. 396, Mar. 1997.
- [23] T. Tsutsui, M. Yahiro, H. Yokogawa, K. Kawano, and M. Yokoyama, “Doubling Coupling-

- Out Efficiency in Organic Light-Emitting Devices Using a Thin Silica Aerogel Layer,” *Adv. Mater.*, vol. 13, no. 15, pp. 1149–1152, Aug. 2001.
- [24] S.-Y. Kim and J.-J. Kim, “Outcoupling efficiency of organic light emitting diodes and the effect of ITO thickness,” *Org. Electron.*, vol. 11, no. 6, pp. 1010–1015, Jun. 2010.
- [25] N. Patel, S. Cina, and J. Burroughes, “High-efficiency organic light-emitting diodes,” *IEEE J. Sel. Top. Quantum Electron.*, vol. 8, no. 2, pp. 346–361, 2002.
- [26] C. F. Madigan, M.-H. Lu, and J. C. Sturm, “Improvement of output coupling efficiency of organic light-emitting diodes by backside substrate modification,” *Appl. Phys. Lett.*, vol. 76, no. 13, p. 1650, 2000.
- [27] T. Nakamura, N. Tsutsumi, N. Juni, and H. Fujii, “Thin-film waveguiding mode light extraction in organic electroluminescent device using high refractive index substrate,” *J. Appl. Phys.*, vol. 97, no. 5, p. 054505, 2005.
- [28] B. W. D’Andrade and J. J. Brown, “Organic light-emitting device luminaire for illumination applications,” *Appl. Phys. Lett.*, vol. 88, no. 19, p. 192908, 2006.
- [29] M.-K. Wei and I.-L. Su, “Method to evaluate the enhancement of luminance efficiency in planar OLED light emitting devices for microlens array,” *Opt. Express*, vol. 12, no. 23, pp. 5777–82, Nov. 2004.
- [30] T. Yamasaki, K. Sumioka, and T. Tsutsui, “Organic light-emitting device with an ordered monolayer of silica microspheres as a scattering medium,” *Appl. Phys. Lett.*, vol. 76, no. 10, p. 1243, 2000.
- [31] K. Neyts, A. U. Nieto, and A. Ullan Nieto, “Importance of scattering and absorption for the outcoupling efficiency in organic light-emitting devices,” *J. Opt. Soc. Am. A*, vol. 23, no. 5, p. 1201, May 2006.
- [32] J. J. Shiang, T. J. Faircloth, and A. R. Ruggal, “Experimental demonstration of increased organic light emitting device output via volumetric light scattering,” *J. Appl. Phys.*, vol. 95, no. 5, p. 2889, 2004.
- [33] R. Bathelt, D. Buchhauser, C. Gärditz, R. Paetzold, and P. Wellmann, “Light extraction from OLEDs for lighting applications through light scattering,” *Org. Electron.*, vol. 8, no. 4, pp. 293–299, Aug. 2007.

- [34] F. Li, X. Li, J. Zhang, and B. Yang, “Enhanced light extraction from organic light-emitting devices by using microcontact printed silica colloidal crystals,” *Org. Electron.*, vol. 8, no. 5, pp. 635–639, Oct. 2007.
- [35] S. Möller and S. R. Forrest, “Improved light out-coupling in organic light emitting diodes employing ordered microlens arrays,” *J. Appl. Phys.*, vol. 91, no. 5, p. 3324, 2002.
- [36] Y. R. Do, Y.-C. Kim, Y.-W. Song, and Y.-H. Lee, “Enhanced light extraction efficiency from organic light emitting diodes by insertion of a two-dimensional photonic crystal structure,” *J. Appl. Phys.*, vol. 96, no. 12, p. 7629, 2004.
- [37] K. Ishihara, M. Fujita, I. Matsubara, T. Asano, S. Noda, H. Ohata, A. Hirasawa, H. Nakada, and N. Shimoji, “Organic light-emitting diodes with photonic crystals on glass substrate fabricated by nanoimprint lithography,” *Appl. Phys. Lett.*, vol. 90, no. 11, p. 111114, 2007.
- [38] Y. Sun and S. R. Forrest, “Enhanced light out-coupling of organic light-emitting devices using embedded low-index grids,” *Nat. Photonics*, vol. 2, no. 8, pp. 483–487, Jul. 2008.
- [39] M. Cai, Z. Ye, T. Xiao, R. Liu, Y. Chen, R. W. Mayer, R. Biswas, K.-M. Ho, R. Shinar, and J. Shinar, “Extremely efficient indium-tin-oxide-free green phosphorescent organic light-emitting diodes,” *Adv. Mater.*, vol. 24, no. 31, pp. 4337–42, Aug. 2012.
- [40] E. Najafabadi, K. A. Knauer, W. Haske, and B. Kippelen, “High-performance inverted top-emitting green electrophosphorescent organic light-emitting diodes with a modified top Ag anode,” *Org. Electron.*, vol. 14, no. 5, pp. 1271–1275, May 2013.
- [41] K. A. Knauer, E. Najafabadi, W. Haske, M. P. Gaj, K. C. Davis, C. Fuentes-Hernandez, U. Carrasco, and B. Kippelen, “Stacked inverted top-emitting green electrophosphorescent organic light-emitting diodes on glass and flexible glass substrates,” *Org. Electron.*, vol. 14, no. 10, pp. 2418–2423, Oct. 2013.
- [42] a. R. Schlatmann, D. W. Floet, a. Hilberer, F. Garten, P. J. M. Smulders, T. M. Klapwijk, and G. Hadziioannou, “Indium contamination from the indium–tin–oxide electrode in polymer light-emitting diodes,” *Appl. Phys. Lett.*, vol. 69, no. 12, p. 1764, 1996.
- [43] H. Aziz, Z. Popovic, C. P. Tripp, N.-X. Hu, A.-M. Hor, and G. Xu, “Degradation processes at the cathode/organic interface in organic light emitting devices with Mg:Ag cathodes,” *Appl. Phys. Lett.*, vol. 72, no. 21, p. 2642, 1998.

- [44] H. Aziz, Z. Popovic, S. Xie, A.-M. Hor, N.-X. Hu, C. Tripp, and G. Xu, "Humidity-induced crystallization of tris (8-hydroxyquinoline) aluminum layers in organic light-emitting devices," *Appl. Phys. Lett.*, vol. 72, no. 7, p. 756, 1998.
- [45] Y.-F. Liew, H. Aziz, N.-X. Hu, H. S.-O. Chan, G. Xu, and Z. Popovic, "Investigation of the sites of dark spots in organic light-emitting devices," *Appl. Phys. Lett.*, vol. 77, no. 17, p. 2650, 2000.
- [46] P. E. Burrows, V. Bulovic, S. R. Forrest, L. S. Sapochak, D. M. McCarty, and M. E. Thompson, "Reliability and degradation of organic light emitting devices," *Appl. Phys. Lett.*, vol. 65, no. 23, p. 2922, 1994.
- [47] R. Phatak, T. Y. Tsui, and H. Aziz, "Dependence of dark spot growth on cathode/organic interfacial adhesion in organic light emitting devices," *J. Appl. Phys.*, vol. 111, no. 5, p. 054512, 2012.
- [48] H. Aziz, Z. D. Popovic, N.-X. Hu, A.-M. Hor, and G. Xu, "Degradation Mechanism of Small Molecule-Based Organic Light-Emitting Devices," *Science (80-.)*, vol. 283, no. 5409, pp. 1900–1902, Mar. 1999.
- [49] H. Aziz and Z. D. Popovic, "Degradation Phenomena in Small-Molecule Organic Light-Emitting Devices," *Chem. Mater.*, vol. 16, no. 23, pp. 4522–4532, Nov. 2004.
- [50] D. Y. Kondakov, W. C. Lenhart, and W. F. Nichols, "Operational degradation of organic light-emitting diodes: Mechanism and identification of chemical products," *J. Appl. Phys.*, vol. 101, no. 2, p. 024512, 2007.
- [51] D. Y. Kondakov, "Role of chemical reactions of arylamine hole transport materials in operational degradation of organic light-emitting diodes," *J. Appl. Phys.*, vol. 104, no. 8, p. 084520, 2008.
- [52] S. Scholz, K. Walzer, and K. Leo, "Analysis of complete organic semiconductor devices by laser desorption/ionization time-of-flight mass spectrometry," *Adv. Funct. Mater.*, vol. 18, no. 17, pp. 2541–2547, 2008.
- [53] V. Sivasubramaniam, F. Brodkorb, S. Hanning, O. Buttler, H. P. Loebel, V. van Elsbergen, H. Boerner, U. Scherf, and M. Kreyenschmidt, "Degradation of HTL layers during device operation in PhOLEDs," *Solid State Sci.*, vol. 11, no. 11, pp. 1933–1940, Nov. 2009.

- [54] F. So and D. Kondakov, "Degradation Mechanisms in Small-Molecule and Polymer Organic Light-Emitting Diodes," *Adv. Mater.*, vol. 22, no. 34, pp. 3762–3777, 2010.
- [55] N. C. Giebink, B. W. D. Andrade, M. S. Weaver, P. B. Mackenzie, J. J. Brown, M. E. Thompson, S. R. Forrest, and B. W. D'Andrade, "Intrinsic luminance loss in phosphorescent small-molecule organic light emitting devices due to bimolecular annihilation reactions," *J. Appl. Phys.*, vol. 103, no. 4, p. 044509, 2008.
- [56] N. C. Giebink, B. W. D'Andrade, M. S. Weaver, J. J. Brown, and S. R. Forrest, "Direct evidence for degradation of polaron excited states in organic light emitting diodes," *J. Appl. Phys.*, vol. 105, no. 12, p. 124514, 2009.
- [57] Q. Wang, G. Williams, and H. Aziz, "Photo-degradation of the indium tin oxide (ITO)/organic interface in organic optoelectronic devices and a new outlook on the role of ITO surface treatments and interfacial layers in improving device stability," *Org. Electron.*, vol. 13, no. 10, pp. 2075–2082, Oct. 2012.
- [58] Q. Wang, Y. Luo, and H. Aziz, "Photodegradation of the organic/metal cathode interface in organic light-emitting devices," *Appl. Phys. Lett.*, vol. 97, no. 6, p. 063309, 2010.
- [59] Q. Wang and H. Aziz, "Poor photo-stability of the organic/LiF/Al contact in organic optoelectronic devices," *Org. Electron.*, vol. 12, no. 9, pp. 1571–1575, Sep. 2011.
- [60] Q. Wang, G. Williams, T. Tsui, and H. Aziz, "Photochemical deterioration of the organic/metal contacts in organic optoelectronic devices," *J. Appl. Phys.*, vol. 112, no. 6, p. 064502, 2012.
- [61] Q. Wang and H. Aziz, "Degradation of Organic/Organic Interfaces in Organic Light-Emitting Devices due to Polaron-Exciton Interactions.," *ACS Appl. Mater. Interfaces*, vol. 5, no. 17, pp. 8733–9, Sep. 2013.
- [62] Q. Wang, B. Sun, and H. Aziz, "Exciton-polaron-induced aggregation of wide-bandgap materials and its implication on the electroluminescence stability of phosphorescent organic light-emitting devices," *Adv. Funct. Mater.*, vol. 24, no. 20, pp. 2975–2985, May 2014.
- [63] D. Y. Kondakov, J. R. Sandifer, C. W. Tang, and R. H. Young, "Nonradiative recombination centers and electrical aging of organic light-emitting diodes: Direct connection between accumulation of trapped charge and luminance loss," *J. Appl. Phys.*, vol. 93, no. 2, p. 1108, 2003.

- [64] M. Matsumura, a Ito, and Y. Miyamae, “Accumulation of positive charges in organic light-emitting diodes with a double-layer structure,” *Appl Phys Lett*, vol. 75, no. 8, pp. 1042–1044, 1999.
- [65] Q. Wang and H. Aziz, “Exciton-Polaron-Induced Aggregation of Organic Electroluminescent Materials: A Major Degradation Mechanism in Wide-Bandgap Phosphorescent and Fluorescent Organic Light-Emitting Devices,” *Adv. Opt. Mater.*, vol. 3, no. 7, pp. 967–975, Jul. 2015.
- [66] V. Bulović, V. Khalfin, G. Gu, P. Burrows, D. Garbuzov, and S. Forrest, “Weak microcavity effects in organic light-emitting devices,” *Phys. Rev. B*, vol. 58, no. 7, pp. 3730–3740, Aug. 1998.
- [67] C. Murawski, P. Liehm, K. Leo, and M. C. Gather, “Influence of cavity thickness and emitter orientation on the efficiency roll-off of phosphorescent organic light-emitting diodes,” *Adv. Funct. Mater.*, vol. 24, no. 8, pp. 1117–1124, 2014.
- [68] T.-Y. Chu and O.-K. Song, “Hole mobility of N,N[^{sup}']-bis(naphthalen-1-yl)-N,N[^{sup}']-bis(phenyl) benzidine investigated by using space-charge-limited currents,” *Appl. Phys. Lett.*, vol. 90, no. 20, p. 203512, 2007.
- [69] J.-W. Kang, S.-H. Lee, H.-D. Park, W.-I. Jeong, K.-M. Yoo, Y.-S. Park, and J.-J. Kim, “Low roll-off of efficiency at high current density in phosphorescent organic light emitting diodes,” *Appl. Phys. Lett.*, vol. 90, no. 22, p. 223508, 2007.
- [70] Z. D. Popovic and H. Aziz, “Delayed Electroluminescence: a New Tool for Studies of OLED Fundamental Properties,” *Proc. SPIE*, vol. 5937, Aug. 2005.
- [71] Y. Zhang, M. M. A. Abdelmalek, Q. Wang, and H. Aziz, “Degradation mechanism in simplified phosphorescent organic light-emitting devices utilizing one material for hole transport and emitter host,” *Appl. Phys. Lett.*, vol. 103, no. 6, p. 063307, 2013.
- [72] C. H. Kim and J. Shinar, “Bright small molecular white organic light-emitting devices with two emission zones,” *Appl. Phys. Lett.*, vol. 80, no. 12, pp. 2201–2203, 2002.
- [73] S. Naka, H. Okada, H. Onnagawa, Y. Yamaguchi, and T. Tsutsui, “Carrier transport properties of organic materials for EL device operation,” *Synth. Met.*, vol. 111–112, pp. 331–333, Jun. 2000.

- [74] T. Ye, S. Shao, J. Chen, L. Wang, and D. Ma, “Efficient phosphorescent polymer yellow-light-emitting diodes based on solution-processed small molecular electron transporting layer,” *ACS Appl. Mater. Interfaces*, vol. 3, no. 2, pp. 410–416, 2011.
- [75] Y. Zhang, Q. Wang, and H. Aziz, “Simplified organic light-emitting devices utilizing ultrathin electron transport layers and new insights on their roles,” *ACS Appl. Mater. Interfaces*, vol. 6, no. 3, pp. 1697–701, Feb. 2014.
- [76] Z. D. Popovic and H. Aziz, “Delayed electroluminescence in small-molecule-based organic light-emitting diodes: Evidence for triplet-triplet annihilation and recombination-center-mediated light-generation mechanism,” *J. Appl. Phys.*, vol. 98, no. 1, p. 013510, 2005.
- [77] D. Song, Q. Wang, S. Zhao, and H. Aziz, “Dependence of carrier recombination mechanism on the thickness of the emission layer in green phosphorescent organic light emitting devices,” *Org. Electron.*, vol. 12, no. 4, pp. 582–588, Apr. 2011.
- [78] R. R. Lunt, N. C. Giebink, A. a. Belak, J. B. Benziger, and S. R. Forrest, “Exciton diffusion lengths of organic semiconductor thin films measured by spectrally resolved photoluminescence quenching,” *J. Appl. Phys.*, vol. 105, no. 5, p. 053711, 2009.
- [79] J.-H. Lee, B.-Y. Lin, Y.-H. Lan, T.-L. Chiu, P.-Y. Lee, and C.-F. Lin, “Electrical and optical characteristics of phosphorescent organic light-emitting device with thin-codoped layer insertion,” *Org. Electron.*, vol. 24, pp. 182–187, 2015.
- [80] Y. Zhang and H. Aziz, “Enhanced stability in inverted simplified phosphorescent organic light-emitting devices and its origins,” *Org. Electron.*, vol. 22, pp. 69–73, 2015.
- [81] G.-C. Choi, D.-E. Kim, J.-W. Park, B.-S. Kim, and Y.-S. Kwon, “Efficiency Improvement of OLED by Aquaregia and RCA Treatment of ITO Substrate,” *Mol. Cryst. Liq. Cryst.*, vol. 504, no. 1, pp. 35–43, Jun. 2009.
- [82] Z. H. Huang, X. T. Zeng, X. Y. Sun, E. T. Kang, J. Y. H. Fuh, and L. Lu, “Influence of plasma treatment of ITO surface on the growth and properties of hole transport layer and the device performance of OLEDs,” *Org. Electron.*, vol. 9, no. 1, pp. 51–62, Feb. 2008.
- [83] G. Liu, J. B. Kerr, and S. Johnson, “Dark spot formation relative to ITO surface roughness for polyfluorene devices,” *Synth. Met.*, vol. 144, no. 1, pp. 1–6, Jul. 2004.
- [84] Y. Tak, K. Kim, H. Park, K.-H. Lee, and J. Lee, “Criteria for ITO (indium–tin-oxide) thin film

- as the bottom electrode of an organic light emitting diode,” *Thin Solid Films*, vol. 411, no. 1, pp. 12–16, May 2002.
- [85] H. Kim, C. M. Gilmore, a. Piqué, J. S. Horwitz, H. Mattoussi, H. Murata, Z. H. Kafafi, and D. B. Chrisey, “Electrical, optical, and structural properties of indium–tin–oxide thin films for organic light-emitting devices,” *J. Appl. Phys.*, vol. 86, no. 11, p. 6451, 1999.
- [86] Y. Zhang and H. Aziz, “Very high efficiency phosphorescent organic light-emitting devices by using rough indium tin oxide,” *Appl. Phys. Lett.*, vol. 105, no. 1, p. 013305, Jul. 2014.
- [87] H. Zamani Siboni, Y. Luo, and H. Aziz, “Luminescence degradation in phosphorescent organic light-emitting devices by hole space charges,” *J. Appl. Phys.*, vol. 109, no. 4, p. 044501, 2011.
- [88] H. Zamani Siboni and H. Aziz, “Triplet-polaron quenching by charges on guest molecules in phosphorescent organic light emitting devices,” *Appl. Phys. Lett.*, vol. 101, no. 6, p. 063502, 2012.
- [89] H. Kanai, S. Ichinosawa, and Y. Sato, “Effect of aromatic diamines as a cathode interface layer,” *Synth. Met.*, vol. 91, no. 1–3, pp. 195–196, Dec. 1997.
- [90] M. A. M. Baldo, D. F. O’Brien, Y. You, A. Shoustikov, S. R. Forrest, M. A. M. Baldo, D. F. O’Brien, Y. You, A. Shoustikov, S. Sibley, and M. E. Thompson, “Highly efficient phosphorescent emission from organic electroluminescent devices,” *Nature*, vol. 395, no. 6698, pp. 151–154, Sep. 1998.
- [91] C. Adachi, M. A. Baldo, M. E. Thompson, and S. R. Forrest, “Nearly 100% internal phosphorescence efficiency in an organic light-emitting device,” *J. Appl. Phys.*, vol. 90, no. 10, p. 5048, 2001.
- [92] S. Wu, B. Huh, T. Yu, and H. Hayase, “OLED Display Market Tracker.” [Online]. Available: <https://technology.ihs.com/553125/oled-display-market-tracker-q4-2015>. [Accessed: 11-Jan-2016].
- [93] H. Zamani Siboni and H. Aziz, “Explaining the different efficiency behaviors of PHOLEDs with/without a hole injection barrier at the hole transport layer/emitter layer interface,” *Org. Electron.*, vol. 14, no. 10, pp. 2510–2517, Oct. 2013.
- [94] S. Lamansky, P. Djurovich, D. Murphy, F. Abdel-Razzaq, H.-E. Lee, C. Adachi, P. E.

- Burrows, S. R. Forrest, and M. E. Thompson, "Highly Phosphorescent Bis-Cyclometalated Iridium Complexes: Synthesis, Photophysical Characterization, and Use in Organic Light Emitting Diodes," *J. Am. Chem. Soc.*, vol. 123, no. 3, pp. 4304–4312, 2001.
- [95] F. Laquai, Y.-S. Park, J.-J. Kim, and T. Basché, "Excitation energy transfer in organic materials: from fundamentals to optoelectronic devices.," *Macromol. Rapid Commun.*, vol. 30, no. 14, pp. 1203–31, Jul. 2009.
- [96] M. H. Tsai, Y. H. Hong, C. H. Chang, H. C. Su, C. C. Wu, A. Matoliukstyte, J. Simokaitiene, S. Grigalevicius, J. V. Grazulevicius, and C. P. Hsu, "3-(9-carbazolyl)carbazoles and 3,6-Di(9-carbazolyl)carbazoles as effective host materials for efficient blue organic electrophosphorescence," *Adv. Mater.*, vol. 19, no. 6, pp. 862–866, 2007.
- [97] S.-J. Su, C. Cai, and J. Kido, "Three-carbazole-armed host materials with various cores for RGB phosphorescent organic light-emitting diodes," *J. Mater. Chem.*, vol. 22, no. 8, p. 3447, 2012.
- [98] L. Xiao, Z. Chen, B. Qu, J. Luo, S. Kong, Q. Gong, and J. Kido, "Recent progresses on materials for electrophosphorescent organic light-emitting devices," *Adv. Mater.*, vol. 23, no. 8, pp. 926–952, 2011.
- [99] S.-J. Su, H. Sasabe, T. Takeda, and J. Kido, "Pyridine-Containing Bipolar Host Materials for Highly Efficient Blue Phosphorescent OLEDs," *Chem. Mater.*, vol. 20, no. 5, pp. 1691–1693, Mar. 2008.
- [100] H. Sasabe, J. Takamatsu, T. Motoyama, S. Watanabe, G. Wagenblast, N. Langer, O. Molt, E. Fuchs, C. Lennartz, and J. Kido, "High-efficiency blue and white organic light-emitting devices incorporating a blue iridium carbene complex.," *Adv. Mater.*, vol. 22, no. 44, pp. 5003–7, Nov. 2010.
- [101] A. P. Kulkarni, C. J. Tonzola, A. Babel, and S. a. Jenekhe, "Electron Transport Materials for Organic Light-Emitting Diodes," *Chem. Mater.*, vol. 16, no. 23, pp. 4556–4573, Nov. 2004.
- [102] R. C. Kwong, M. R. Nugent, L. Michalski, T. Ngo, K. Rajan, Y.-J. Tung, M. S. Weaver, T. X. Zhou, M. Hack, M. E. Thompson, S. R. Forrest, and J. J. Brown, "High operational stability of electrophosphorescent devices," *Appl. Phys. Lett.*, vol. 81, no. 1, p. 162, 2002.
- [103] B. W. D'Andrade, S. R. Forrest, A. B. Chwang, and B. W. D. Andrade, "Operational stability of electrophosphorescent devices containing p and n doped transport layers," *Appl. Phys. Lett.*,

vol. 83, no. 19, p. 3858, 2003.

- [104] G. Schwartz, T.-H. Ke, C.-C. Wu, K. Walzer, and K. Leo, "Balanced ambipolar charge carrier mobility in mixed layers for application in hybrid white organic light-emitting diodes," *Appl. Phys. Lett.*, vol. 93, no. 7, p. 073304, 2008.
- [105] T.-Y. Chu, Y.-S. Wu, J.-F. Chen, and C. H. Chen, "Characterization of electronic structure of aluminum (III) bis(2-methyl-8-quinolinato)-4-phenylphenolate (BAIq) for phosphorescent organic light emitting devices," *Chem. Phys. Lett.*, vol. 404, no. 1–3, pp. 121–125, Mar. 2005.
- [106] I. Tanaka, Y. Tabata, and S. Tokito, "Förster and Dexter energy-transfer processes in fluorescent BAIq thin films doped with phosphorescent Ir(ppy)₃ molecules," *J. Appl. Phys.*, vol. 99, no. 7, p. 073501, 2006.
- [107] T.-Y. Chu, J.-F. Chen, S.-Y. Chen, C.-J. Chen, and C. H. Chen, "Highly efficient and stable inverted bottom-emission organic light emitting devices," *Appl. Phys. Lett.*, vol. 89, no. 5, p. 053503, 2006.
- [108] S.-Y. Chen, T.-Y. Chu, J.-F. Chen, C.-Y. Su, and C. H. Chen, "Stable inverted bottom-emitting organic electroluminescent devices with molecular doping and morphology improvement," *Appl. Phys. Lett.*, vol. 89, no. 5, p. 053518, 2006.
- [109] M. Thomschke, S. Hofmann, S. Olthof, M. Anderson, H. Kleemann, M. Schober, B. Lüssem, and K. Leo, "Improvement of voltage and charge balance in inverted top-emitting organic electroluminescent diodes comprising doped transport layers by thermal annealing," *Appl. Phys. Lett.*, vol. 98, no. 8, p. 083304, 2011.
- [110] J.-B. J.-J. Kim, J.-H. Lee, C.-K. Moon, and J.-B. J.-J. Kim, "Highly efficient inverted top emitting organic light emitting diodes using a transparent top electrode with color stability on viewing angle," *Appl. Phys. Lett.*, vol. 104, no. 7, p. 073301, Feb. 2014.
- [111] D. Yokoyama, "Molecular orientation in small-molecule organic light-emitting diodes," *J. Mater. Chem.*, vol. 21, no. 48, p. 19187, 2011.
- [112] S.-Y. Kim, W.-I. Jeong, C. Mayr, Y.-S. Park, K.-H. Kim, J.-H. Lee, C.-K. Moon, W. Brütting, and J.-J. Kim, "Organic Light-Emitting Diodes with 30% External Quantum Efficiency Based on a Horizontally Oriented Emitter," *Adv. Funct. Mater.*, vol. 23, no. 31, pp. 3896–3900, Aug. 2013.

- [113] S.-Y. Chang, J. Kavitha, S.-W. Li, C.-S. Hsu, Y. Chi, Y.-S. Yeh, P.-T. Chou, G.-H. Lee, A. J. Carty, Y.-T. Tao, and C.-H. Chien, "Platinum(II) complexes with pyridyl azolate-based chelates: synthesis, structural characterization, and tuning of photo- and electrophosphorescence.," *Inorg. Chem.*, vol. 45, no. 1, pp. 137–46, 2006.
- [114] Q. Wang, I. W. H. Oswald, X. Yang, G. Zhou, H. Jia, Q. Qiao, Y. Chen, J. Hoshikawa-Halbert, and B. E. Gnade, "A Non-Doped Phosphorescent Organic Light-Emitting Device with Above 31% External Quantum Efficiency," *Adv. Mater.*, vol. 26, no. 48, pp. 8107–8113, 2014.
- [115] K.-H. Kim, J.-L. Liao, S. W. Lee, B. Sim, C.-K. Moon, G.-H. Lee, H. J. Kim, Y. Chi, and J.-J. Kim, "Crystal Organic Light-Emitting Diodes with Perfectly Oriented Non-Doped Pt-Based Emitting Layer," *Adv. Mater.*, vol. 28, no. 13, pp. 2526–2532, Apr. 2016.
- [116] H. Ishii, K. Sugiyama, E. Ito, and K. Seki, "Energy Level Alignment and Interfacial Electronic Structures at Organic/Metal and Organic/Organic Interfaces," *Adv. Mater.*, vol. 11, no. 8, pp. 605–625, Jun. 1999.